Studies of

Large Scale Atmospheric Energetics

Department of Meteorology
The University of Wisconsin
Madison, Wisconsin 53706

Contributions by

R. A. Anthes
L. H. Horn
P. J. Smith
D. R. Johnson
W. C. Shen

L. H. Horn and D. R. Johnson, Joint Principal Investigators

ANNUAL REPORT

The research in this document has been supported
by the National Environmental Satellite Center of the
Environmental Science Services Administration under Grant WBG 52

December 1967

Studies of

Large Scale Atmospheric Energetics

Department of Meteorology
The University of Wisconsin
Madison, Wisconsin 53706

Contributions by

R. A. Anthes
L. H. Horn
P. J. Smith
D. R. Johnson
W. C. Shen

L. H. Horn and D. R. Johnson, Joint Principal Investigators

ANNUAL REPORT

The research in this document has been supported
by the National Environmental Satellite Center of the
Environmental Science Services Administration under Grant WBG 52

December 1967

Scanner's note:

This page is blank.

TABLE OF CONTENTS

400-109

Scanner's note:

This page is blank.

INTRODUCTION

The research presented here in the form of an annual report consists of continuing studies primarily involving the large scale energetics of the atmosphere. The last paper in the report, an error analysis of the radiometersonde, is reprinted with permission of the Journal of Geophysics and was completed to support our research on the diabatic effects of infrared irradiance on large scale motions. Also during 1967, the paper "The Theory of Available Potential Energy and a Variational Approach to Atmospheric Energetics," co-authored by Professors John A. Dutton of Pennsylvania State University and Donald R. Johnson, was published in Vol. 12, Advances in Geophysics. The monograph represents a contribution partially evolving from previous research supported by WBG 10 and WBG 25.

The research in this report consists of studies primarily supported by the Environmental Science Services Administration under grant WBG 52.

Partial support was provided by the Wisconsin Alumni Research Foundation and National Science Foundation through the University Research Committee in the form of a grant for computational funds and the use of computer facilities.

Lyle H. Horn
Donald R. Johnson
Joint Principal Investigators

Madison, Wisconsin
December, 1967

Scanner's note:

This page is blank.

ENERGY EQUATIONS AND THEIR APPLICATION TO A LIMITED REGION OF THE ATMOSPHERE

Phillip J. Smith, Lyle H. Horn, Donald R. Johnson

ABSTRACT

Energy budget equations applicable to any limited atmospheric region are developed employing the concept of available potential energy and used to calculate the energy budget over North America for March, 1962. These equations contain, in addition to the customary generation, conversion, and dissipation terms, expressions for the boundary fluxes. Since it appears necessary to use a global reference state, the local available potential energy (A) is defined as the contribution the limited region makes to the global available potential energy. In this study this leads to mean values of A that are negative.

The energy budget estimates obtained here differ in a number of ways from the global, annual budget values. The generation value obtained here is quite small, probably reflecting the reduced zonal heating effects in this region. The boundary fluxes and pressure work estimates, both of which are zero in the global budget, demonstrate the significant interaction between the limited region and its environment. The large values of $\overline{\omega}\overline{\alpha}$ (identified in this paper as A-conversion) and $\overline{\omega'\alpha'}$ compared with $-\overline{\underline{V}} \cdot \nabla_p \overline{\phi}$ (identified as K-conversion) indicate that neither A-conversion nor $\overline{\omega'\alpha'}$ represent direct production of kinetic energy for the area and time of this study.

The errors in the daily estimates to a large extent cancelled in the monthly means. Given the limited data sample utilized in this study, the largest errors are probably associated with the technique used to determine partial derivatives. In addition it seems possible that filtering the raw wind data may have caused underestimates of K-conversion, which in turn have led to underestimates of the dissipation.

TABLE OF SYMBOLS

I. Physical variables and constants

ρ	density
α	specific volume
p	pressure
p_{00}	$p = 1000$ mb
p_1, p_2	arbitrary pressure levels
p_0	surface pressure
p_r	reference pressure (equal to the global mean pressure on a θ surface)
p''	$p - p_r$
T	temperature
z	height in geopotential units
z_0	geopotential height of the surface
z_T	geopotential height of the top of the atmosphere
ϕ	gz
$\underline{V}$	horizontal wind vector
ω	$\frac{dp}{dt}$ (referred to as vertical motion in this paper)
θ	potential temperature
θ_T	potential temperature at z_T
Q	diabatic heating rate per unit mass
t	time
P	gravitational potential energy
I	internal energy
K	kinetic energy
Π	total potential energy $(I + P)$
Π_r	reference total potential energy
A	available potential energy
C_A	A-conversion
HF_A	horizontal flux of A
VF_A	vertical flux of A
PW	pressure work
G	generation of A
C_K	K-conversion
HF_K	horizontal flux of K
VF_K	vertical flux of K
D	dissipation
ε_A	available potential energy error
ε_C	conversion error
E	efficiency factor
g	980 cm sec^{-2}
c_v	specific heat of dry air at constant volume
c_p	specific heat of dry air at constant pressure

R	gas constant for dry air
κ	R/c_p
X	weighted mass change

II. Mathematical operations

$\int d\sigma$	area integral
$\int dz$	height integral
$\int dp$	pressure integral
$\int dM$	mass integral
	$= \iint \rho \, dz \, d\sigma$
	$= \frac{1}{g} \iint dp \, d\sigma$ for hydrostatic balance
∇_p	del operator on constant pressure surface
$\cdot$	scalar product of vector quantities
$(\overline{\overline{\ }})$	local area average of a potential temperature surface
$(\overline{\ })$	local area average on a pressure surface
$(\ )'$	deviation from $(\overline{\ })$

1. INTRODUCTION

The kinetic energy of all scales of atmospheric motion is produced by complex thermodynamic processes. Of fundamental interest is the question of how these processes maintain the kinetic energy against frictional dissipation. One method of investigating this problem is to examine the time change of energy and the mechanisms which produce these changes, i.e., study the atmosphere's energy budget. Most previous investigations have been concerned with the general circulation and have, therefore, interpreted results in terms of global or hemispheric energetics. The purpose of this study is to: (1) develop equations which describe the energy budget for any limited region of the atmosphere; and (2) compute the energy budget over North America for March, 1962.

Of primary importance in studies of atmospheric energetics has been the concept of available potential energy. Originally applied to the atmosphere by Margules (1903), it remained for Lorenz (1955a) to present the concept in a mathematical form which could be used in studies of the general circulation. Lorenz defined the available potential energy as the

difference between the existing total potential energy of the atmosphere and that which would exist if the atmospheric mass were adiabatically redistributed to a horizontal, hydrostatically stable state. This idealized atmosphere, which has been referred to as the reference state, can be shown to represent the minimum total potential energy under the constraints of adiabatic mass redistribution and hydrostatic equilibrium (Van Mieghem, 1956). Since the minimizing of total potential energy by adiabatic processes also maximizes the kinetic energy, this concept allows one to consider that part which is "energetically active." Lorenz's equations and those developed in this paper reveal that nonfrictional diabatic heating is the basic process in maintaining the mean, global kinetic energy against frictional dissipation.

Many authors have used Lorenz's equations (or equations equivalent to Lorenz's) to provide numerical estimates of the atmosphere's global energy cycle. Some of the more significant studies are noted below. Estimates of available potential energy and kinetic energy have been made by Saltzman and Fleisher (1961, 1962), Winston and Krueger (1961), and Krueger, et al. (1965). In order to define a global energy cycle it is of course also necessary to describe production (generation), destruction (dissipation), and interaction (conversion) of these energies.

The diabatic generation was first computed by Wiin-Nielsen and Brown (1962) who estimated diabatic heating indirectly using the first law of thermodynamics. Employing harmonic analysis they then computed generation as a function of wave number. Computing diabatic heating by the same method, Winston and Krueger (1961) made independent estimates of the generation. Clapp (1961) computed the generation by evaluating each diabatic term independently and then summing, while Krueger, et al. (1965) calculated generation as a residual term after computing the other terms of the energy budget. Attempts have also been made to determine the generation due to individual components of the diabatic heating. The influence of infrared cooling has been estimated by Suomi and Shen (1963) (Explorer VII data), Corcoran and Horn (1965) (Tiros II data), and Johnson (1967) (Suomi-Kuhn radiometer data). The influence of released latent heat has been estimated by Danard (1966).

In order to determine the extent to which the generation term describes the energy source necessary to maintain the kinetic energy, the results of the studies cited above have been compared with estimates of frictional dissipation provided by Jensen (1961) and Holopainen (1964). The conversion of available potential energy to kinetic energy has also been extensively investigated by Saltzman and Fleisher (1960a, b, 1961), Wiin-Nielsen (1959), White and Saltzman (1956), Winston and Krueger (1961), and Krueger, et al. (1965). Finally, many of these authors (e.g., Saltzman and Fleisher, 1960a, and Wiin-Nielsen, et al., 1963) have estimated the

transfer of available potential and kinetic energy between the various scales of motion. Particular emphasis in this area has been given to the transfer of energy between the eddy (all wave numbers) and zonal (mean) components of the two energy forms.

Although Lorenz's equations have been used extensively over the past decade, they do possess certain limitations when applied to actual data. These limitations can be placed in two general classes: (1) the mathematical approximations employed in their development; and (2) the absence of boundary terms which are needed for studying energetics of limited regions. Lorenz (1955b) was the first to point out that his original equations were approximate and in this later paper developed more general expressions for the available potential energy. Recently Dutton and Johnson (1967), who re-examined the basic concepts of available potential energy, obtained equations extending Lorenz's later work. One approximation made by Lorenz was to use a binomial expansion of the terms $(p_r + p'')^\kappa$ (see Table of Symbols), and then to neglect terms with p'' raised to powers greater than two. Dutton and Johnson have found that this yields values of the global mean available potential energy which are generally about 5% higher than the exact value, with a few deviations as large as 10%. A second approximation made by Lorenz was to assume a constant static stability on any isobaric surface. The errors induced by this approximation depend on the particular constant lapse rate assumed.

In addition to producing errors in the estimates of available potential energy, these approximations can also lead to underestimates of the generation term. Using the exact form of the generation term, Dutton and Johnson obtained generation estimates which were nearly three times larger than those obtained using the approximate expression. These results, combined with revised estimates of frictional dissipation by Holopainen (1963) and Kung (1966a, b), indicate that the atmospheric energy cycle may be considerably more intense than previously thought.

Rather than further detailing the results of the above mentioned studies, the authors have summarized them in the flow diagram presented in Figure 1. This diagram includes values which Oort (1964) derived from various other studies as well as the more recent estimates of Dutton and Johnson (1967) and Kung (1966a, 1967). Individual studies will be reviewed as needed later in this paper.

As noted earlier, a further limitation encountered when Lorenz's equations are used in empirical studies is that they lack boundary terms. Energy budget studies using data from limited regions of the earth, as is the case in this paper, must investigate the importance of boundary fluxes. Many of the studies mentioned above used data from limited regions, but,

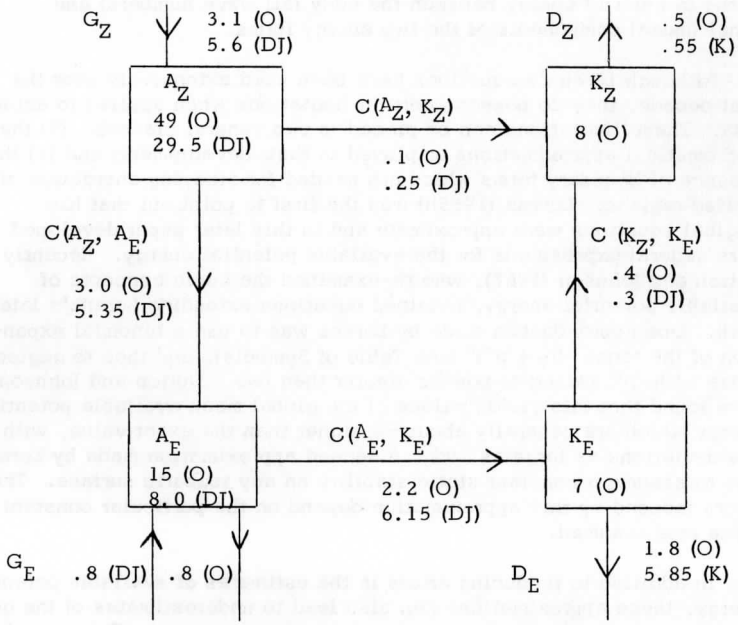

Figure 1. Flow diagram of atmospheric energy. Values indicated by O, DJ, or K are from Oort, Dutton and Johnson, or Kung, respectively. C, G, D are conversion, generation, and dissipation, respectively, while subscripts Z and E represent the zonal and eddy components.

Units: A, K = 10^5 joule m^{-2}; C, G, D = watts m^{-2}

since they involved time averages, the results were assumed to be representative of the entire earth and boundary terms were thus neglected. However, some work on the inclusion of boundary terms based on the approximate formulation has been done by Muench (1965), Julian and Labitzke (1965) and Danard (1966). An additional factor to be considered is that, as pointed out by Pfeffer (1957), restriction to a limited region requires more care in interpreting the conversion term. This problem will be discussed more completely in Chapter 3.

2. ENERGY BUDGET EQUATIONS

In this chapter the energy budget equations for a limited region of the atmosphere are developed from basic definitions. For the entire atmosphere the internal, gravitational potential, and kinetic energy are given, respectively, by

$$I = \int_{\sigma}\int_{z_0}^{z_T} \rho\, c_v T\, dz\, d\sigma \tag{1}$$

$$P = \int_{\sigma}\int_{z_0}^{z_T} \rho\, g\, z\, dz\, d\sigma \tag{2}$$

$$K = \int_{\sigma}\int_{z_0}^{z_T} \rho\, \frac{\underline{V}\cdot\underline{V}}{2}\, dz\, d\sigma \tag{3}$$

where σ is the area of the earth.

Assuming the local hydrostatic balance throughout the atmosphere, (2) and (3) can be written in pressure coordinates as

$$P = \int_{\sigma}\int_{0}^{p_0} z\, dp\, d\sigma \tag{4}$$

$$K = \frac{1}{g}\int_{\sigma}\int_{0}^{p_0} \frac{\underline{V}\cdot\underline{V}}{2}\, dp\, d\sigma. \tag{5}$$

Integrating the interior integral of (4) by parts and applying the equation of state yields

$$P = \int_{\sigma}\int_{z_0}^{z_T} \rho\, R\, T\, dz\, d\sigma. \tag{6}$$

Adding (1) to (6), again assuming hydrostatic balance, and changing back to pressure coordinates yields the expression for the total potential energy of the entire atmospheric mass

$$\Pi = P + I = \frac{c_p}{g} \int_{\sigma} \int_{0}^{p_0} T \, dp \, d\sigma \tag{7}$$

which, using Poisson's equation, can also be written as

$$\Pi = c_p \int_{M} \frac{\theta \, p^{\kappa}}{p_{00}^{\kappa}} \, dM \tag{8}$$

where M is the entire mass of the atmosphere.

To arrive at an expression for available potential energy, it is first necessary to specify the total potential energy of the reference state. Recall from Chapter 1 that the reference state, as defined by Lorenz, is achieved by adiabatic redistribution of the entire atmosphere to a horizontal, hydrostatically stable state. In the reference state the pressure in equation (8) is given by its reference value p_r, while the potential temperature remains unchanged. Hence, the reference total potential energy of the entire atmosphere is

$$\Pi_r = c_p \int_{M} \frac{\theta \, p_r^{\kappa}}{p_{00}^{\kappa}} \, dM. \tag{9}$$

Under the assumption of hydrostatic balance, the reference pressure at any point is given by the global mean pressure of the potential temperature surface passing through that point. It can be expressed as

$$p_r(\theta, t) = \frac{1}{\sigma} \int_{\sigma} \int_{\theta_T}^{\theta} \frac{\partial p}{\partial \theta} \, d\theta \, d\sigma \tag{10}$$

where $p_r(\theta_T, t) = 0$.

Subtracting (9) from (8) and again applying Poisson's equation yields the expression for the available potential energy of the entire atmosphere

$$A = \Pi - \Pi_r = c_p \int_{M} \frac{p^{\kappa} - p_r^{\kappa}}{p^{\kappa}} \, T \, dM. \tag{11}$$

Since (11) can be written as the sum of integrals over limited atmospheric masses M_j (where $\sum_j M_j = M$), the contribution from any particular limited region (j), defined by the area σ_j and the vertical pressure limits p_{1j} and p_{2j} ($p_{1j} > p_{2j}$), to the available potential energy of the entire atmosphere is

$$A_j = c_p \int_{M_j} \frac{p^\kappa - p_r^\kappa}{p^\kappa} T\,dM = \frac{c_p}{g} \int_{\sigma_j} \int_{p_{2j}}^{p_{1j}} \frac{p^\kappa - p_r^\kappa}{p^\kappa} T\,dp\,d\sigma. \tag{12}$$

Over this same limited region the kinetic energy equation (from (5)) is

$$K_j = \frac{1}{g} \int_{\sigma_j} \int_{p_{2j}}^{p_{1j}} \frac{V \cdot V}{2}\,dp\,d\sigma. \tag{13}$$

The final budget equations, representing the local time change of the contribution from a limited region to the available potential and kinetic energy of the entire atmosphere, are formulated by taking the local time derivatives of (12) and (13). For convenience, the subscript j in (12) and (13) will be dropped. Using Poisson's equation, (12) may be rewritten as

$$A = \frac{c_p}{g} \int_{\sigma} \int_{p_2}^{p_1} T - \frac{p_r^\kappa \theta}{p_{00}^\kappa}\,dp\,d\sigma \tag{14}$$

and, assuming the area of the region remains constant, the local time derivative becomes

$$\frac{\partial A}{\partial t} = \frac{c_p}{g} \int_{\sigma} \int_{p_2}^{p_1} \left(\frac{\partial T}{\partial t} - \frac{p_r^\kappa}{p_{00}^\kappa} \frac{\partial \theta}{\partial t} - \frac{\theta}{p_{00}^\kappa} \frac{\partial p_r^\kappa}{\partial t} \right) dp\,d\sigma$$

$$+ \frac{c_p}{g} \int_{\sigma} \left[\frac{p_1^\kappa - p_{r_1}^\kappa}{p_1^\kappa} T_1 \frac{\partial p_1}{\partial t} - \frac{p_2^\kappa - p_{r_2}^\kappa}{p_2^\kappa} T_2 \frac{\partial p_2}{\partial t} \right] d\sigma. \tag{15}$$

The first integral of (15) contains implicitly the source (diabatic heating), sink (conversion to kinetic energy), and boundary flux terms required in the final budget equation of A. To express these terms explicitly it is necessary to rewrite the local time derivatives contained in this integral as the difference between the total time derivatives and the advection terms. Thus, the first integral of (15) becomes

$$\frac{c_p}{g}\int_\sigma\int_{p_2}^{p_1}\left\{\left(\frac{dT}{dt}-\underline{V}\cdot\nabla_p T-\omega\frac{\partial T}{\partial p}\right)-\frac{p_r^\kappa}{p_{00}^\kappa}\left(\frac{d\theta}{dt}-\underline{V}\cdot\nabla_p\theta-\omega\frac{\partial\theta}{\partial p}\right)\right.$$

$$\left.-\frac{\theta}{p_{00}^\kappa}\left(\frac{dp_r^\kappa}{dt}-\underline{V}\cdot\nabla_p p_r^\kappa-\omega\frac{\partial p_r^\kappa}{\partial p}\right)\right\}dp\,d\sigma \qquad (16)$$

In (16) it is assumed that the mean pressure on each θ surface is constant with time. Application of the first law of thermodynamics, the continuity equation, and Poisson's equation transforms (16) into

$$\frac{1}{g}\int_\sigma\int_{p_2}^{p_1}\omega\alpha\,dp\,d\sigma+\frac{1}{g}\int_\sigma\int_{p_2}^{p_1}\frac{p^\kappa-p_r^\kappa}{p^\kappa}Q\,dp\,d\sigma$$

$$-\frac{c_p}{g}\int_\sigma\int_{p_2}^{p_1}\frac{p^\kappa-p_r^\kappa}{p^\kappa}\nabla_p\cdot T\underline{V}\,dp\,d\sigma+\frac{c_p}{g}\int_\sigma\int_{p_2}^{p_1}\left(\frac{p_r^\kappa}{p_{00}^\kappa}\frac{\partial\omega\theta}{\partial p}-\frac{\partial\omega T}{\partial p}\right)dp\,d\sigma$$

$$-\frac{c_p}{g}\int_\sigma\int_{p_2}^{p_1}\frac{T}{p^\kappa}\left(\frac{dp_r^\kappa}{dt}-\underline{V}\cdot\nabla_p p_r^\kappa-\omega\frac{\partial p_r^\kappa}{\partial p}\right)dp\,d\sigma\,. \qquad (17)$$

Again using Poisson's equation and combining the fourth and fifth integrals of (17) yields

$$-\frac{c_p}{g}\int_\sigma\int_{p_2}^{p_1}\frac{\partial}{\partial p}\left(\frac{p^\kappa-p_r^\kappa}{p^\kappa}\right)\omega T\,dp\,d\sigma$$

$$-\frac{c_p}{g}\int_\sigma\int_{p_2}^{p_1}\frac{T}{p^\kappa}\left(\frac{dp_r^\kappa}{dt}-\underline{V}\cdot\nabla_p p_r^\kappa\right)dp\,d\sigma. \qquad (18)$$

Using (18) and the relation

$$-\left(\frac{p^\kappa-p_r^\kappa}{p^\kappa}\right)\nabla_p\cdot T\underline{V}+\frac{T}{p^\kappa}\underline{V}\cdot\nabla_p p_r^\kappa=-\nabla_p\cdot\frac{p_r^\kappa}{p^\kappa}T\underline{V}+\left\{p_r^\kappa\nabla_p\cdot\frac{T\underline{V}}{p^\kappa}+T\underline{V}\cdot\nabla_p\left(\frac{p_r^\kappa}{p^\kappa}\right)\right\}$$

$$=-\nabla_p\cdot\frac{p_r^\kappa}{p^\kappa}T\underline{V}+\nabla_p\cdot\left(\frac{p_r^\kappa}{p^\kappa}T\underline{V}\right)$$

$$=-\nabla_p\cdot\frac{p^\kappa-p_r^\kappa}{p^\kappa}T\underline{V}$$

permits (17) to be expressed as

$$\frac{1}{g}\int_{\sigma}\int_{p_2}^{p_1}\omega\,\alpha\,dp\,d\sigma+\frac{1}{g}\int_{\sigma}\int_{p_2}^{p_1}\frac{p^{\kappa}-p_r^{\kappa}}{p^{\kappa}}\,Q\,dp\,d\sigma$$

$$-\frac{c_p}{g}\int_{\sigma}\int_{p_2}^{p_1}\nabla_p\cdot\frac{p^{\kappa}-p_r^{\kappa}}{p^{\kappa}}\,T\underline{V}-\frac{c_p}{g}\int_{\sigma}\int_{p_2}^{p_1}\frac{\partial}{\partial p}\left(\frac{p^{\kappa}-p_r^{\kappa}}{p^{\kappa}}\right)T\omega\;\;dp\,d\sigma \tag{19}$$

$$-\frac{c_p}{g}\int_{\sigma}\int_{p_2}^{p_1}\frac{T}{p^{\kappa}}\frac{dp_r^{\kappa}}{dt}\,dp\,d\sigma.$$

By using Leibnitz's rule to evaluate the time derivative of the right-hand side of (10) and then applying the continuity equation in (x, y, θ) coordinates, it may be shown that $dp_r^{\kappa}/dt = 0$. This result and substitution of (19) into (15) yield the final budget equation for A

$$\frac{\partial A}{\partial t}=\overbrace{\frac{1}{g}\int_{\sigma}\int_{p_2}^{p_1}\frac{p^{\kappa}-p_r^{\kappa}}{p^{\kappa}}\,Q\,dp\,d\sigma}^{a}+\overbrace{\frac{1}{g}\int_{\sigma}\int_{p_2}^{p_1}\omega\,\alpha\,dp\,d\sigma}^{b}$$

$$\overbrace{-\frac{1}{g}\int_{\sigma}\int_{p_2}^{p_1}\nabla_p\cdot\left(c_p\frac{p^{\kappa}-p_r^{\kappa}}{p^{\kappa}}\,T\underline{V}\right)dp\,d\sigma}^{c}\overbrace{-\frac{1}{g}\int_{\sigma}\int_{p_2}^{p_1}\frac{\partial}{\partial p}\left(c_p\frac{p^{\kappa}-p_r^{\kappa}}{p^{\kappa}}\,T\omega\right)dp\,d\sigma}^{d} \tag{I}$$

$$\overbrace{+\frac{1}{g}\int_{\sigma}\left(c_p\frac{p_1^{\kappa}-p_{r_1}^{\kappa}}{p_1^{\kappa}}T_1\frac{\partial p_1}{\partial t}-c_p\frac{p_2^{\kappa}-p_{r_2}^{\kappa}}{p_2^{\kappa}}T_2\frac{\partial p_2}{\partial t}\right)d\sigma}^{e}.$$

The local time derivative of (13) is

$$\frac{\partial K}{\partial t}=\frac{1}{g}\int_{\sigma}\int_{p_2}^{p_1}\frac{\partial}{\partial t}\frac{\underline{V}\cdot\underline{V}}{2}\,dp\,d\sigma+\frac{1}{g}\int_{\sigma}\left(\frac{\underline{V}_1\cdot\underline{V}_1}{2}\frac{\partial p_1}{\partial t}-\frac{\underline{V}_2\cdot\underline{V}_2}{2}\frac{\partial p_2}{\partial t}\right)d\sigma. \tag{20}$$

As was the case in (15), the first integral of (20) contains the source (conversion from A), sink (frictional dissipation), and boundary flux terms required in the final budget equation for K. These terms can be introduced quite simply by taking the scalar product of $\underline{V}$ with the horizontal equation of motion and applying the continuity equation to yield

$$\frac{\partial}{\partial t}\left(\frac{\underline{V}\cdot\underline{V}}{2}\right) = -\underline{V}\cdot\nabla_p\phi + \underline{V}\cdot\underline{F} - \nabla_p\cdot\left(\frac{\underline{V}\cdot\underline{V}}{2}\right)\underline{V} - \frac{\partial}{\partial p}\left(\omega\,\frac{\underline{V}\cdot\underline{V}}{2}\right) \qquad (21)$$

Substituting (21) into (20) yields the final budget equation for K,

$$\frac{\partial K}{\partial t} = \overbrace{\frac{1}{g}\int_\sigma\int_{p_2}^{p_1}\underline{V}\cdot\underline{F}\,dp\,d\sigma}^{a} \overbrace{- \frac{1}{g}\int_\sigma\int_{p_2}^{p_1}\underline{V}\cdot\nabla_p\phi\,dp\,d\sigma}^{b}$$

$$\overbrace{- \frac{1}{g}\int_\sigma\int_{p_2}^{p_1}\nabla_p\cdot\left(\frac{\underline{V}\cdot\underline{V}}{2}\right)\underline{V}\,dp\,d\sigma}^{c} \overbrace{- \frac{1}{g}\int_\sigma\int_{p_2}^{p_1}\frac{\partial}{\partial p}\left(\omega\frac{\underline{V}\cdot\underline{V}}{2}\right)dp\,d\sigma}^{d} \qquad (II)$$

$$\overbrace{+ \frac{1}{g}\int_\sigma\left(\frac{\underline{V}_1\cdot\underline{V}_1}{2}\frac{\partial p_1}{\partial t} - \frac{\underline{V}_2\cdot\underline{V}_2}{2}\frac{\partial p_2}{\partial t}\right)d\sigma}^{e}.$$

Note that the boundary terms of equations I and II (Ic, Id, IIc, IId) integrate to zero when the entire atmosphere is considered. Also, note that although the development is performed in (x, y, p) coordinates, terms Ie and IIe still allow the possibility of variable vertical boundaries (e.g., surface and tropopause level). However, if constant pressure levels are assumed as the vertical boundaries, terms Ie and IIe will vanish.

3. DISCUSSION OF BUDGET TERMS

In this section the physical significance of each of the terms of equations I and II is considered. In the following discussion it is important to remember that each of the terms represents the contribution of a limited region to the corresponding global mean; however, for simplicity the word contribution will usually not be included. This convention will also be followed in later chapters.

Term Ia describes the generation of available potential energy by diabatic processes. Although this term appears quite different from Lorenz's (1955a) approximate generation expression, it is identical to that obtained in later work by Lorenz (1955b) and very similar to the expression obtained more recently by Dutton and Johnson (1967). The factor $E = \frac{p^\kappa - p_r^\kappa}{p^\kappa}$ has been called the efficiency factor by Dutton and Johnson.[1] This factor specifies where the addition (or subtraction) of heat is most efficient for generating available potential energy. The strongest positive generation will occur when centers of positive and negative efficiency coincide, respectively, with centers of diabatic heating and cooling.

Computations by Dutton and Johnson show that on the average the larger positive efficiencies are found at levels below 400 mb in equatorial latitudes ($p > p_r$), while the larger negative values occur slightly above the 400 mb level in polar latitudes ($p < p_r$). In the atmosphere the presence of zonally averaged heating (or cooling) fields which tend to be positively correlated with the efficiency factors results in a positive zonal generation of A. This is equivalent to viewing the atmosphere as an energy producing heat engine with heat being added (subtracted) at relatively higher (lower) temperatures and pressures.

Dutton and Johnson point out that the approximate expression obtained by Lorenz can underestimate the generation. For example, they computed the annual mean zonal generation as 5.6 watts m^{-2}, while the studies summarized by Oort (1964) based on Lorenz's approximate expression obtained 3.1 watts m^{-2}. Furthermore, Dutton and Johnson point out that the exact form yields positive generation in mid-latitude cyclogenetic areas east of Asia and North America, while the approximate form yields negative generation in these areas.

Term Ib represents the change in A due to vertical redistribution of mass, resulting in a change in the total potential energy with no effect on the reference potential energy. Term IIb represents the change of K produced by cross-isobaric flow. In nearly all of the published papers on atmospheric energetics term Ib is the basic expression from which the conversion of A to K has been estimated. However, term IIb, described by Kung (1966a, b) as the kinetic energy generation, also represents conversion.

---

[1] Actually, they defined the efficiency factor as $\frac{p^\kappa - p_r^\kappa}{p^\kappa} \frac{\partial z}{\partial \theta}$; however, this difference does not alter the physical interpretation of the expression.

From the expression

$$\underline{V} \cdot \nabla_p \phi = \nabla_p \cdot \phi \underline{V} - \phi \nabla_p \cdot \underline{V}$$

and the continuity equation, Ib and IIb are related by

$$\frac{1}{g} \int\int \omega \alpha \, dp \, d\sigma = \frac{1}{g} \int\int \underline{V} \cdot \nabla_p \phi \, dp \, d\sigma - \frac{1}{g} \int\int \nabla_p \cdot \phi \underline{V} \, dp \, d\sigma - \frac{1}{g} \int\int \frac{\partial}{\partial p} \omega \phi \, dp \, d\sigma. \tag{22}$$

The last two terms of (22) represent the work of the pressure gradient forces on the boundaries of the limited region. When these terms are zero (closed system), a change in available potential energy as given by Ib will be accompanied by an equal change in kinetic energy in the opposite sense as given by IIb, entirely within the same atmospheric region. This is the sense in which conversion is usually considered. In cases in which the pressure work terms of (22) are not zero (open system), as pointed out by Pfeffer (1957), neither Ib nor IIb can be thought of as representing conversion processes in the usual sense. This suggests that the usual concept of conversion is inappropriate when discussing any arbitrary limited atmospheric region. In order to retain the label "conversion" the authors suggest that the concept be generalized to include the possibility of production of one form of energy within a region at the expense of this same form of energy and/or another form of energy outside of the region. For example, the depletion of A within a region, as given by a negative value of Ib, might be accompanied by a corresponding increase of A or K outside of the region, rather than an increase of K within the region. With this broader concept of conversion in mind the author will refer to terms Ib and IIb as A-conversion and K-conversion, respectively.

Terms Ic, Id, IIc, IId, represent the horizontal and vertical transport of mass which can change the contribution that the region makes to the available potential or kinetic energy of the entire atmosphere. Of course, when the entire atmosphere is considered, the change of energy by the flux of mass is zero. However, in investigations over limited regions these terms may be quite significant since they determine to what extent the region is energetically independent of external processes.

Term IIa is a deceivingly simple expression for the complicated processes involved in the dissipation of kinetic energy. Although long recognized as a significant feature of motions in the boundary layer, Holopainen (1963) and Kung (1966a, b) have provided evidence that it can also be very significant in the free atmosphere.

As mentioned in Chapter 2 the remaining terms, Ie and IIe, reflect changes in the vertical boundaries of the limited regions and will be zero

when fixed pressure levels are used as boundaries. In pressure coordinates these terms represent the changes in A and K that occur when the total mass under consideration changes (i.e., the surface pressure changes while the pressure at the top remains constant).

4. DATA AND COMPUTATIONAL METHODS

Data for this study consisted of March, 1962, daily radiosonde data (temperature, horizontal winds, and height of pressure levels at 50 mb intervals for 00 and 12 Z) from the network of North American stations shown in figure 2. These data, spanning an area and time period of significant synoptic activity, provide spatial and temporal coverage for the budget area which contains 65 stations (outlined in figure 2 by the heavier line) and an additional 28 stations required for computations on the boundary of the budget area. The data for these stations were obtained from the MIT General Circulation Data Library[1] and the National Weather Records Center.

Although the original data extended as high as 7 mb, because of incomplete data coverage this study utilized only data obtained at or below the 250 mb level. Of course, missing data levels were still present below 250 mb at some of the stations. If missing data occurred between levels of existing data, the missing data were estimated by linear interpolation. If, however, the missing data did not occur between levels of existing data, the energy terms which utilized these data were not computed.

With the exception of the linear interpolation, the temperature and height data were used directly, while the wind data were filtered using a five-point "least squares" approximating polynomial to suppress the effects of random errors (Schmidt and Johnson, 1967).

After the data modifications were performed, the integrands of the terms of equations I, II and (22) were computed. Nearly all of the terms depend either directly or indirectly on computations involving the del operator. The general method used for the del operator estimation of the gradient and divergence terms is discussed in the Appendix. The vertical motion (ω) was estimated at each level by the kinematic method using the estimates of horizontal divergence ($\nabla_p \cdot \underline{V}$) and the assumption that at the ground $\omega = \frac{\partial p}{\partial t}$. The net diabatic heating (Q) was estimated by the

---

[1] Processed by Travelers Research Center, Inc., under National Science Foundation grants GP 820 and GP 3657.

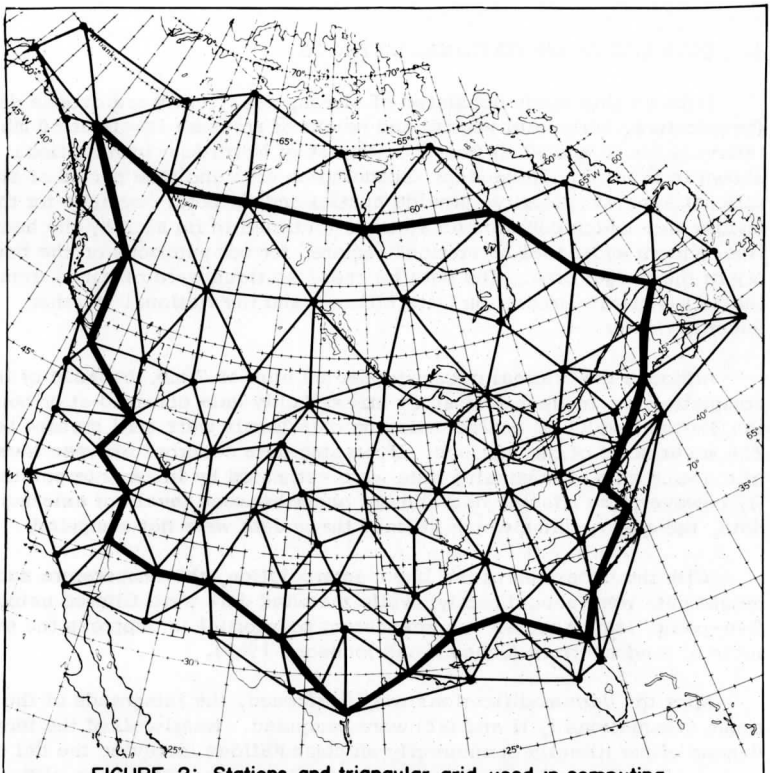

FIGURE 2: Stations and triangular grid used in computing energy budgets. Heavy line defines budget region.

thermodynamic method; i.e., by evaluating the right-hand side of the first law of thermodynamics in the form

$$Q = c_p \frac{\partial T}{\partial t} + c_p \underline{V} \cdot \nabla_p T + (c_p \frac{\partial T}{\partial p} - \alpha)\omega$$

where $\frac{\partial T}{\partial p}$ was estimated by finite difference and $\nabla_p T$ by the del operator method.

The only parameter required and not available in the original data is the global reference pressure for each isentropic surface. The global estimates used in this study were determined by averaging the monthly mean reference pressures computed by Dutton and Johnson from data along the 75° W meridian. Table 1 lists the mean annual reference pressures corresponding to particular potential temperature surfaces. Reference pressures for other potential temperature surfaces were obtained by linear interpolation between the values in this table. Note that the reference pressures used in this study specify a global reference state; i.e., the hypothetical redistribution process must occur simultaneously over the entire atmosphere. This may seem paradoxical in view of the fact that this study is concerned with energetics within a limited atmospheric region. However, since equation (12) represents the contribution of a limited region to the global available potential energy, it is seen that some provision must be made for the global state of the atmosphere. If one were to hypothetically define a local reference state in the same way as the global reference state, the realization of the local reference state (independent of the behavior of the rest of the atmosphere) could yield at least first order discontinuities in the pressure and height fields at the horizontal boundaries of the region. Thus, despite a disadvantage which will be discussed later it appears necessary to consider the entire atmosphere when defining the reference state used in this study.

It should be further pointed out that even when the global reference state is used, some question exists as to how this state should be defined, and indeed other global reference states have been proposed by Van Mieghem (1956) and Pfeffer, et al. (1966). However, as pointed out by Dutton and Johnson (1967), selection of an optimum reference state would be useful only if the resulting available potential energy would yield information on the future state that the atmosphere attempts to reach and why particular modes of circulation are chosen. Unfortunately the concepts of available potential energy does not yield this information, but instead is useful only in describing existing energy transformations. Hence, no advantage is gained by using some more complicated definition of the reference state in the equations developed in this paper.

Table 1

Potential Temperature and Corresponding Reference Pressures

θ, °K	p_r, mb
240	998.4
250	996.3
260	990.4
270	975.7
280	940.7
290	866.3
300	751.0
310	597.6
320	453.2
330	342.2
340	253.3
350	187.8
360	155.7
370	136.3

After the integrands of the terms of equations I and II were evaluated, the vertical integrals were estimated by the trapezoidal method using 50 mb increments and divided into three separate layers (Layer 1 = Surface to 750 mb; Layer 2 = 750 to 500 mb; Layer 3 = 500 to 250 mb). These integrals were then averaged over the entire budget area by multiplying the integral at each station by an area weight for that station, summing over all of the stations, and dividing by the total area. To compute the area weights a triangular grid with the data stations as vertices was constructed over the budget area. The area weight for each station was then computed as one-third of the sum of the area of the triangles for which the station was a vertex. The triangular grid is depicted in figure 2. When missing data occurred, the station at which the data was missing was not considered in the area average. Finally, the local time derivatives of A, K, T, and surface pressure for time t_0 were estimated by a centered 24 hour finite difference.

5. RESULTS

The data and computational procedures described in Chapter 4 were used to compute the average energy budget for each day of March, 1962. The daily values were then arithmetically averaged to produce monthly mean

estimates of each of the budget terms. When considering the monthly mean values it should be realized that the value of any energy term is dependent on several parameters and could be the result of a number of physical processes. Because of this lack of uniqueness the discussion will sometimes seem speculative, reflecting the authors' attempts to specify the particular process which most likely accounts for the computed energy value. In order to aid in the discussion of the results it seems desirable to first examine the vertical motion and diabatic heating.

The monthly mean vertical motion and diabatic heating profiles are depicted in figure 3. The vertical motion profile shows subsidence in the layer between the surface and 300 mb and rising motion in the 300-250 mb layer. The diabatic heating profile indicates warming in the surface to 850 mb and 300-250 mb layers and cooling in the 850-300 mb layer. The integrated value of -2.3 ly day^{-1} compares with -1.3 ly day^{-1} estimated by Davis (1963) for April for a zonal ring extending from 30 to 60°N and from the surface to 200 mb. The heating below 850 mb can be attributed to eddy conduction and direct solar heating (Hanson, et al., 1967) during this spring period, while the cooling above 850 mb is undoubtedly due to infrared radiation. The warming above 300 mb is quite likely also due to infrared processes, the 250 mb value obtained in this study agreeing well with the infrared warming estimates of between 0 and 1 deg day^{-1} at tropopause altitudes for the spring season by Kuhn, Cox and Stearns (1967).

The monthly mean energy budget estimates are summarized in Table 2, which contains values of the various energy parameters for each of the layers defined in Chapter 4. The kinetic energy K for the total layer (11.70×10^5 joules m^{-2}) is somewhat less than the global annual estimate of 15×10^5 joules m^{-2} made by Oort (1964) and Kung's (1966a) estimate of 18.96×10^5 joules m^{-2} for the same period and area of this study. Kung's value is probably larger because his study included the atmosphere to 50 mb.

The negative value obtained here for the contribution to the available potential energy is not comparable with earlier studies, all of which have yielded positive quantities. Previous estimates were greater than zero because they were determined from Lorenz's (1955a) approximate expression, which always yields a positive number. The sign of A within a local region is determined by the selection of the reference state. In a region containing air which is colder than the global mean one finds $p < p_r$ and $A < 0$. The concept of the available potential energy of a limited region can be examined further by rewriting (12) as

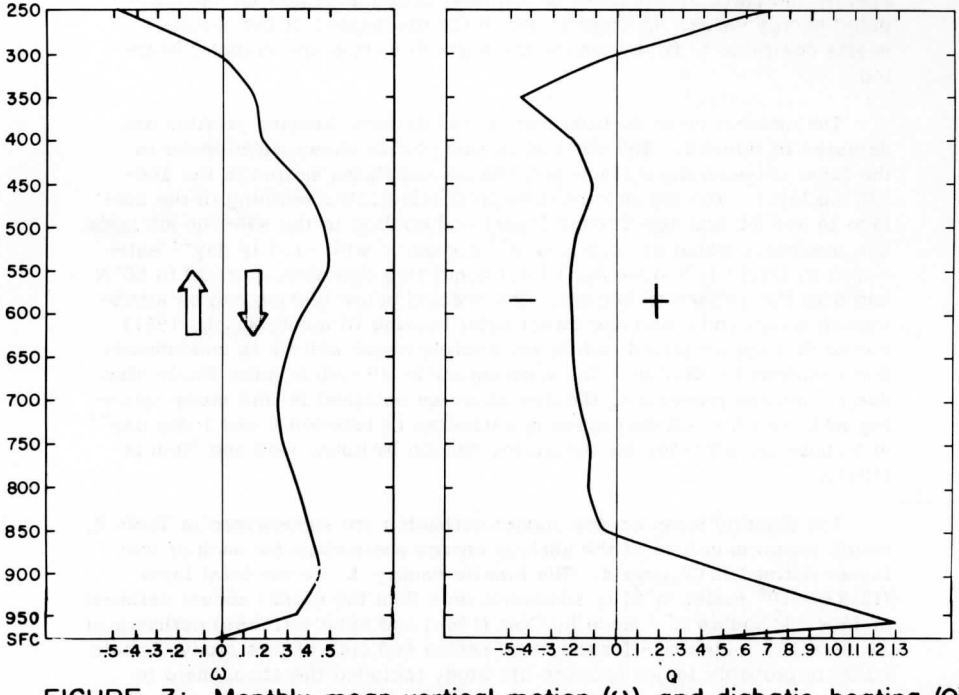

FIGURE 3: Monthly mean vertical motion (ω) and diabatic heating (Q) profiles for North America, March, 1962.

UNITS: $\omega = 10^{-4}$ mb sec^{-1}; Q = deg day^{-1}

Table 2

Monthly mean energy budget by layers for North America, March, 1962. 1, 2, 3, T indicate layers as defined in Chapter 4.

Units: A, K = 10^5 joules m^{-2}; energy transformations and fluxes = watts m^{-2}.

	1	2	3	4
A	-1.03×10^2	-4.95×10^2	-9.27×10^2	-15.25×10^2
K	.95	2.83	7.92	11.70
$\frac{\partial A}{\partial t}$	3.53	5.58	7.97	17.08
G	- 0.06	0.68	- 0.77	- 0.15
C_A	6.55	6.23	-23.53	-10.75
HF_A	8.88	8.88	- 0.71	17.05
VF_A	-14.59	-15.37	43.40	13.44
X	- 0.33			- 0.33
ε_A	3.08	5.16	-10.42	- 2.18
$\frac{\partial K}{\partial t}$	0.00	- 0.05	- 0.14	- 0.19
D	- 0.64	- 0.14	- 0.30	- 1.08
C_K	0.69	- 0.09	- 0.32	0.28
HF_K	0.01	- 0.25	0.59	0.35
VF_K	- 0.06	0.43	- 0.11	0.26
PW	8.40	8.89	-27.14	- 9.85
ε_C	- 1.16	- 2.75	3.29	- 0.62
$\overline{\omega' \alpha'}$	0.08	- 4.37	-24.46	-28.75
$\bar{\omega}\,\bar{\alpha}$	6.47	10.60	0.93	18.00

$$A = \frac{c_p}{g} \int_{\sigma} \int_{p_2}^{p_1} \frac{p^\kappa - \bar{\bar{p}}^\kappa}{p^\kappa} T \, dp \, d\sigma + \frac{c_p}{g} \int_{\sigma} \int_{p_2}^{p_1} \frac{\bar{\bar{p}}^\kappa - p_r^\kappa}{p^\kappa} T \, dp \, d\sigma . \quad (24)$$

The first term on the right side of (24) is the local available potential energy that would be present if the local system were not allowed to interchange mass with its environment, leaving the second term to represent the available potential energy existing due to the departure of the characteristics of the local region from the remaining atmosphere. As is the case when σ is the entire globe, the first term is always positive. Hence, negative A values occur when the interaction term is negative and its absolute value is greater than the first term. The relatively cold air in this region leads to values of $\bar{\bar{p}}$ which are considerably less than p_r, resulting in a large negative value for A_j.

Within the set of estimates involving the time rate of change of the energy parameters, perhaps the most surprising feature is the very small size of the generation G for the total layer (-0.15 watts m^{-2}) compared to the other terms in the A budget. However, this value is not greatly different from the -0.8 watts m^{-2} obtained by Oort (1964) and the 0.8 watts m^{-2} obtained by Dutton and Johnson for the eddy generation. This suggests that in this study the generation is dominated by eddy heating processes and that the role of zonal generation is limited, probably because of the absence of data from tropical and polar latitudes.

The generation is also relatively small in each of the three layers. A better insight into the physical processes affecting G can be gained by writing the generation expression as

$$G = \frac{1}{g} \int_{p_2}^{p_1} \bar{E} \, \bar{Q} \, dp + \frac{1}{g} \int_{p_2}^{p_1} \overline{E'Q'} \, dp. \quad (25)$$

The first term represents the effect of the mean heating field. Lorenz (1955b) notes that the second term which describes the influence of differential heating is similar to the approximate expression of the generation.

In layer 1 both the mean efficiency factors and mean diabatic heating have predominantly the same sign within the layer and, therefore, would be expected to produce positive generation. However, since the observed value is near zero (-0.06 watts m^{-2}), it appears that the effect of mean heating is offset by a horizontal distribution (described by the second term of equation 25) which produces heating of relatively cold air and cooling of relatively warm air. In the middle layer the positive generation (0.68 watts m^{-2}) corresponds to the diabatic cooling and negative efficiency

factors normally found there. In addition, while the release of latent heat is not dominant in the monthly mean, it does tend to occur in regions of positive efficiency and would, therefore, also contribute to this positive result. In the upper layer the correlation of mean cooling and negative efficiency factors would yield a positive generation. Therefore, the observed negative value (-0.77 watts m^{-2}) would indicate that again there is heating of relatively cold air and cooling of relatively warm air. Since the spatial and temporal variations of the efficiency factors and diabatic heating are so complex, it is impossible to identify all of the processes contributing to the generation estimates.

The A-conversion (C_A) for the total layer (-10.75 watts m^{-2}) compares with Dutton and Johnson's global annual value (-6.4 watts m^{-2}), which was partially based on Kung's (1966b) global annual estimate of frictional dissipation. Both results are considerably larger than Oort's estimate of -2.3 watts m^{-2}. The studies from which Oort derived his value may have underestimated C_A because they employed the quasi-geostrophic vorticity equation or the adiabatic method to determine the vertical motion. These methods tend to smooth out the smaller synoptic scales. In contrast the authors feel that the vertical motion estimates in this study retain much of the influence of the entire range of synoptic scales. The major problem encountered in the method used here, however, is that the vertical motion, and terms utilizing the vertical motion, are sometimes overestimated in the upper levels. If one assumes that ω is frequently overestimated in the third layer, the total A conversion may be less than computed here. The details of this problem are discussed in Chapter 6.

The role of C_A in the energetics of a limited region is perhaps best seen by comparing it with the K-conversion (C_K) and pressure work (PW) estimates, which are linked through equation (22). In these results PW and C_A are of the same size, with C_K much smaller. This means that although C_A indicates a reduction of A in layer 3 and increases in layers 1 and 2, it is not accompanied by corresponding increases or decreases of K within any of the layers. Therefore, because of the considerable interaction with the environment, C_A apparently does not represent energy conversion in the conventional sense, at least within the area and time period studied here.

In an effort to provide an alternate representation of the conversion process many authors have used $\overline{\omega'\alpha'}$ rather than C_A, e.g., White and Saltzman (1956), Winston and Krueger (1961), Oort (1964), and Danard (1966). The term $\overline{\omega'\alpha'}$ has been described as the conversion of available potential to kinetic energy by vertical overturnings within atmospheric waves. Under this formulation a decrease of available potential energy occurs when relatively warm air rises and cold air sinks.

C_A, $\overline{\omega'\alpha'}$, and $\bar{\omega}\,\bar{\alpha}$ are related according to

$$C_A = \frac{1}{g}\int_{p_2}^{p_1} \overline{\omega'\alpha'}\, dp + \frac{1}{g}\int_{p_2}^{p_1} \bar{\omega}\,\bar{\alpha}\, dp. \qquad (26)$$

When the entire atmosphere is considered, the last term is zero and $C_A = \frac{1}{g}\int_0^{p_0} \overline{\omega'\alpha'}\, dp$; however, this relation is not valid in limited regions. One can interpret $\overline{\omega'\alpha'}$ as that portion of C_A which can be attributed to scales of vertical motion completely contained in the region, while $\bar{\omega}\,\bar{\alpha}$ is associated with scales which are only partially sampled in the region.

The values of $\bar{\omega}\,\bar{\alpha}$ agree well with the mean vertical motion profile (Figure 3). The subsidence in layers 1 and 2 produces positive values (6.47 and 10.60 watts m^{-2}), while the reversal in the mean vertical motion profile in layer 3 results in a near zero value (0.93 watts m^{-2}). On the other hand $\overline{\omega'\alpha'}$ is very small in layer 1, a somewhat surprising result in view of the fact that to a large extent it reflects the influence of synoptic scale phenomena. A small value in this layer can be partially accounted for by the presumably small values of ω'. In addition, however, the negative $\overline{\omega'\alpha'}$ normally associated with developing synoptic scale motions is apparently balanced by a near equal positive value resulting from rising cold air and sinking warm air as might occur in an occluded storm. In layers 2 and 3, the horizontal variations in vertical motion associated with developing synoptic processes are evidently large enough to yield large values of $\overline{\omega'\alpha'}$. The vertical distribution obtained here agrees qualitatively with the distribution obtained by Eddy (1965) during a three day storm period (January 21-23, 1959) for the portion of $\overline{\omega'\alpha'}$ associated with 1600 and 3500 n. mi. scales. In addition, the relative size of C_A and $\overline{\omega'\alpha'}$ for the total layer ($\overline{\omega'\alpha'} \simeq 2\frac{1}{2}\, C_A$) agrees with the ratio of Danard's (1966) one day estimate of $\overline{\omega'\alpha'}$ over the United States of about -19.0 watts m^{-2} versus Dutton and Johnson's global estimate of C_A, -6.40 watts m^{-2}. A significant feature of $\overline{\omega'\alpha'}$ is that it seems to bear no direct relation to C_K. It would appear, therefore, that over the period and limited region of this study $\overline{\omega'\alpha'}$, like C_A, does not represent the conventional conversion process.

Considering again the values contained in the energy budgets, it is interesting to note that in spite of the size of the region and the length of the time period the horizontal and vertical fluxes are still very significant. The flux of A is accomplished by a net transport which changes the contribution that a local region makes to the available potential energy of the entire atmosphere. In particular, a positive flux can occur with either an inflow of air warmer than the global mean or an outflow of air

colder than the global mean. The dominance of horizontal flux of A (HF_A) in layers 1 and 2 indicates that this term may be largely influenced by major synoptic features. Low pressure centers which tend to form or deepen east of the Rocky Mountains and inject warm air into the budget region from the Gulf area probably provide an important source of positive A flux. In addition increases of A may be noted when cold Canadian highs exit the budget region. The net effect of this process would depend on whether the highs are replaced by warmer air from perhaps the Pacific or Gulf area or colder Arctic air. The vertical flux of A (VF_A), agrees qualitatively with the mean vertical motions in Figure 3. The remaining term (X) indicates that the mean surface pressure, and hence the mass within the region decreased during March, 1962.

The net change in A during the month was 17.08 watts m^{-2}, which is of course considerably different from the zero value one would expect for a global annual mean. However, this value is comparable with the estimate of about 10 watts m^{-2} obtained by Danard during a one day period (January 21, 1959) of cyclonic activity over the United States. The local change of K (-0.19 watts m^{-2}) is almost identical to Kung's (1966a) estimate of -0.20 watts m^{-2}.

In the kinetic energy budget the dominant term for the total layer is the frictional dissipation (D), -1.08 watts m^{-2}. This estimate is less than the global, annual estimate of -2.3 watts m^{-2} given by Oort, and considerably less than Kung's (1966b) annual estimate of -6.40 watts m^{-2}. In addition it is also smaller than the value of -4.87 watts m^{-2} given by Kung (1966a) for the month and area of this study. However, it should be noted that Kung's March, 1962, result includes a dissipation of about -1.0 watts m^{-2} in the 250-50 mb layer, a layer which was not used in this study. In a recent paper Kung (1967) has found that the inclusion of 12 Z data with the 00 Z data used in his earlier studies resulted in a 36% reduction of his original annual dissipation estimate. Applying this reduction to the surface to 250 mb value of -3.87 watts m^{-2} for March, 1962, yields a revised figure of -2.46 watts m^{-2}. Therefore, depending on which estimate is accepted the result obtained in this study is smaller by a factor of 2 or 3. It is interesting to note that Kung (1966a) and Julian and Labitzke (1965) obtained values of -0.28 watts m^{-2} and -0.30 watts m^{-2} for HF_K and VF_K, respectively. Although of opposite sign to those obtained here, their results indicate that the small values obtained in this study are reasonable. Quite likely any error in D results primarily from underestimates of the production of K by cross-isobaric flow (C_K). The possible causes of the discrepancy between Kung's value of D and that obtained here are considered in Chapter 6.

Finally, an indication of the reliability of the budget estimates can be obtained by considering the discrepancies between the calculated local

changes and the sum of the processes which produce the changes. These discrepancies, referred to as ε_A (available potential energy error) and ε_C (conversion error), are

$$\varepsilon_A = \frac{\partial A}{\partial t} - (G + C_A + HF_A + VF_A + X) \tag{27}$$

and

$$\varepsilon_C = (C_A + C_K) - PW. \tag{28}$$

Table 2 shows that ε_A and ε_C are not large when compared with the more important budget terms. Since the signs of ε_A and ε_C in layers 1 and 2 are opposite to the signs in layer 3, the errors tend to cancel, leaving relatively small values for the total layer ($\varepsilon_A = -2.18$, $\varepsilon_C = -0.62$).

6. ERRORS

Throughout the discussion of the results, comparisons were made with other studies. While some studies compared well, others did not. The differences are either real, temporal or spatial variations or are discrepancies due to errors. The possible errors in this study which may have contributed to these differences are more fully examined in this chapter.

Any investigation must contend with four sources of error—inadequate defining equations, erroneous data, inadequate data sample, and approximate computing techniques. The equations used here contain the assumption of hydrostatic balance. Since this assumption is quite reasonable over an area as large as is used here, the equations would not be expected to provide a significant source of error. The presence of errors in the original observations or in their subsequent transcription is a problem which can never be completely resolved. However, the checking procedures used by the agencies which processed the data and the restriction of this study to levels below 250 mb would tend to reduce this difficulty. Although the data sample used here provides as complete a coverage in space and time as is currently available, it is quite likely that the sample is inadequate to determine unbiased estimates of the various parameters. Thus, given this limited data sample, it seems reasonable to assume that the computing techniques provide the primary source of error.

Inherent in the computation of nearly all of the budget terms is the procedure used for determining the partial derivatives. Recall from the appendix that the technique employed here involves the expansion of a parameter in terms of a truncated Taylor series containing one second-order and two first-order partial derivatives. The inclusion of one second-order derivative allows the consideration of some nonlinear effects;

however, in general there may have been other non-linearities which produced significant bias errors.

Nonlinearities are probably most prominent in the horizontal wind field, suggesting that bias errors exist in the horizontal divergence, flux, and pressure work estimates. The impact of biased divergence values on vertical motion values obtained by the kinematic method is quite significant (Schmidt and Johnson, 1967). In this method the vertical motion at a particular level is determined from the sum of the divergence estimates from all of the lower levels, resulting in an accumulation of bias errors which sometimes becomes quite large. The authors have found that the vertical motion estimates up to 500 mb are of reasonable magnitude (i.e., between $\pm$ .008 mb sec^{-1}), but above this level are sometimes as large as $\pm$ .02 mb sec^{-1}, which seems quite unreasonable. The main effect of such errors should appear in estimates of A-conversion, vertical flux, and vertical pressure work. Although the horizontal flux and horizontal pressure work are not affected by such cumulative bias errors, they, nevertheless, can also contain appreciable errors. In each case the wind field is multiplied by a scalar quantity, either $c_p ET$, $\underline{V} \cdot \underline{V}/2$, or ϕ which could result in a vector field which is more non-linear than the basic wind field. Since $c_p ET$ and ϕ are generally at least two orders of magnitude larger than $\underline{V} \cdot \underline{V}/2$, this effect would be expected to produce larger errors in the horizontal flux of A and horizontal pressure work than in the horizontal flux of K. The proposed relations between errors and horizontal winds seem to be verified by noting that the monthly mean ε_A and ε_C are maximum in layer 3, where nonlinearities in the wind field are probably most prominent.

It was pointed out in Chapter 5 that another discrepancy occurs in the estimates of K-conversion, which in turn results in errors in the dissipation values. The authors feel that this may be partially caused by filtering the winds, which, while leading to improved divergence estimates, may have smoothed out some of the ageostrophic components of the wind. For example, for a 250 mb thick layer a three degree error in the direction of a 10 m sec^{-1} wind would give an error in C_K of 1.25 watts m^{-2}, which is twice as large as the monthly mean value obtained in this study for layer 1. It is interesting to note that Kung (1966a, b), who obtained cross-isobaric flow by a similar technique did not filter the winds, obtained a larger and probably more realistic estimate of C_K over the same period and area.

7. SUMMARY

In this study the basic definition of internal, gravitational potential, and kinetic energy and Lorenz's (1955a) definition of available potential energy were used to derive a set of energy equations which can be applied to any limited region of the atmosphere. These equations were then employed to obtain the monthly mean energy budget of North America for March, 1962. In developing the necessary equations and applying them to real data, the following significant points and difficulties stand out:

1. The energy equations for a limited region can be written in a form containing, in addition to the customary generation, conversion and dissipation terms, expressions for the horizontal and vertical fluxes through the boundaries of the region. The generation term is identical to that of Lorenz (1955b) and very similar to that of Dutton and Johnson (1967).

2. It appears necessary to use a global reference state to define the energetics of a limited region. This requires that the local available potential energy be defined as the contribution the region makes to the global available potential energy. It was also noted that hypothetically the region could not attain its own minimum state, independent of the rest of the atmosphere, without inducing at least first order discontinuities in the height field. Since the region of the atmosphere for the period studied here was in general colder than the global mean, the use of a global reference state leads to monthly mean values of A which are negative.

3. The energy budget estimates obtained in this study differ from the global, annual budget as given by Dutton and Johnson (see Figure 4). The generation value obtained here is much smaller than the global estimate, probably because the zonal effects are greatly reduced in the limited region. The boundary fluxes and pressure work terms, which are zero in the global budget, apparently play an important role in the energetics of limited regions. The size of these terms demonstrates the significant interaction between the limited region and its environment. The large values of A-conversion (C_A) and $\overline{\omega'\alpha'}$ compared with K-conversion (C_K) indicate that neither C_A nor $\overline{\omega'\alpha'}$, which have been used as conversion terms in other studies, represent direct production of kinetic energy for the area and time of this study.

4. The relatively small error terms ε_A and ε_C (see Table 3) show that the equations are nearly balanced.

5. Given the limited data sample, it appears that of the various sources of error present, the most important is probably the technique used to determine partial derivatives, which primarily affects HF_A, VF_A, PW, and C_A. In addition it seems possible that filtering the winds may have caused underestimates of C_K, which in turn have led to underestimates of the dissipation.

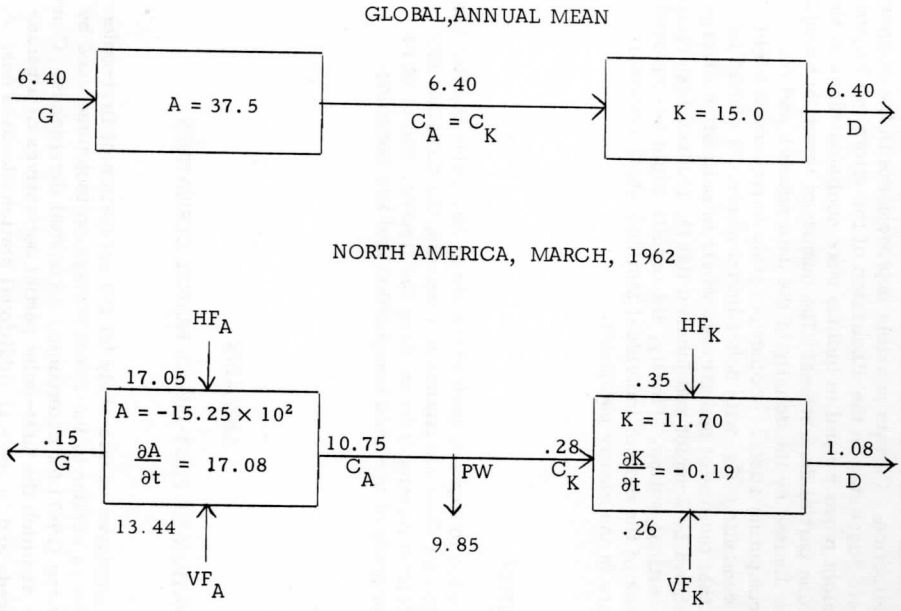

Figure 4. Flow diagrams of energy budgets for the global, annual mean and North America, March, 1962.

Units: A, K = 10^5 joules m^{-2}; energy transformations and fluxes = watts m^{-2}

Future studies of the energetics of limited regions will require several improvements over the procedures used here. Obviously one of the most important is the need for improved vertical motion estimates. Of equal benefit of course would be the direct determination of diabatic heating and frictional dissipation. Certain possible improvements in the computing techniques were suggested in the discussion of the errors in Chapter 6. For example, it might prove fruitful to include more nonlinear terms in the scheme for obtaining partial derivatives. The number of terms that could be added would be limited by the density of the data network and the potentially high computing costs. Another possible improvement might be obtained from computing C_K with non-filtered winds. It should be noted, however, that the use of non-filtered winds in estimating divergence would, as shown by Schmidt and Johnson (1967), produce less reliable estimates of the vertical motion. Finally, the results might be improved by a detailed check of the data of individual stations which obviously contribute to errors in the energy parameter.

ACKNOWLEDGMENTS

The authors wish to express their gratitude to Mr. Peter Guetter and Mr. Robert Chalice for their assistance in preparing the computer programs, to Mr. Stephen Newcomb for drafting the figures, and to Miss Sue Piotrowski for much of the hand computation and key punching.

APPENDIX

ESTIMATION OF FIRST-ORDER PARTIAL DERIVATIVES

The method employed in this study for the estimation of first-order partial derivatives is similar to the linear regression technique used by Schmidt and Johnson (1967) for determining horizontal divergence. Consider station A, at which the first-order partial derivatives of a parameter ψ are desired, and n $(n > 3)$ additional stations located near A. The difference between ψ at the j^{th} additional station and A can be approximated by the truncated Taylor series

$$\Delta\psi_{jA} \simeq \left.\frac{\partial\psi}{\partial x}\right|_A \Delta x_{jA} + \left.\frac{\partial\psi}{\partial y}\right|_A \Delta y_{jA} + \frac{1}{2}\frac{\partial^2\psi}{\partial x\partial y}\Delta x_{jA}\Delta y_{jA} \qquad (1*)$$

Although only $\frac{\partial\psi}{\partial x}$ and $\frac{\partial\psi}{\partial y}$ are desired, the inclusion of the second-order term allows some consideration of the nonlinear behavior of the ψ field.

The set of n equations of the form (1*) can be written as the matrix equation

$$\Delta\psi = \chi B \qquad (2^*)$$

where

$$\chi = \begin{bmatrix} \Delta x_{1A} & \Delta y_{1A} & \frac{1}{2}\Delta x_{1A}\Delta y_{1A} \\ \Delta x_{2A} & \Delta y_{2A} & \frac{1}{2}\Delta x_{2A}\Delta y_{2A} \\ \vdots & \vdots & \vdots \\ \Delta x_{nA} & \Delta y_{nA} & \frac{1}{2}\Delta x_{nA}\Delta y_{nA} \end{bmatrix}$$

$$B = \begin{bmatrix} \frac{\partial\psi}{\partial x}\Big|_A \\ \frac{\partial\psi}{\partial y}\Big|_A \\ \frac{\partial^2\psi}{\partial x\partial y}\Big|_A \end{bmatrix} \qquad \Delta\psi = \begin{bmatrix} \Delta\psi_{1A} \\ \Delta\psi_{2A} \\ \vdots \\ \Delta\psi_{nA} \end{bmatrix}$$

Equation (2*) specifies a set of n equations in 3 unknowns, with χ and $\Delta\psi$ representing measured parameters and B the unknowns. Since n exceeds the number of unknowns and since (2*) is linear, the method of linear regression may be used to approximate B. To do so, let (2*) be approximated by

$$\Delta\hat{\psi} = \chi\hat{B} \qquad (3^*)$$

where $\Delta\hat{\psi}$ and $\hat{B}$ are estimates of the true values $\Delta\psi$ and B. The best linear estimate of $\Delta\hat{\psi}$ is obtained by minimizing the difference between $\Delta\psi$ and $\Delta\hat{\psi}$, i.e., by requiring that $(\Delta\psi - \Delta\hat{\psi})$ be orthogonal to χ, which defines the space containing $\Delta\hat{\psi}$. Thus,

$$\chi^T(\Delta\psi - \Delta\hat{\psi}) = 0. \qquad (4^*)$$

Employing (3*) and (4*), one obtains

$$\hat{B} = [X^T X]^{-1} X^T \Delta\psi \qquad (5^*)$$

which contains the desired estimates of the partial derivatives.

In this study, the n additional stations were chosen such that they were the closest available to A and such that A was located near the center of the area defined by the n stations. In all cases, n was initially specified at between five and eight; however, missing data at some stations sometimes reduced the number. If the final n was less than four, the computation was not performed.

BIBLIOGRAPHY

Clapp, P. F. (1961): Normal heat sources and sinks in the lower troposphere in winter. Monthly Weather Review, 89. No. 5, 147-162.

Climatological Data. National Survey, March, 1962: ESSA, U. S. Department of Commerce.

Corcoran, J. L., and L. H. Horn (1965): The role of synoptic scale variations of infrared radiation in the generation of available potential energy. Journal of Geophysical Research, 70, No. 18, 4521-4528.

Danard, M. B. (1966): On the contribution of released latent heat to changes in available potential energy. Journal of Applied Meteorology, 5, No. 1, 81-84.

Davis, P. A. (1963): An analysis of the atmospheric heat budget. Journal of Atmospheric Sciences, 20, No. 1, 5-22.

Dutton, J. A., and D. R. Johnson (1967): The theory of available potential energy and a variational approach to atmospheric energetics. Advances in Geophysics, Vol. 12, Academic Press, New York, 333-436.

Hanson, K. J., T. H. Vonder Haar, and V. E. Suomi (1967): Reflection of sunlight to space and absorption by the earth and atmosphere over the United States during Spring 1962. Monthly Weather Review, 95, No. 6, 354-362.

Holopainen, E. O. (1963): On the dissipation of kinetic energy in the atmosphere. Tellus, 15, No. 1, 26-32.

Holopainen, E. O. (1964): Investigation of friction and diabatic processes in the atmosphere. Papers No. 101, Department of Meteorology, University of Helsinki.

Jensen, C. E. (1961): Energy transformation and vertical flux processes over the Northern Hemisphere. Journal of Geophysical Research, 66, No. 4, 1145-1156.

Johnson, D. R. (1967): The role of terrestrial radiation in the generation of zonal and eddy available potential energy. Tellus, 19, No. 4, pp. 517-539.

Julian, P. R., and K. B. Labitzke (1965): A study of atmospheric energetics during the January-February 1963 stratospheric warming. Journal of the Atmospheric Sciences, 22, No. 6, 597-610.

Krueger, A. F., J. S. Winston, and D. Haines (1965): Computations of atmospheric energy and its transformation for the Northern Hemisphere for a recent five-year period. Monthly Weather Review, 93, No. 4, 227-238.

Kuhn, P. M., S. K. Cox, and L. Stearns (1967): The observed radiation budget of the atmosphere. Unpublished manuscript.

Kung, E. C. (1966a): Kinetic energy generation and dissipation in the large-scale atmospheric circulation. Monthly Weather Review, 94, No. 2, 67-82.

Kung, E. C. (1966b): Large-scale balance of kinetic energy in the atmosphere. Monthly Weather Review, 94, No. 11, 627-640.

Kung, E. C. (1967): Diurnal and long-term variations of the kinetic energy generation and dissipation for a five-year period. Monthly Weather Review, 95, No. 9, pp. 593-606.

Lorenz, E. N. (1955a): Available potential energy and the maintenance of the general circulation. Tellus, 7, No. 2, 157-167.

Lorenz, E. N. (1955b): Generation of available potential energy and the intensity of the general circulation. Large Scale Synoptic Processes, University of California (Los Angeles), Department of Meteorology, Final Report, J. Bjerknes, Project Director.

Margules, M. (1903): Uber die energie der sturme. Jahrb. Zentralanst Meteorol., 1-26. (Translation by C. Abbe (1910) in Smithsonian Institute Miscellaneous Collection, 51, 553-595).

Muench, H. S. (1965): On the dynamics of the wintertime stratospheric circulation. Journal of Atmospheric Sciences, 22, No. 4, 349-360.

Oort, A. H. (1964): On estimates of the atmospheric energy cycle. Monthly Weather Review, 92, No. 11, 483-493.

Pfeffer, R. L. (1957): On the physical significance of energy transformation functions. Studies of the Atmospheric General Circulation II, Massachusetts Institute of Technology, Department of Meteorology, Final Report, General Circulation Project, V. P. Starr, Director.

Pfeffer, R. L., D. Mardon, P. Sterbenz, and W. Fowlis (1966): A new concept of available potential energy. Report No. 66-1, Florida State University, Department of Meteorology.

Posey, J. W. (1962): The weather and circulation of March, 1962—a month with an unusually strong high-latitude block. Monthly Weather Review, 90, No. 6, 252-258.

Saltzman, B. and A. Fleisher (1960a): Spectrum of kinetic energy transfer due to large-scale horizontal Reynolds stresses. Tellus, 12, No. 1, 110-111.

Saltzman, B. and A. Fleisher (1960b): The modes of release of available potential energy in the atmosphere. Journal of Geophysical Research, 65, No. 4, 1215-1222.

Saltzman, B. and. A. Fleisher (1961): Further statistics on the modes of release of available potential energy. Journal of Geophysical Research, 66, No. 7, 2271-2273.

Saltzman, B. and A. Fleisher (1962): Spectral statistics of the wind at 500 mb. Journal of Atmospheric Sciences, 19, No. 2, 195-204.

Schmidt, P. J. and D. R. Johnson, (1967): Vertical profiles of polynomial filtered winds, divergence and vertical motion. Paper presented at the American Meteorological Society Conference on Numerical Prediction, October, 1967. Abstract, Bulletin of the American Meteorological Society, Vol. 48, No. 8, p. 583.

Suomi, V. E., and W. C. Shen (1963): Horizontal variation of infrared cooling and the generation of eddy available potential energy. Journal of Atmospheric Sciences, 20, No. 1, 62-65.

Van Mieghem, J. (1956): The energy available in the atmosphere for conversion into kinetic energy. Beitrage zur Physik der Atmosphare, 29, 129-142.

White, R. M. and B. Saltzman (1956): On conversion between potential and kinetic energy in the atmosphere. Tellus, 8, No. 3, 357-363.

Wiin-Nielsen, A. (1959): A study of energy conversion and meridional circulation for large scale motion in the atmosphere. Monthly Weather Review, 87, No. 9, 319-332.

Wiin-Nielsen, A., and J. A. Brown (1962): On diagnostic computations of atmospheric heat sources and sinks and the generation of available potential energy. Proceedings of the International Symposium on Numerical Weather Prediction, 1960, Tokyo, Meteorological Society of Japan, 593-613.

Wiin-Nielsen, A., J. A. Brown, and M. Drake (1963): On atmospheric conversions between the zonal flow and the eddies. Tellus, 15, No. 3, 261-279.

Winston, J. S. and A. F. Krueger (1961): Some aspects of a cycle of available potential energy. Monthly Weather Review, 89, No. 9, 307-318.

Scanner's note:

This page is blank.

THE GENERATION OF AVAILABLE POTENTIAL ENERGY IN HURRICANE HILDA (1964)

Richard A. Anthes and Donald R. Johnson

ABSTRACT

The energetics of Hurricane Hilda (1964) are studied through the theory of available potential energy applied to a limited fixed region surrounding the storm. The generation of available potential energy is shown to be closely dependent on differential heating within the baroclinic structure of the hurricane, occurring primarily in the middle and upper troposphere of the core of the storm. The diabatic heating components (condensation, emission of long wave radiation, direct absorption of solar radiation, and sensible heating) are modeled and the contribution to the total generation from each component computed. The results from the latent heating model based on Kuo's work portray the dependence of the deep cumulus convection on the sea surface temperature. The best estimate of the total generation of available potential energy within the hurricane scale is 10.3×10^{12} watts, of which 77 percent is generated by latent heating, 17 percent by infrared cooling, and 6 percent by direct solar absorption. The total generation compares favorably with estimates of kinetic energy production in mature hurricanes. Energy considerations in the steady state condition of the hurricane system are discussed within the framework of the available potential energy theory.

I. INTRODUCTION

The hurricane is comprised of many scales of atmospheric motion. The large scale circulation is a warm core barocolinc vortex with characteristic wind speeds of 50 meters per second in the vicinity of the eye wall. This horizontal motion comprises nearly all the kinetic energy in the storm. Superimposed on this horizontal motion is a slow quasi-steady thermally driven direct circulation characterized by inflow in the low level,

relatively intense ascending motion near the core, outflow at high levels and slow sinking motion around the fringe of the storm. The radial extent of this circulation is typically on the order of 1000 km.

A second important scale of motion in the hurricane system is the convection near the hurricane's core, as emphasized in the "hot tower" concept by Riehl and Malkus (1961). Although the dimension of this scale is two orders of magnitude smaller than that of the hurricane circulation itself, the vertical motion in the convection provides the vital link between the source of thermal energy at the convective scale and the production of kinetic energy for the large scale.

Recently, Charney and Eliassen (1964), Ooyama (1964), Kuo (1965), and Ogura (1964) have attempted to separate the cumulus scale motion from the macroscale motion while retaining the cumulative effect of the latent heat release by the cumulus convection. In this way the large scale motion is thermally driven by the net heating effect of the many small convective elements.

For the large scale thermally direct circulation to develop, the cumulus convection must be organized to produce horizontal temperature gradients and baroclinicity associated with the hurricane's warm core. The importance of the warm core in the production of kinetic energy on the large scale was recognized by Palmén (1948) and recently reemphasized by Yanai (1964). Yanai shows that baroclinicity is a necessary requirement for the maintenance of kinetic energy in the tropical cyclone since the solenoid field associated with the warm core vortex is in the kinetic energy producing sense, tending to accelerate the direct circulation.

Within the realm of atmospheric energetics, the rising motion in the warm core and subsidence near the fringe of the hurricane implies a conversion from potential to kinetic energy in this region. Both of these conditions suggest studying the hurricane energetics from the framework of available potential energy. In this paper the theory of available potential energy is used to determine the effect of differential heating. Such an approach will delineate the regions of a hurricane where heating will be most important in the production of energy available for conversion to kinetic energy.

II. GENERATION OF AVAILABLE POTENTIAL ENERGY WITHIN THE HURRICANE SCALE

The atmosphere's available potential energy is defined by Lorenz (1955) as the difference between the sum of the internal and the gravitational potential energies of a given state of the atmosphere and the sum of the energies

which would exist after an adiabatic mass redistribution to a statically stable horizontal density stratification. During this redistribution process the available potential energy is converted to kinetic energy as the warm air rises and the cold air sinks. The source of the available potential energy is the differential heating of the atmosphere by the diabatic processes.

In their recent paper, Dutton and Johnson (1967) extended Lorenz's work on the theory of available potential energy by showing that the theory is valid for all scales of atmospheric motion. Dutton and Johnson stress the importance of adding heat at high pressure and extracting heat at low pressure in the generation of available potential energy. This effect, noted by Lorenz (1955), is disregarded in studies of the diabatic generation based on the concept that the source of available potential energy is due primarily to isobaric differential heating. Both effects are incorporated in the exact expression for the generation of available potential energy (after Dutton and Johnson (1967)), given by

$$G = \int_A \int_{\theta_0}^{\theta_T} [1 - (\frac{\bar{p}}{p})^{\kappa}] J_\theta \dot{Q} \, d\theta \, dA \qquad (1)$$

where p is the pressure, θ is potential temperature, J_θ is the Jacobian of transformation $|\frac{\partial h}{\partial \theta}|$ between height h and potential temperature, $\dot{Q}$ is the rate of heat addition per unit volume and κ is the ratio of the gas constant R to the specific heat at constant pressure c_p. The integration extends horizontally over the entire area A of each isentropic surface and vertically from the coldest potential temperature of the atmosphere θ_0 to θ_T equal to infinity at the top of the atmosphere.

Since the mean pressure in (1) is determined by integrating over the entire global isentropic surface, its direct application for the estimation of the generation of available potential energy is only possible when global data are available. Ideally one would prefer to separate the available potential energy associated with each scale of atmospheric motion. However, since this is a formidable problem because of scale interactions, only a scale-wise decomposition of the generation integral is attempted. The local generation associated with a particular scale is based on the concept that the mass distribution may be considered to be a superposition of scales.

For the scale decomposition, the global generation is divided into two portions,

$$G = G_{R_1} + G_{R_2} \qquad (2)$$

where

$$G_{R_1} = \int_{A_1} \int_{\theta_0}^{\theta_T} [1 - (\frac{\bar{\bar{p}}}{p})^{\kappa}] J_\theta \dot{Q} \, d\theta \, dA \tag{3}$$

and

$$G_{R_2} = \int_{A_2} \int_{\theta_0}^{\theta_T} [1 - (\frac{\bar{\bar{p}}}{p})^{\kappa}] J_\theta \dot{Q} \, d\theta \, dA \tag{4}$$

G_{R_1} represents the contribution to the global generation by the atmosphere surrounding the hurricane scale of motion and G_{R_2} is the contribution to the global generation within a region R_2 containing the hurricane.

Over most of the subtropical region, the pressure $p(x, y, \theta)$ equals a mean pressure $\bar{p}(\theta)$ and only in the tropical depressions, hurricanes or small scale convection does the pressure distribution depart significantly from this condition. Thus in the tropics it seems reasonable to consider that the hurricane is an isolated scale superimposed on the nearly flat horizontal barotropic mass distribution.

From this consideration, G_{R_2} is further divided into two components given by

$$G_{R_2} = \bar{G}_{R_2} + G'_{R_2} \tag{5}$$

where

$$\bar{G}_{R_2} = \int_{A_2} \int_{\theta_0}^{\theta_T} \left[\frac{\bar{p}^{\kappa} - \bar{\bar{p}}^{\kappa}}{p^{\kappa}} \right] J_\theta \dot{Q} \, d\theta \, dA \tag{6}$$

$$G'_{R_2} = \int_{A_2} \int_{\theta_0}^{\theta_T} [1 - (\frac{\bar{p}}{p})^{\kappa}] J_\theta \dot{Q} \, d\theta \, dA \tag{7}$$

$\bar{G}_{R_2}$ is the generation associated with the barotropic tropical scale and G'_{R_2} is the generation within the hurricane scale due to its baroclinic nature. Mathematically the three generation expressions sum to the original generation integral and the scale-wise interpretation of the generation seems justified.

Since we wish to determine if the hurricane is an energetically self-sustaining thermodynamic system, we only investigate in detail G'_{R_2}. If the region R_2 were isolated with no advection through the lateral boundaries, (7) would be the exact expression for the generation of available energy in R_2. However, since R_2 interacts with the region R_1, $\bar{G}_{R_2}$

should be considered. In (6), $(\bar{p}^{\kappa} - \bar{\bar{p}}^{\kappa})$ will be positive below 300 mb since the average pressure of the θ surface within the tropics will be higher than the global average. Thus, a contribution to the generation of available potential energy for the global scale occurs from the net heating within the region.

III. STRUCTURE OF HURRICANE: BAROCLINICITY AND THE EFFICIENCY FACTOR

The effects of the various diabatic processes within the hurricane scale can be studied through the concept of an efficiency factor. Following Dutton and Johnson (1967), the efficiency factor for the hurricane scale from (7) is

$$\epsilon = [1 - (\frac{\bar{p}}{p})^{\kappa}] J_{\theta} \tag{8}$$

The physical explanation for the efficiency factor lies in the definition that available potential energy is the difference of the total potential energy of an actual atmosphere and the total potential energy of the hypothetical reference atmosphere. In the presence of heating or cooling, the total potential energies of both states change by different amounts. The efficiency factor field provides the proper weighting of the heating field to determine the change of this difference, i.e., the change of available potential energy. Note: 1) that heating (cooling) at high pressure and cooling (heating) at low pressure relative to the mean pressure of an isentropic surface within the region creates (destroys) available potential energy and 2) that the distribution of ϵ illustrates quantitatively where heating and cooling will be effective in the generation of available energy. To apply this concept, an efficiency factor cross section for hurricane Hilda (1964) was constructed from the available data.

On October 1, 1964 at 12Z hurricane Hilda was located at 25° N 91° W near the center of the Gulf of Mexico as shown in Fig.1 and in the Tiros VII satellite photograph (Fig. 2). An area extending radially 1000 km from the center of the storm in all directions was selected to be the representative region R_2 for the storm. Data for this region were provided mainly from three flights of ESSA Research Flight Facility planes at approximately 800, 600 and 200 mb. Conventional radiosonde data around the Gulf of Mexico supplemented the aircraft data.

Using the flight data, radiosonde data and mean soundings for the area (Jordan, 1958), an east-west potential temperature and efficiency factor cross section through the region R_2 enclosing Hilda was constructed (Fig. 3).

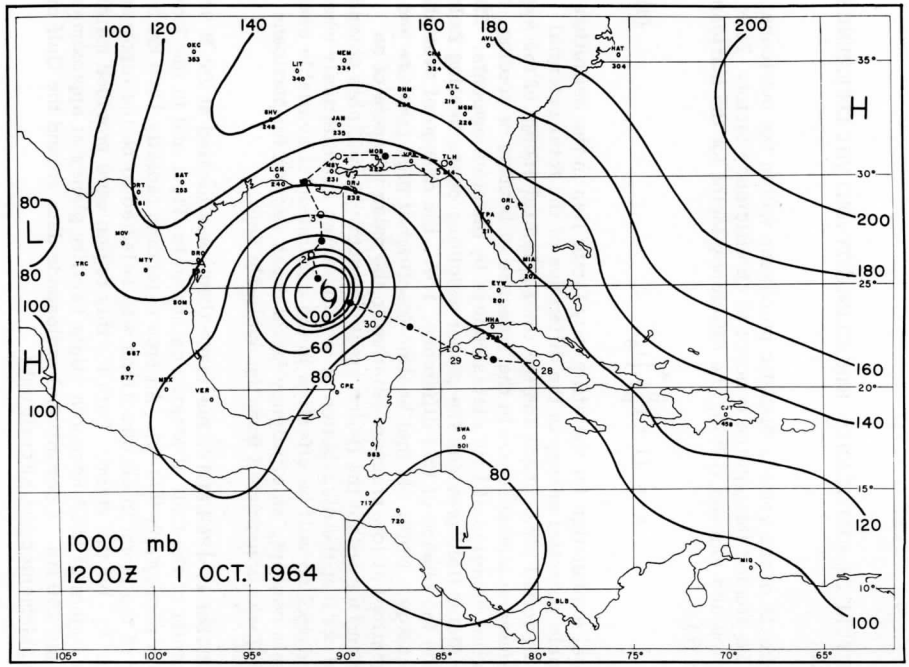

Fig. 1. 1000 mb geopotential surface, from Hawkins and Rubsam (1968). Track of Hilda indicated by dashed line. Daily 00Z and 12Z positions indicated by ● and O respectively.

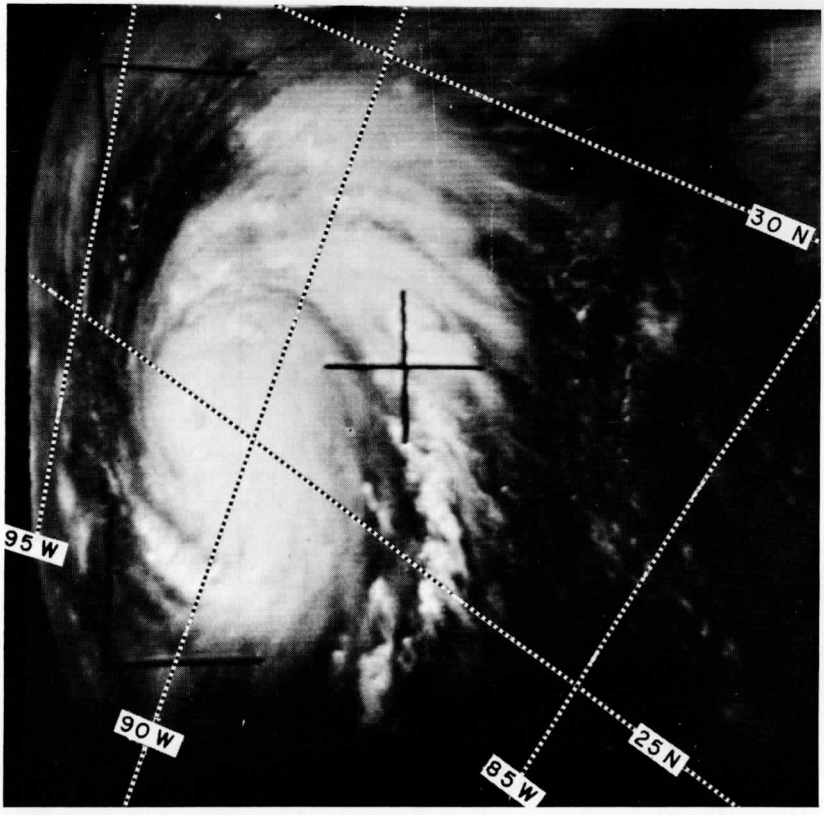

Fig. 2. Tiros VII photograph of hurricane Hilda, 1456Z 10 October 1964, orbit 6952/51.

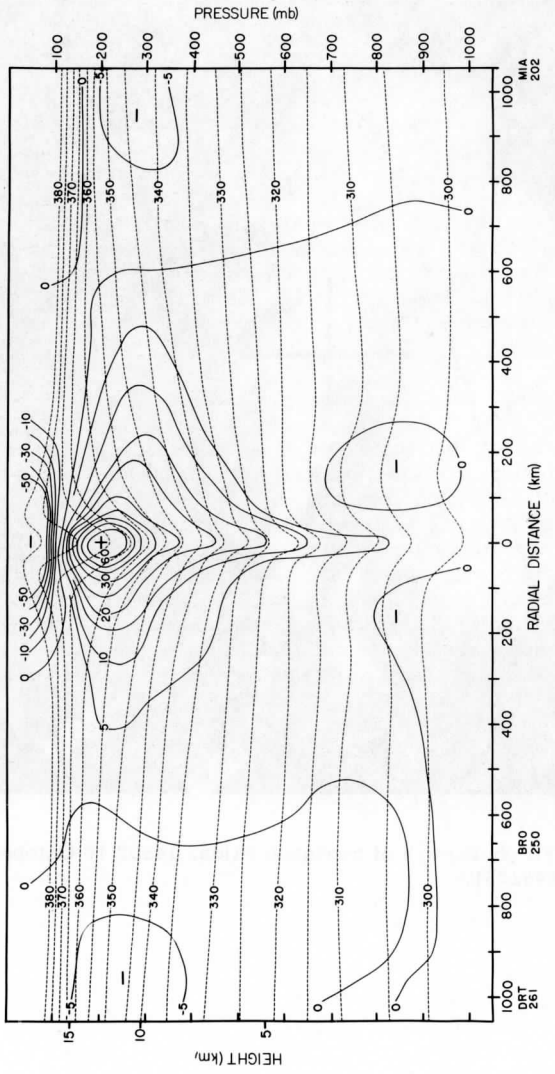

Fig. 3. Potential temperature (°K) and efficiency factor (m/deg) cross section through Hilda, 1 October 1964.

In the warm core pressures are higher than the isentropic average of the hurricane region and the positive efficiency factors are large. In the outer region of the storm, pressures are lower and the efficiency factors are negative.

As expected, the magnitude of the efficiency factors is also dependent on the size of the region over which the mean pressure of each θ surface is determined. However, the dependence is slight. Beyond a certain radial distance the change of $\bar{p}(\theta)$ by enlarging the horizontal extent of the region R_2 is extremely small since $\bar{p}(\theta)$ is nearly equal to the pressure $p(x, y, \theta)$ in the added region. To study the influence of the areal extent, efficiency factors were computed again over a region 1/4 the size, i.e., an area with a radius of 500 km. The reduction in size affected the maximum efficiency factors by no more than 20 percent and shifted the zero line inwards about 200 km. Since we are mainly interested in the differential effects of heating, these differences do not appear to be significant.

Another important element in the relationship between the efficiency factor, baroclinicity and heating is the tendency for a "feedback" mechanism. On an isentropic surface heating at high pressure, the positive efficiency area, results in a steeper slope of the isentropic surfaces in the region separating the cold and warm air, an increase in the baroclinicity, and a creation of additional available potential energy. Conversely, cooling at high pressure results in a decreased slope of the isentropic surfaces, a decrease in the baroclinicity, and a destruction of available potential energy. Thus, heating distributions which tend to increase the baroclinicity also increase the magnitude of the efficiency factors and subsequent heating and cooling is even more efficient in producing available potential energy. The converse is true for a decrease in the baroclinicity.

IV. AVAILABLE POTENTIAL HEAT GENERATION BY THE COMPONENTS OF HEAT ADDITION

In this section, estimates of the generation of available potential energy within Hilda by the diabatic processes are made. The five physical processes of heating in the atmosphere are:

1) release of latent heat,
2) emission of long wave radiation,
3) direct absorption of solar radiation,
4) sensible heat transfer through the earth-atmosphere interface, and
5) frictional dissipation of mechanical energy.

In the boundary layer where frictional dissipation is high, efficiency factors are quite small, indicating that the direct generation contribution from this source will be slight. In the free atmosphere, the generation contribution from internal friction is possibly weakly positive since higher values may be expected in the inner region of positive efficiency factors where the kinetic energy and the vertical shears are greatest. However, because of the positive and negative efficiency factor weighting, the generation within the entire hurricane region by frictional dissipation may be presumably neglected. From these considerations only the first four processes are modeled and their contributions to the total generation of available energy are computed.

Release of Latent Heat

As is generally emphasized, the primary source of energy in the hurricane is the release of latent heat through cumulus convection. It is evident that both the vertical and the horizontal distribution of the components of heat addition as well as the efficiency factor distribution must be known to determine the generation of available potential energy. Two methods are developed to estimate the spatial distribution of latent heating. The first is a simple statistical cloud model and the second is a more sophisticated one based on Kuo's model for latent heat release (1965).

First Method for Latent Heat Release

In the first model surface air is lifted dry adiabatically to the lifting condensation level, then essentially moist adiabatically to 100 mb. During the moist adiabatic process the cloud parcel properties are modified every 100 mb by entraining environmental air. Since this results in a temporary desaturation, the resultant parcel lapse rate lies between the dry and moist adiabatic lapse rate. Under the assumption that condensation occurs when the relative humidity reaches 100 percent and that all condensed water vapor falls out of the system, the amount of latent heat released within each 100 mb layer is approximated by

$$\Delta H = L \Delta q \bar{\rho} \tag{9}$$

where $\bar{\rho}$ is the mean density of the layer. Δq, the difference of the specific humidity between the top (t) and bottom (b) of each layer, is defined by

$$\Delta q = q_{s_t} - [(1-\alpha) q_{s_b} + \alpha\, q_b] \tag{10}$$

where α is the entrainment percentage (20 percent in this initial study (Byers and Braham, 1949)), q_s is the saturation specific humidity and q is the environmental specific humidity.

The heating rate $\dot{Q}$ in (7) is obtained from the release of latent heat within the convective clouds ΔH, the time dependency of the heat release, and the percentage of area covered by convective clouds. If the percentage area of cloud cover in an incremental radial ring is B and the time for the cloud to ascent 100 mb is Δt, the average rate of heat addition becomes

$$\dot{Q} = \Delta H \, B/\Delta t \qquad (11)$$

Assuming the parcel's ascent rate to be linear with respect to pressure, Δt is determined by the lifetime of the cloud, i.e., the time required for the cloud to ascend from the point of initial condensation to the 100 mb level. Based on Ogura's estimates (1964), the cloud lifetime was set equal to 60 minutes, yielding a Δt of 6.6 minutes, which is higher than Gray's estimate of 30 minutes (1967).

The following percentages of areal cloud coverage by cumulonimbi based on Gentry's study (1964) of rainbands within a hurricane were assigned:

Radius (km)	B - percent areal coverage
0 - 100	15
100 - 200	10
200 - 300	4
300 - 400	3
400 - 500	1

Second Method for Latent Heat Release

The second method of estimating the latent heat release is adapted from Kuo (1965). This approach assumes that the latent heat release is determined by the flux of moisture from the boundary layer induced dynamically by the hurricane. The source of moisture is evaporation into the boundary layer and frictional cross-isobaric inflow of moist air.

In parameterizing the rate of latent heat release, Kuo introduces the concept of "rate of cloud production," defined as the ratio of the net moisture convergence in a vertical column, I, to the amount of moisture, Q, that is needed to saturate and warm the column to a saturation specific

humidity q_s and temperature T_s. If the differential horizontal advection of moisture is negligible in comparison with the vertical flux of moisture from the boundary layer, I is given by

$$I = \begin{cases} -\omega_0 q_0 g^{-1} & \omega_0 < 0 \\ 0 & \omega_0 \geq 0 \end{cases} \tag{12}$$

where ω_0 and q_0 are the individual derivative of pressure and specific humidity at the top of the boundary layer, and g is the acceleration of gravity. Q is given by

$$Q = g^{-1} \int_{p_0}^{p_t} (q_s - q)dp + g^{-1} \int_{p_0}^{p_t} c_p L^{-1} (T_s - T)\, dp \tag{13}$$

where p_0 is the pressure at cloud base and p_t is the pressure at cloud top.

In Kuo's model the rate of heat addition to the environment is

$$\dot{Q} = \rho c_p (T_s - T) \frac{I}{Q} \tag{14}$$

T_s and q_s are given by the moist adiabat through the lifting condensation level, T and q are known from the aircraft data and ω_0 is modeled after Ogura (1964).

In Ogura's model the radial profile of ω_0 is estimated from the surface stress and the absolute vorticity and given by

$$\omega_0 = -\frac{g}{r} \frac{\partial}{\partial r} \left[r \tau_0 / \left(f + \frac{\partial (r v_0)}{\partial r} \right) \right] \tag{15}$$

where τ_0 is the surface stress, v_0 is the tangential wind speed at the top of the boundary layer, and f is the Coriolis parameter. An empirical model for the radial distribution of the tangential wind speed of the form, $v_0 r^{1/2} = C$ was assumed, with the constant C determined by a least squares fit of the model to the observed winds beyond the radius of the maximum tangential wind. Details are presented in the Appendix. Using the solution for the steady state mean vertical motion from (15) (Fig. 4), and this model, realistic estimates of the latent heating rate were determined.

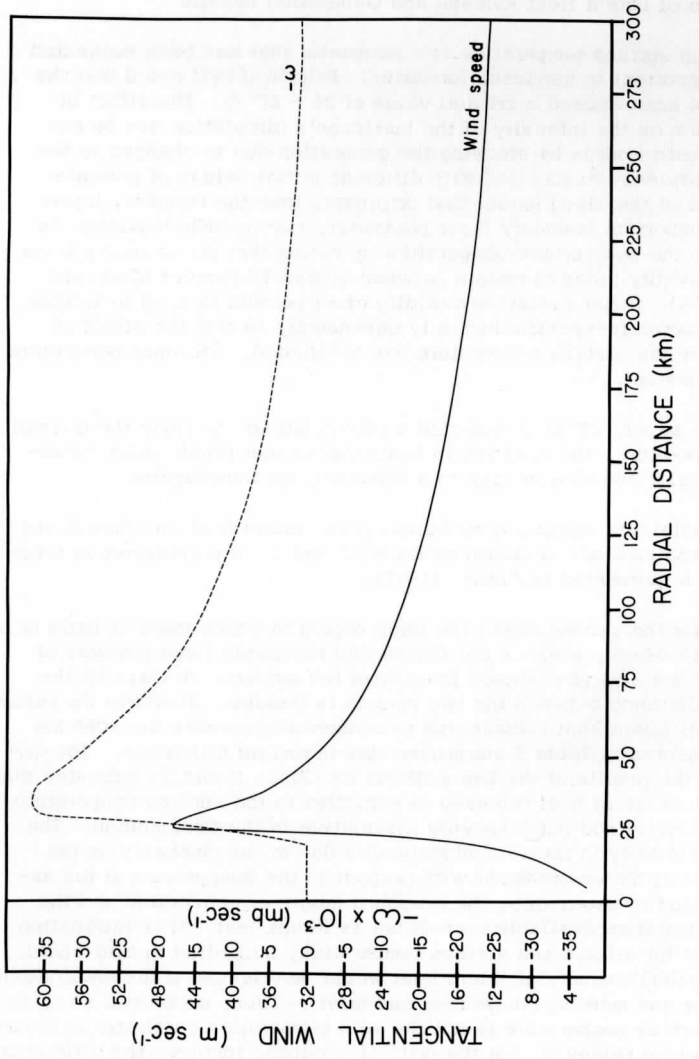

Fig. 4. Tangential wind speed and vertical motion computed from analytical model.

Comparison of Latent Heat Release and Generation Results

The sea surface temperature is a parameter that has been suggested as being important in hurricane formation. Palmén (1948) noted that the temperature must exceed a critical value of 26 - 27° C. The effect of this criterion on the intensity of the hurricane's circulation can be examined in both models by studying the generation due to changes in the latent heat release associated with different initial values of potential temperature of the cloud parcel that originates from the boundary layer. The other important boundary layer parameter, the specific humidity, is related to the sea surface temperature by noting that the boundary layer relative humidity tends to remain between 80 and 90 percent (Dunn and Miller (1964). A fixed relative humidity of 85 percent is used to provide unique temperature-specific humidity dependency so that the effect of varying only the surface temperature can be studied. All other parameters are held constant.

In this paper, 27° C is selected as the reference to study the critical ocean temperature, and changes in heat release that result under conditions 3° cooler and warmer than this reference are investigated.

The radial and vertical distribution of the latent heat for Case II and III using both methods is shown in Tables 1 and 2. A corresponding table for Case I is presented by Anthes (1967).

Note for the second model the large region in which there is little or no latent heat release, while in the first model relatively large amounts of latent heat are always released throughout the system. In Case III the striking difference between the two models is lacking. Similarly the results for the total latent heat release due to condensation within the 1000 km region presented in Table 3 summarize this important difference. The difference in the results of the two methods for Cases II and III indicates that the amount of latent heat released is sensitive to the surface temperature in the second method but relatively insensitive in the first method. The greater sensitivity in the second method is due to the emphasis on the temperature of the environment with respect to the temperature of the ascending cloud in determining the maximum height of convection and the amount of moisture available for release as latent heat. It is interesting to note that for a fixed sea surface temperature, according to this model, larger (smaller) amounts of latent heat would be released if the environment were cooler and more moist (warmer and drier). Thus, model two stresses that the surface temperature is not the sole temperature parameter in determining the heat released, but the critical condition involves the difference of the equivalent potential temperature of the surface air and the potential temperature distribution of the environment.

Table 1. Latent heat release and generation for moderate case (T_0 = 27° C)

.02	.02	.06	.06	.10	.11	.34	.26	1.2	1.8
0	0	0	0	0	0	0	0	0	0
.19	.08	.60	.36	.92	.71	2.9	4.0	7.4	25.
0	0	0	0	.10	.10	2.3	3.0	2.1	7.
.54	.20	1.7	.77	2.5	1.9	7.4	9.3	14.	40.
.30	.08	.50	.20	.90	.60	4.9	6.0	4.4	10.
.88	.09	2.7	.55	3.8	1.4	11.	6.8	18.	26.
.5	.06	1.0	.20	2.0	.8	6.2	4.0	12.	19.
1.1	.11	3.4	.55	4.7	1.0	13.	3.1	20.	18.
.5	.04	.8	.1	2.3	.4	10.	2.0	23.	21.
1.3	.09	3.8	.34	5.4	.52	15.	1.4	22.	11.
.3	.02	.7	.07	2.3	.2	13.	1.0	46.	25.
1.5	.15	4.5	.38	6.1	.39	17.	.54	24.	7.9
.3	.03	.5	.04	2.6	.20	16.	.50	35.	9.7
2.6	.02	8.0	.06	12.	0	33.	-.2	49.	6.5
.6	0	1.3	.01	5.0	0	18.	-.1	71.	6.2

100
200
300
400
500
600
700
800
1000
Pressure (mb)

500 400 300 200 100 0
Radial distance (km)

$\dot{Q}_1$	G_1
$\dot{Q}_2$	G_2

Plotting Model

$\dot{Q}_1$: latent heat release method 1 (10^{-2} watt m^{-3})

G_1: generation from method 1 (watt m^{-2})

$\dot{Q}_2$: latent heat release from method 2 (10^{-2} watt m^{-3})

G_2: generation from method 2 (watt m^{-2})

Table 2. Latent heat release and generation for warm case (T_0 = 30°C)

.02	.02	.08	.08	.13	.14	.47	.35	1.5	2.3
0	0	0	0	.04	.04	1.4	1.0	7.8	17.
.24	.10	.78	.47	1.2	.93	3.7	5.1	8.9	30.
.32	.10	.84	.50	2.3	1.9	7.7	12.	22.	76.
.66	.21	3.0	.95	3.1	2.4	8.6	11.	16.	45.
.60	.20	1.4	.60	3.2	2.4	9.5	11.	23.	55.
1.0	.10	3.2	.64	4.4	1.6	12.	7.6	19.	28.
.77	.1	1.6	.40	3.8	1.5	10.	6.3	28.	46.
1.3	.12	3.9	.63	5.3	1.2	14.	3.4	22.	19.
.73	.06	1.5	.2	4.0	.7	13.	2.9	34.	31.
1.4	.10	4.3	.45	6.0	.59	16.	1.6	23.	12.
.62	.04	1.5	.1	4.0	.4	14.	1.3	41.	23.
1.6	.06	5.0	.43	6.8	.44	19.	.6	26.	8.4
.63	.03	1.4	.10	4.3	.3	16.	.6	43.	12.
2.8	.01	9.0	.03	13.	0	34.	-.2	51.	4.2
.08	0	1.9	.01	5.2	0	18.	-.1	51.	1.9

Pressure (mb): 100, 200, 300, 400, 500, 600, 700, 800, 1000

500 400 300 200 100 0

Radial distance (km)

$\dot{Q}_1$	G_1
$\dot{Q}_2$	G_2

Plotting Model

$\dot{Q}_1$: latent heat release method 1 (10^{-2} watt m^{-3})

G_1: generation from method 1 (watt m^{-2})

$\dot{Q}_2$: latent heat release from method 2 (10^{-2} watt m^{-3})

G_2: generation from method 2 (watt m^{-2})

The failure of the first model to be sensitive to the surface temperature is due to the fact that there is no control by the environment on the convection since the area cloud coverage B and cloud lifetime are fixed. In this model the rate of convection is implicitly fixed and the cloud parcel always penetrates to 100 mb. The latent heat released in the three cases is nearly identical. The quantitative effect of varying the parameters B and Δt is evident since they are linearly related to the heating and generation. For example, if Gray's estimate (1967) of 30 minutes for the cloud lifetime is used, the generation is doubled. However, if this estimate is combined with Malkus' et al. (1961) estimate for cloud coverage which is approximately one-half of Gentry's, the generation estimates are identical to the results presented.

A deficiency in model II is the use of a technique designed for obtaining the cumulative effects of latent heat through the process of free convection while in certain stages of a hurricane the release of latent heat through forced convection may be significant. The use of Kuo's model in a case of forced convection in an unsaturated environment in which $T_S \approx T$ is invalid. In this case the numerator of (14) is zero while the denominator is finite, and the heating rate is underestimated. In the 24° C sea surface case the difference between T_S and T is small; hence the estimates of latent heat release and generation are possibly underestimated if forced convection is significant.

In spite of the possible deficiencies, the total latent heat release for the warmer temperatures for both models compares favorably with Riehl's (1954) estimate of $2 - 5 \times 10^{14}$ watts for a mature storm, and Hughes (1952) result of 5×10^{14} watts for 28 Pacific tropical cyclones. In future experiments it would be interesting to extend the dependency of the generation to other parameters in addition to the sea surface temperature by using models which are more realistically based on cloud dynamics, such as the model proposed by Malkus (1960).

Best Estimation of Generation Due to Latent Heat

Measurements of the water temperature immediately before Hilda's passage through the Gulf of Mexico indicated fairly uniform temperatures at about 29° - 30° (Leipper, 1967). However, Leipper indicates that the sea surface temperature lowered to 28° C during the hurricane's passage due primarily to mixing of the Gulf's surface layer by the wind. Thus, an extrapolated value of 3.2×10^{14} watts for latent heat release from the results for Case II and III of the second method is probably the most realistic estimate of the latent heat release.

Using the distribution of latent heat from the three cases for both models, the generation of available potential energy within the region R_2 was estimated using a finite evaluation of (7). The heating rates and generation results are presented in Tables 1 and 2 and summarized in Table 3. The vertical and horizontal distribution of latent heating and the associated generation is presented in Figs. 5 and 6.

Table 3. Total latent heat release (10^{14} watts) and generation due to latent heat release (10^{12} watts)

		First Method		Second Method	
	T_0	Heating	Generation	Heating	Generation
Case I	24° C	4.1	7.3	0.7	0.4
Case II	27° C	4.6	8.5	2.5	5.3
Case III	30° C	5.2	10.4	4.4	13.0

In the results, it is clear that the greatest generation occurs within 100 km of the eye in the middle troposphere. In this region the efficiency factors are high and the latent heat release is large. As the radial distance increases, the efficiency factors and latent heat release decrease rapidly, so that over 50 percent of the generation occurs in the inner 100 km.

The vertical distribution of generation shows that approximately 90 percent occurs in the middle troposphere between 700 and 200 mb and is associated with large positive efficiency factors. Below 700 mb, even though the latent heat release is strong, the efficiency factors are smaller and there is little direct generation. Above 200 mb, the release of latent heat is relatively unimportant.

In a comparison of the results for the 30° C case the generation estimates are greater for the second model even though the latent heat release by the first model is larger. This difference emphasizes that not only the amount but also the distribution of the heat released is important in the generation of available potential energy.

Therefore, we conclude: 1) that although both methods give reasonable results for the warm case (III), the second method is physically more realistic, and 2) that the best estimate of the generation due to latent heating is an interpolated value of 7.9×10^{12} watts associated with a sea surface temperature of 28° C.

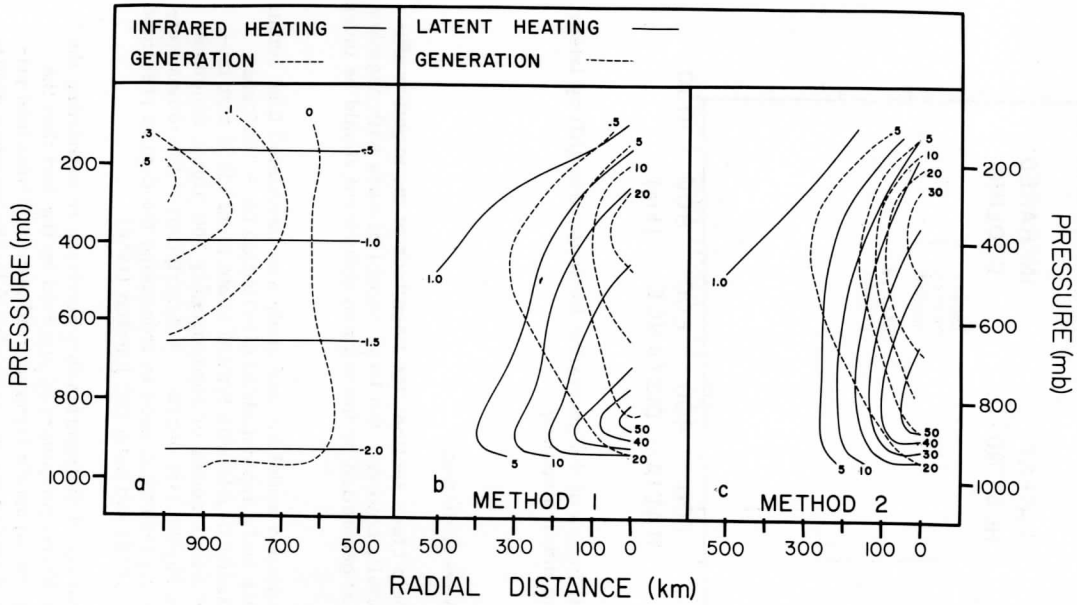

Fig. 5. Heating (10^{-2} watts/m^{-3}) and generation (10^{-3} watts m^{-3}) rates due to infrared cooling and latent heating (Case III).

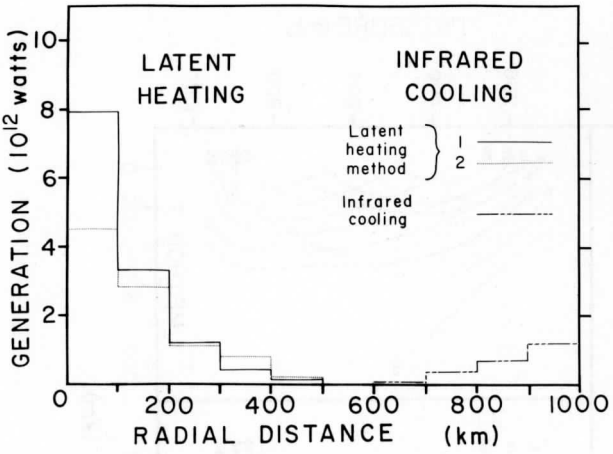

Fig. 6. Radial distribution of the generation for warm case (III) by latent heating and infrared cooling.

Emission of Long Wave Radiation

In the hurricane's cross section, the magnitude of the negative efficiency factors is small, however, the large amount of mass with negative values suggests that generation by the infrared component should be investigated.

The infrared radiation model for this study was formulated from actual radiometersonde data and a typical cloud distribution for a hurricane. Several radiometersonde flights with typical subtropical cloud distributions were selected from a series of approximately 100 flights conducted in the Caribbean during the last decade. A description of the radiometersonde and the filtering technique used in processing the data is presented by Suomi and Kuhn (1958) and Kuhn and Johnson (1966).

Use of a typical cloud distribution in a hurricane in estimating the generation by the infrared component is justified by the fact that the modification of the atmosphere's infrared irradiance is determined primarily by the cloud distribution and secondarily by the moisture distribution. In a typical hurricane extensive multileveled cloudiness with

cumulonimbi penetrating to the tropopause occurs in the central region of the storm. A cirrus deck near the tropopause covers this region. From both radiometersonde evidence and theoretical considerations, such a region under the cirrus shield is nearly in radiational equilibrium and the infrared cooling rate is near zero. However, above the cirrus shield strong cooling of 4-6° C per day occurs. At some distance from the center, the hurricane is characterized by a sharp break in cloudiness beyond which practically clear conditions prevail (Fett, 1964). In this region the infrared cooling may be typified by the "clear air" rate of 1-2° C per day.

The relationship between the heat addition rate per unit volume and the instantaneous change of temperature $\frac{\partial T}{\partial t_I}$ is

$$\dot{Q} = c_p \rho \frac{\partial T}{\partial t_I} \tag{16}$$

Using (16) and (7), the infrared component of the generation was computed. However, because the exact infrared cooling was not known, a satellite picture was used to indicate cloud coverage and the generation was computed for the extremes of a range of cooling rates.

The satellite picture (Fig. 2) of hurricane Hilda indicates that beyond 500 km, the region R_2 is free of significant layered clouds; hence the "clear air" cooling rate of 1 to 2° C/day was used for the representative range in this region. For the inner 500 km region above the cirrus shield a range of 4 to 6° C/day was used while under the cirrus shield the range was 0.0 to 0.3° C/day. Furthermore, since the vertical gradient of efficiency factors in the upper troposphere was large, the infrared generation was computed under two different cirrus distributions, one at 100 mb where the mean efficiency factors are weakly positive, and the other with the top at 200 mb where the efficiencies are strongly positive. The contributions of the various regions to the generation due to the infrared cooling are listed in Table 4.

From various combinations of cooling rates, the total infrared generation ranges between 0.6×10^{12} watts (combination yielding the minimum) and 2.7×10^{12} watts (combination yielding the maximum). Taking the mean cooling rate for each region and assuming the more likely cirrus level of 100 mb, the best estimate for the generation due to the infrared heating component is 1.8×10^{12} watts. The significant contribution to the infrared generation is from the outer "clear" regions of the hurricane environment in the upper troposphere, as shown in Figs. 5 and 6. This is due to the dominating effect of the large amount of mass and the small negative efficiency factors over the large positive efficiency factors and small amount of mass in the inner area.

Table 4: Infrared and direct solar components of generation

Region and cloud condition		Heating rate and generation extremes		
Infrared				
0 < R < 500	under cirrus	0	-.3	Heating (°C/day)
		0	-.33	Generation (10^{12} watts)
500 < R < 1000	clear air	-1.0	-2.0	Heating
		1.4	2.8	Generation
0 < R < 500	top of cirrus 200 mb.	-4.0	-6.0	Heating
		-0.3	-0.5	Generation
0 < R < 500	top of cirrus 100 mb.	-4.0	-6.0	Heating
		-.07	-.11	Generation
Solar				
0 < R < 500		0.5	1.0	Heating
		0.55	1.10	Generation
500 < R < 1000		0.1	0.3	Heating
		-0.14	-.42	Generation

In a comparison of the infrared generation with the latent heat component associated with the sea surface temperature of 28° C, the ratio of the infrared to the latent heat generation is 1: 4. These results indicate that the infrared generation represents a significant source of available potential energy and the cooling in the descending branch of the hurricane circulation is an important feature.

Direct Absorption of Solar Radiation

Since the atmosphere is nearly transparent to direct solar radiation, the generation by this component is presumably small. A simple calculation is made to establish its order of magnitude. From Korb and Möller (1962) representative extremes for the range of direct solar heating in cloudy moist regions would be 0.5 to 1.0° C/day while in a clear dry atmosphere values range from 0.1 to 0.3° C/day. Again, combining extremes from the two regions of differing cloud conditions the maximum solar generation is 0.96 and the minimum is 0.13×10^{12} watts while the best estimate associated with the mean heating rate in each region is 0.55×10^{12} watts. The ratio of the solar to the latent heating component is 1 : 15 while compared to the infrared component the ratio is 1 : 3.3.

Sensible Heat Addition

The fourth generation component studied is that due to sensible heat addition at the earth's interface. The occurrence of both positive and negative efficiency factors in the boundary layer implies that there is both local destruction and production of available energy by the component of sensible heat addition.

Malkus and Riehl (1960) show that the process of interface sensible heat transfer does not become effective until the air–sea temperature difference is 2° C or greater. In outer portions of the region, R_2, it is reasonable to assume that there is little sensible heat transfer since there will be essentially no difference in temperature across the interface. However, in the inner region the air flows horizontally toward lower pressure and tends to cool by adiabatic expansion. Observations show that in spite of the tendency for adiabatic cooling, the temperature remains constant throughout the inflow layer, thus indicating that sensible heat is added. Since observational evidence further indicates that the major reduction in surface pressure occurs in the inner 150 km of the storm, significant adiabatic expansion and sensible heat addition should occur mainly in this region.

Hawkins and Rubsam (1968) calculated a total of 0.15×10^{14} watts for the sensible heat addition in the ring bounded by the 20 and 150 km radii from the center of Hilda. If this sensible heat is distributed uniformly throughout a boundary layer 1.1 km in depth, the heating rate per unit volume is 0.204 watts m^{-3}. These results are in excellent agreement with the Malkus-Riehl (1960) estimate of 720 ly/day sensible heat addition over a depth of 1.1 km in the inner 90 km of a moderate hurricane, which yields a total of 0.11×10^{14} watts.

Using the Hawkins-Rubsam estimate of 0.204 watts m^{-3}, a mean efficiency factor of 1.5 m/deg, and a $\Delta\theta$ of 3° C for a boundary layer 1.1 km in depth over a region 150 km radial extent, a crude estimate for the sensible heat generation is 6.5×10^{10} watts. Because of the choice of a large efficiency factor and $\Delta\theta$, this estimate is probably high. Even so, it is two orders of magnitude smaller than the generation components of latent heat and radiation indicating that sensible heat addition is not important in the direct generation of available energy.

The role of sensible heat addition within the framework of the theory of available potential energy is indirect. As the air flows toward lower pressure, sensible heating serves to raise the equivalent potential temperature and is a necessary element in the maintenance of convection surrounding the eye. Ultimately, the latent heat release occurring in the air with the higher equivalent potential temperature maintains the warm core, baroclinicity and the high efficiency factors, thus making the release of latent heat in this region more effective in the direct generation of available potential energy. Although the sensible heat generation is small, the role of sensible heating in maintaining the core of high equivalent potential temperature is an essential process in the energetics of hurricanes.

Total Heat Budget and Global Generation Contribution

Summing the latent heat estimate of 3.1×10^{14} watts, the infrared heating estimate of -3.7×10^{14} watts from a mean cooling rate of 1.2° C/day, the solar heating estimates of 0.9×10^{14} watts from a mean heating rate of 0.3° C/day, and the sensible heat estimate of 0.15×10^{14} watts, the net heat addition is 0.45×10^{14} watts. This corresponds to a mean heating rate of about 0.2° C/day unless sensible heat is transported from the region of the hurricane. Riehl's results (1959), although for a smaller volume in the Gulf, indicates that significant sensible heat transport away from a tropical storm does occur. However, in this study the near equality of the two dominating components, infrared cooling and latent heating, indicates the tendency for the hurricane to operate thermodynamically as a closed system over the region R_2.

As mentioned earlier, the net heating within R_2 would provide a positive contribution to the generation of available potential energy for the global scale in addition to the generation for the hurricane scale. Using estimates of $\bar{\bar{p}}(\theta)$ from Dutton and Johnson (1967) and the $\bar{p}(\theta)$ from this study, tentative estimates were made from (6) for $\bar{G}_{R_2}$. The generation contribution from the four heating components for the 28°C case, method two, are latent heat 9.8×10^{12} watts, infrared -8.0×10^{12} watts, solar absorption 1.6×10^{12} watts and sensible heating 0.9×10^{12} watts. Thus the total generation contribution for the global scale of 4.3×10^{12} watts, or an average of 1.4 watts m^{-2} from $\bar{G}_{R_2}$ is significant.

V. TOTAL GENERATION WITHIN HURRICANE HILDA AND KINETIC ENERGY PRODUCTION

The total generation for the hurricane scale, G'_{R_2}, given by the sum of the components of latent heating, infrared cooling, direct solar absorption, and sensible heating is listed below for both models of latent heat release and the three surface conditions:

Total generation of available energy (10^{12} watts).

Case		Total Using First Model of Latent Heat	Total Using Second Model of Latent Heat
I	$T_0 = 24°$ C	9.7	2.8
II	$T_0 = 27°$ C	10.9	7.7
III	$T_0 = 30°$ C	12.8	15.4

Our interpolated estimate for total generation rate associated with the Gulf sea surface temperature of 28° C is 10.3×10^{12} watts which may be compared with estimates of kinetic energy produced in tropical storms, summarized in Table 5.

Because of the different areas involved, direct comparisons are difficult. However, it is clear that the total generation of 10.3×10^{12} watts compares favorably with other investigators' estimates. The close agreement between the generation estimate and the estimate for kinetic energy production and advection for Hilda (Hawkins and Rubsam (1968)) is especially interesting considering the independent nature of the two methods.

Table 5: Kinetic energy production in hurricanes

Author	Region of Storm	Kinetic Energy Production $\times 10^{12}$ Watts
Gentry (1951)	0 - 110 km	3.2
Miller (1962)	0 - 110 km	8.0
Riehl and Malkus (1961)	0 - 110 km	5.2
Palmén and Jordan (1955)	0 - 220 km	4.6
Palmén and Riehl (1957)	0 - 666 km (entire storm)	15.0
Hawkins and Rubsam (1968) for hurricane Hilda	0 - 150 km	8.6

While the numerical comparisons are striking, the physical validity of using computed values of the generation of available potential energy associated with the barocolinic component to also estimate the kinetic energy production depends on the condition that this component of global generation is actually converted into kinetic energy within the system itself. Several observational results in addition to the numerical results indicate that this is true and give validity to the argument that the baroclinic mass distribution of the hurricane may be treated as a scale superposition on the flat barotropic distribution of the tropics. Among these are: 1) the relatively quiescent state of the hurricane's barotropic environment, 2) the direct circulation associated with the ring of subsidence surrounding the cirrus shield and the ascending branch near the eye, and 3) the slow erratic movement of most hurricanes indicating negligible momentum exchange with the environmental flow. Of the three supporting facts, the ring of clear subsiding air indicates the existence of the direct circulation and provides the best evidence that the thermodynamic concept of the generation of the available potential energy associated with the hurricane's baroclinic component is valid. The sinking of the cold environment and the rising of the warm air is the mechanism by which the locally generated available potential energy is continually transformed into kinetic energy. The diabatic components of latent heat and infrared cooling maintain the baroclinicity of the hurricane and the store of available potential energy against the adiabatic conversion process. Furthermore, if the hurricane is a self-sustaining scale of motion, the direct

generation within the system must be the primary source of the kinetic energy to offset the sink of frictional dissipation.

The total generation for the three cases for the second method provides an interesting result which indicates the importance of high equivalent potential temperatures in the boundary layer. In Case 1 with a 24° C surface temperature, the generation of 2.8×10^{12} watts is insufficient to maintain a well developed hurricane, in Case II with a 27° C surface temperature the generation of 7.7×10^{12} watts is probably sufficient but marginal, while in Case III with a 30° C surface temperature the generation is sufficient to maintain an intense hurricane. The actual dynamics of the generation are related to the difference of the environment's potential temperature and the equivalent potential temperature of the surface air. Quite likely for a characteristic potential temperature for the environment, there is a corresponding sea surface temperature for which the hurricane tends to exist in a steady state, in which the direct generation, the rate of kinetic energy production and the frictional dissipation are nearly equal. An imbalance between the three processes will result in a change of intensity in the storm. For example, if the hurricane moves over a warmer sea surface, the model indicates that the generation will increase. Unless the adiabatic cooling due to the direct circulation immediately increases, thus compensating for the increased rate of latent heat release, greater baroclinicity and higher efficiency factors are the immediate result. The increased baroclinicity is important in that the associated increased thermal wind component eventually allows for higher wind speeds and greater amounts of kinetic energy to be maintained in a balanced state in the hurricane system. The increased kinetic energy results from an increase in the rate of production of kinetic energy over that dissipated by friction. Eventually the dissipation of kinetic energy will also increase due to the greater shears in both the boundary layer and free atmosphere until a new steady state condition is reached in which the generation, production of kinetic energy and frictional dissipation are again nearly equal, but are all greater than the rates corresponding to the lower sea surface temperature.

VII. SUMMARY

In this study the estimates of the generation of available potential energy associated with the hurricane's baroclinicity from four components of heat addition have been determined. To obtain these estimates a scale decomposition of the generation integral was attempted, two models for the release of latent heat were used, and an infrared cooling and solar absorption model formulated.

The following conclusions may be made:

1) The component of the generation integral associated with the hurricane's baroclinicity can be utilized to provide physically realistic estimates of the rate of production of energy available for conversion to kinetic energy within the hurricane scale.

2) The local generation of available potential energy by the latent heat component occurs mainly in the middle and upper troposphere within 200 km of the hurricane center and not only depends on the sea surface temperature but also on the difference between the equivalent potential temperature of the boundary layer and the potential temperature distribution of the environment.

3) The local generation of available potential energy by the infrared component occurs primarily in the upper troposphere of the region beyond 500 km.

4) The generation for the hurricane scale by direct solar absorption and sensible heat addition is negligible. However, the dynamic role of the sensible heating in maintaining the deep cumulus convection is undoubtedly important.

5) The total generation estimate for Hilda using a sea surface temperature of 28° C is 10.3×10^{12} watts with approximately 6 percent being contributed by direct solar absorption, 17 percent by infrared cooling and 77 percent by the release of latent heat.

6) According to available potential energy considerations, the latent heat release necessary for the formation of tropical storms should occur in a region of positive efficiency factors.

In future studies, detailed isentropic cross sections through several disturbances that develop into hurricanes should be made. Particular emphasis should be placed on the determination of the location where the intense precipitation and deep cumulonimbus convection develops in relation to the efficiency factor distribution.

APPENDIX. BOUNDARY LAYER VERTICAL MOTION

According to Ogura (1964) under the assumption of steady state symmetry for the hurricane and the condition that the stress vanishes at the top of the boundary layer, the vertical motion at the top of the boundary layer is

$$\omega_0 = -\frac{g}{r}\frac{\partial}{\partial r}\left[\frac{r\,\tau_0}{f+\frac{1}{r}\frac{\partial (r\,v_0)}{\partial r}}\right] \tag{A1}$$

In this study the surface stress τ_0 was estimated from the semi-empirical drag formula given by

$$\tau_0 = C_D V_s^2 \rho \tag{A2}$$

where V_s is the surface wind speed and C_D is the dimensionless drag coefficient. For this study a drag coefficient value of 4×10^{-3} was selected from various estimates of C_D over water (Fig. 7).

The radial wind profiles used to estimate the vertical motion were provided by the low level (800 mb) aircraft data. The winds were measured by an AN/APN-82 system (Gray, 1965 and 1966) and a nearly continuous radial profile of tangential winds with about 1 km horizontal separation was available. In the initial attempt, centered finite differences over an interval of 5 km were used to estimate the derivatives in (A1). Due to the extreme sensitivity of (A1) to small values of the denominator the ω_0 estimates deteriorate rapidly with increasing radial distance and nearly infinite values of ω_0 of either sign occur.

To avoid this problem several filtering techniques including a quadratic least squares polynomial and a running mean over seven points were utilized to smooth the tangential winds. Some of the wild fluctuations were reduced by the polynomial filtering however the ω_0 profile was still far from satisfactory. The running mean results were similarly poor.

A suitably smooth radial profile of the tangential wind was only obtained by assuming an analytic function for the tangential wind speed. The model (Riehl, 1954)

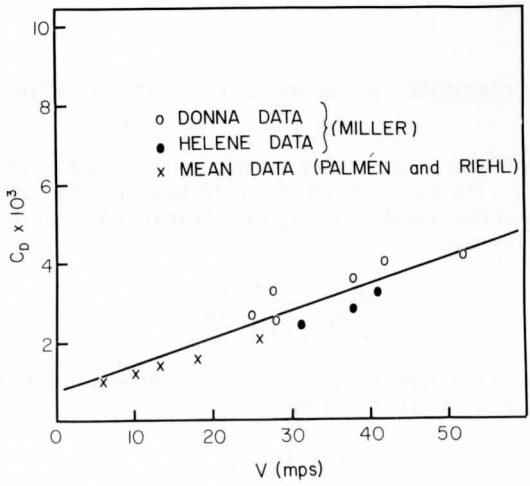

Fig. 7. Drag coefficient estimates over water versus wind speed from Miller (1962) and Palmén and Riehl (1957).

$$V_0 \, r^{1/2} = C \tag{A3}$$

was used to represent the wind profile beyond the radial distance of the maximum wind. The constant C was determined by a least squares fit of the observed wind profile to the model. Since the dependent observation is V_i for each independent variable r_i $(i = 1, \ldots, n)$, the model is transformed to

$$V_0 = r^{-1/2} \, C \tag{A4}$$

Using the transformation variable

$$x = r^{-1/2} \tag{A5}$$

the substitution of (A5) into (A4) yields

$$V_0 = Cx \tag{A6}$$

which is the equation of a straight line. The solution for C, after transforming back to the actual radial distances, r_i, is

$$C = \sum_{i=1}^{n} V_i r_i^{-1/2} \Big/ \sum_{i=1}^{n} r_i^{-1} \qquad \text{(A7)}$$

Using the least squares estimate of C, first and second derivatives of the tangential velocity profile were provided by differentiating the model (A3) and a well behaved vertical motion profile was produced (Fig. 4). These ω_0 values were used in the computation of latent heat by the second method from the radial distance of maximum horizontal wind outward. Inside this distance ω_0 values were set equal to zero.

This ω_0 field cannot be interpreted as the field that is instantaneously associated with the convective updrafts but must be interpreted as the mean radial profile of vertical motion for the hurricane. The actual convective vertical motion at any instance is closely related to horizontal fluctuations in the wind occurring within a scale smaller than the larger scale for which equation (A1) is valid.

ACKNOWLEDGMENTS

The authors wish to express their appreciation to the personnel of the National Hurricane Research Laboratory, ESSA, to Professor Werner Schwerdtfeger of the University of Wisconsin for his helpful review of the manuscript and to Mr. Dave Morgan for drafting. Support was provided by the National Science Foundation through a graduate fellowship, National Environmental Satellite Center of ESSA under grant WBG-52, and the National Hurricane Research Laboratory of ESSA.

REFERENCES

R. A. Anthes, 1967: "The generation of available potential energy in hurricane Hilda (1964)," M.S. Thesis, University of Wisconsin, Madison, Wisconsin, 84 pp.

H. R. Byers and R. R. Braham Jr., 1949: The Thunderstorm, U.S. Dept. of Commerce, Washington.

J. G. Charney and A. Eliassen, 1964: "On the growth of the hurricane depression," Journal of the Atmospheric Sciences, Vol. 21, pp. 68-75.

G. Dunn and B. Miller, 1964: Atlantic Hurricanes, Louisiana State University Press, Baton Rouge, 1964, 377 pp.

J. A. Dutton and D. R. Johnson, 1967: "The theory of available potential energy and a variational approach to atmospheric energetics," Advances in Geophysics, Vol. 12, pp. 333-436.

R. W. Fett, 1964: "Aspects of hurricane structure. New model considerations suggested by Tiros and Project Mercury observations," Monthly Weather Review, Vol. 92, pp. 43-60.

R. C. Gentry, 1951: "Forecasting the formation and movement of the Cedar Keys Hurricane, Sept. 1-7, 1950," Monthly Weather Review, Vol. 79, pp. 107-115.

R. C. Gentry, 1964: "A study of hurricane rainbands," National Hurricane Research Project Report, No. 69, U.S. Weather Bureau, 85 pp.

W. M. Gray, 1965: "Calculation of cumulus vertical draft velocities in hurricanes from aircraft observations," Journal of Applied Meteorology, Vol. 4, No. 4, pp. 463-474.

W. M. Gray, 1966: "On the scales of motion and internal stress characteristics of the hurricane," Journal of the Atmospheric Sciences, Vol. 23, pp. 278, 288.

W. M. Gray, 1967: "The mutual variation of wind, shear, and baroclinicity in the cumulus convective atmosphere of the hurricane," Monthly Weather Review, Vol. 95, No. 2, pp. 55-73.

H. Hawkins and D. Rubsam, 1968: Personal communication, to be published in the Monthly Weather Review in 1968.

L. A. Hughes, 1952: "On the low level wind structure of tropical storms," Journal of Meteorology, Vol. 9, Dec., pp. 422-428.

C. L. Jordan, 1958: "Mean soundings for the West Indies area," Journal of Meteorology, Vol. 15, pp. 91-97.

G. Korb and F. Möller, 1962: "Theoretical investigations of energy gain by absorption of solar radiation in clouds," Ludwig-Maximilious Universitat, Meteorologisches Institut, München, Germany, Contract DA-91-591-EUC-1621.

P. M. Kuhn and D. R. Johnson, 1966: "Improved radiometersonde observations of atmospheric infrared irradiance," Journal of Geophysical Research, Vol. 71, No. 2, pp. 367-373.

H. L. Kuo, 1965: "On the formation and intensification of tropical cyclones through latent heat release by cumulus convection," Journal of the Atmospheric Sciences, Vol. 22, pp. 40-63.

D. F. Leipper, 1967: "Observed ocean conditions and hurricane Hilda, 1964," Journal of the Atmospheric Sciences, Vol. 24, No. 2, pp. 182-196.

E. N. Lorenz, 1955: "Available potential energy and the maintenance of the general circulation," Tellus, Vol. 7, No. 2, pp. 157-167.

E. N. Lorenz, 1955: "Generation of available potential energy and the intensity of the general circulation," in Large Scale Synoptic Processes (J. Bjerknes, Project Director) Department of Meteorology, Final Report, 1957, Contract AF 19(604)-1286. University of California, Los Angeles, California.

J. S. Malkus, 1960: "Recent developments in studies of penetrative convection and an application to hurricane cumulonimbus towers," Cumulus Dynamics, Pergamon Press, pp. 65-83.

J. S. Malkus and H. Riehl, 1960: "On the dynamics and energy transformations in steady-state hurricanes," Tellus, Vol. 12, No. 1, pp. 1-20.

J. S. Malkus, C. Ronne and M. Chaffee, 1958: "Cloud patterns in hurricane Daisy," Tellus, Vol. 13, No. 1, 1961.

B. I. Miller, 1962: "On the momentum and energy balance of Hurricane Helene (1958)," National Hurricane Research Project Report No. 53, U.S. Weather Bureau, 19 pp.

Y. Ogura, 1964: "Frictionally controlled, thermally driven circulations in a circular vortex with applications to tropical cyclones," Journal of the Atmospheric Sciences, Vol. 21, pp. 610-621.

K. Ooyama, 1964: "A dynamical model for the study of tropical cyclone development" Proceedings of the Third Technical Conference on Hurricane Tropical Meteorology, Mexico City 6-12, June 1963.

B. I. Miller, 1964: "A study of the filling of hurricane Donna (1960) over land," Monthly Weather Review, Vol. 92, pp. 389-406.

E. Palmén, 1948: "On the formation and structure of tropical hurricanes," Geophysica (Helsinki), Vol. 3, pp. 26-38.

E. Palmén and C. Jordan, 1955: "Note on the release of kinetic energy in tropical cyclones," Tellus, Vol. 7, No. 2, pp. 186-188.

E. Palmén and H. Riehl, 1957: "Budget of angular momentum and kinetic energy in tropical cyclones," Journal of Meteorology, Vol. 14, pp. 150-159.

H. Riehl, 1954: Tropical Meteorology, McGraw-Hill, New York, 382 pp.

H. Riehl, 1959: "On production of kinetic energy from condensation heating," The Atmosphere and the Sea in Motion, Rockefeller Institute Press, New York, and Oxford University Press, London, pp. 381-399.

H. Riehl and J. S. Malkus, 1961: "Some aspects of hurricane Daisy, 1958," Tellus, Vol. 13, No. 2, p. 181-213.

V. E. Suomi and P. M. Kuhn, 1958: "An economical net radiometer," Tellus, Vol. 10, No. 1, pp. 160, 163.

M. Yanai, 1964: "Formation of tropical cyclones," Reviews of Geophysics, Vol. 2, No. 2, pp. 367-414.

PROFILES OF INFRARED IRRADIANCE AND COOLING THROUGH A JET STREAM

Donald R. Johnson
Department of Meteorology
University of Wisconsin

William C. Shen*
Control Data Corporation

ABSTRACT

Vertical atmospheric cross sections of upward, downward and net infrared irradiance, infrared cooling, temperature, potential temperature, and water vapor through a jet stream are constructed for 7 and 9 January, 1961, along a line from International Falls to Willemsted, Curacao. The profiles of irradiance and infrared cooling determined from filtered radiometersonde measurements clearly portray the influence of clouds. Variations of infrared irradiance and cooling associated with the zonal, secondary and convective scales are discussed. Primarily attention is focused on radiation features associated with the jet stream and its associated cloud distribution. The contrast between profiles of net irradiance and infrared cooling between clear and cloudy regions is clearly portrayed. The range of infrared heating at the base of the clouds to the cooling at the top of the clouds exceeds 5-7° C/day. Appreciable variations of infrared cooling are found in the stratosphere indicating the presence of water vapor, dust, tenuous cirrus or other attenuating particles. The data indicates that a major factor controlling the horizontal variations of stratospheric infrared cooling is the high level cloudiness. The presence or absence of high level clouds primarily controls the source of infrared energy emitted from the earth and the troposphere, i.e., the upward irradiance which is available for stratospheric absorption.

*The research presented in this paper was conducted while the author was a member of the Department of Meteorology at the University of Wisconsin.

INTRODUCTION

Of the diabatic processes occurring in the earth-atmosphere system, infrared emission alone serves to discharge the thermal energy. A question of considerable significance is whether infrared emission is important in determining the various modes of the atmosphere's circulation, or is merely a passive physical process to extract heat from the system. Presently the question is unanswered. However, from certain physical considerations, it is known that its dynamic importance is a function of scale size. With the recent addition of satellite radiation information, added impetus in the search for the determination of the importance of infrared processes is occurring. However, observational studies using satellite irradiance information can only describe the horizontal variation of the various components of irradiance at the atmosphere's fringe (Winston and Rao [24]; Allison, Gray and Warnecke [1]; Astling and Horn [2]) even though vertically the atmosphere is a highly nonisotropic radiator.

The purpose of this study is threefold: 1) to present a synoptic description of the vertical distribution of infrared irradiance to emphasize its nonisotropic structure, 2) to aid in the interpretation of the satellite's vertically integrated irradiance observations, and 3) to further elaborate on the irradiance processes associated with different scales (Kuhn and Suomi [6]). Primary attention is given to the infrared processes associated with the jet stream. However, the infrared structure of larger and smaller scales is evident from the analyses. The sparsity of radiometersonde data in time and space allows only tentative statements concerning infrared processes and the scales of motion. Still, we are satisfied that the analyses portray many interesting features that are important and that radiometersonde data supplementing satellite irradiance data on a synoptic scale would be valuable for both research and operational purposes.

ANALYSES AND DATA

Vertical cross sections portraying the fields of upward, downward and net infrared irradiance and the instantaneous infrared cooling, as well as the temperature, potential temperature, water vapor and wind fields are prepared along a line from the northernmost station, International Falls, to the southernmost, Willemstad, Curacao. The data for the vertical cross sections were provided by radiometersonde flights at International Falls, Peoria, Nashville, Montgomery, Grand Cayman, and Willesmstad at the regularly scheduled synoptic times of 0000Z, 7 and 9 January, 1961. Supplementary 0000Z data were provided by the radiosonde flights at Green Bay and Tampa. Filtered estimates of the

irradiance components and infrared cooling were determined from radiometersonde data using the polynomial filtering technique described by Kuhn and Johnson [10]. The frequency response of this polynomial filtering technique for the radiometersonde data is 0.23 for a vertical wavelength of 0.8 km, 0.65 for 1 km and 0.92 for 1.6 km.

Surface and constant pressure charts based on analyses from the National Meteorological Center are presented with slight modifications in Figures 1 through 3. Since our purpose is to discuss several characteristic features of the irradiance field, synoptic considerations are limited to a brief discussion of the broad scale circulation features of 7 and 9 January, 1961.

SYNOPTIC DISCUSSION

On the 0000Z surface chart for 7 January, Figure 1, the predominant surface features are the high pressure area located in the Southeastern U.S. and a developing low pressure area in Northern Minnesota. The high pressure area centered in Georgia was of maritime polar origin, having migrated from the Pacific across the Southwest U.S. Since the high was slowly weakening, the developing low pressure area was the dominant surface feature by 8 January, 1961. By 9 January the Minnesota low pressure area moved eastward to the Nova Scotia peninsula and deepened from a central pressure of 1002 mb on the 7th to 998 mb on the 9th (see Figure 2). The cold front trailed southwestward over the Atlantic Ocean to northern Florida with the extremely cold continental arctic (cA) air and the overlying, deep tropospheric, continental polar (cP) air having moved behind the cold front from the lee of the Canadian Rockies southeastward over the eastern half of the U.S. The high pressure center of 1041 mb remained in Canada and by virtue of its strength and position continued to feed cold air from Canada to the eastern U.S. Another surface feature of interest was the weak stable wave in the Gulf of Mexico east of Brownsville. On 7 January the stationary portion of an old polar front extending from the central North Atlantic into the Gulf of Mexico was undergoing frontolysis, but since the stable wave had vertical continuity to the cut-off 500 mb low over western Texas (Figure 3), it maintained its identity.

At the 500 mb level on 7 January, Figure 3, two distinct trajectories were embedded in the westerly flow over the eastern half of the U.S. One trajectory from the west-northwest was associated with the polar jet which was located in the upper troposphere along the northern U.S. border above the north-south temperature contrast between the maritime polar (mP) air over the central United States and the colder cP air

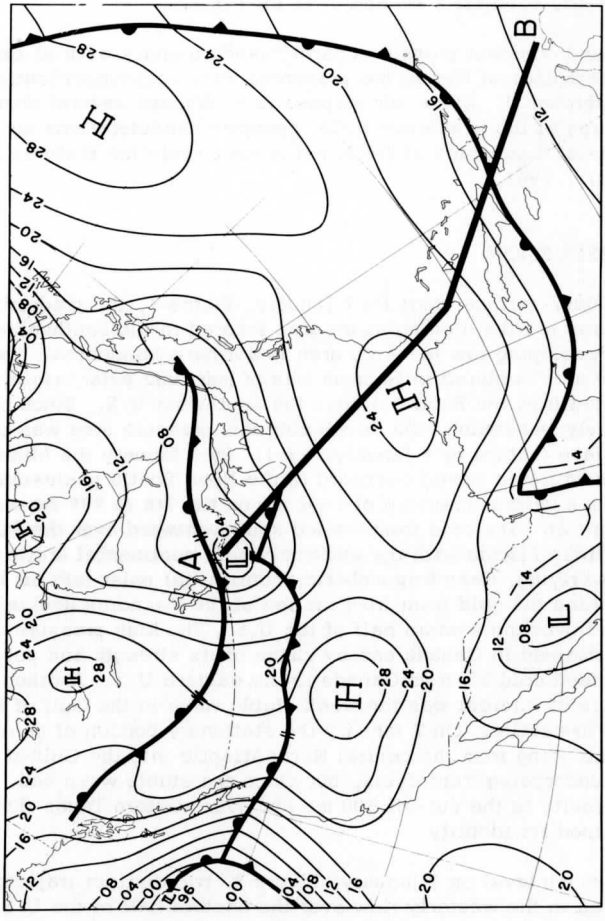

Figure 1. Surface chart, 0000Z, 7 January 1961. Solid line from A to B is the position of the vertical cross section.

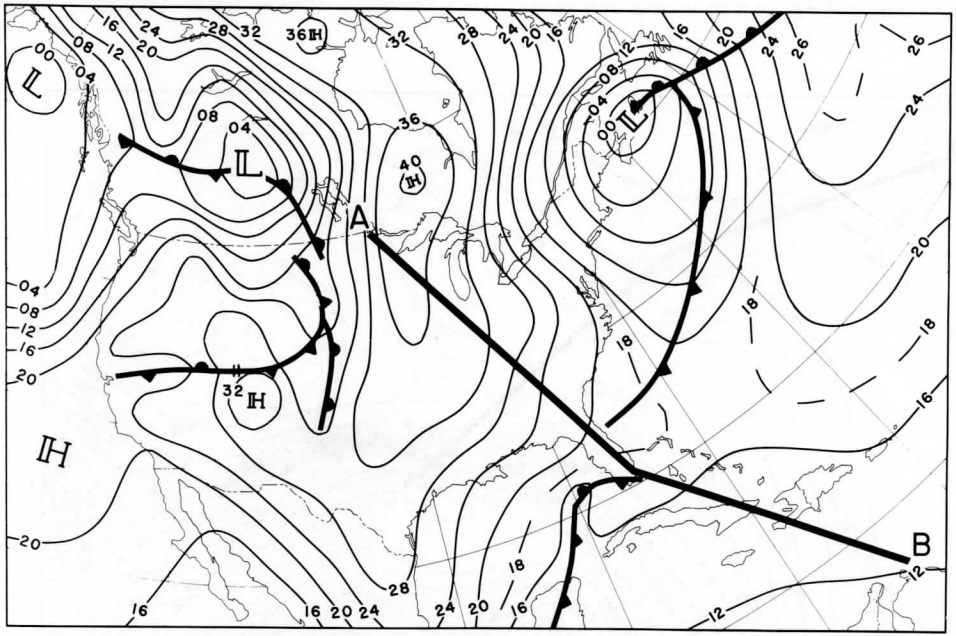

Figure 2. Surface chart, 0000Z, 9 January 1961. Solid line from A to B is the position of the vertical cross section.

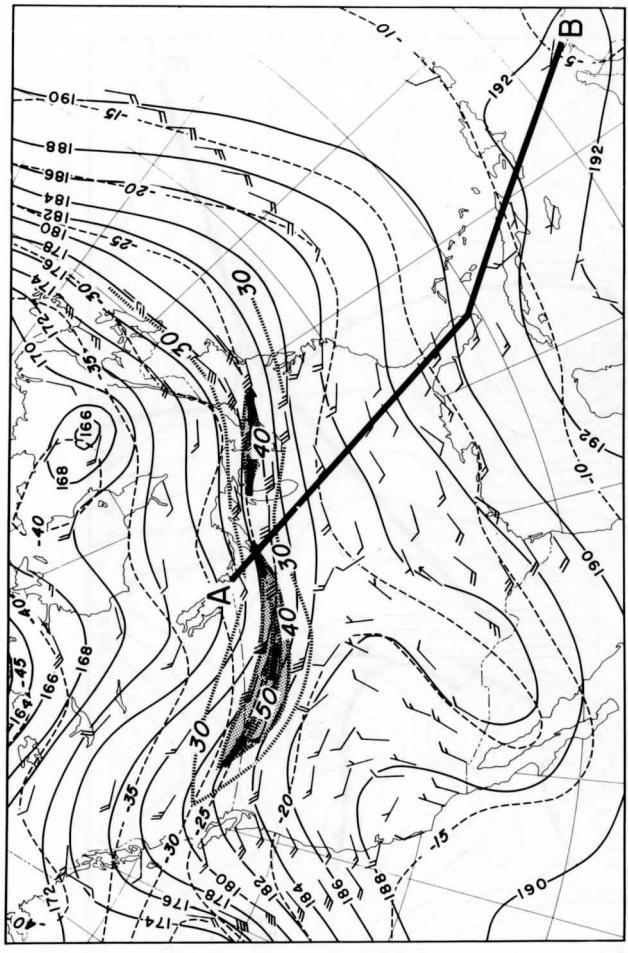

Figure 3. 500 mb chart, 0000Z, 7 January 1961. Solid line from A to B is the position of the vertical cross section.

over Canada. The maximum velocity of the jet was approximately 45 m/sec at the 300 mb level over Green Bay. In all analyses shaded regions indicate wind speeds greater than 40 m/sec.

Further south, the other trajectory was associated with the high tropospheric subtropical jet. The subtropical jet was situated above a weak baroclinic zone in the middle and upper troposphere between the mP air over the central U. S. and the maritime subtropical (mT) air of the Caribbean. At 200 mb, the upper tropospheric jet extends along the Gulf and appears as a broad band of moderate velocities with a maximum near 55 m/sec.

By the 9th, the two jets had merged into a broad band of maximum winds with a particularly complicated structure as the cold polar air of the upper troposphere moved over the eastern U. S. The sequence of events during the 48 hour period and pattern of the merged jets is similar to that described by Reiter [13]. The maximum wind velocities are located at the southern edge of the strongly developed cold upper-level trough lying over the New England States. The subtropical portion of the merged jet at the 200 mb surface on the 9th, had velocities in excess of 70 m/sec as the frontal zones become juxtaposed and the baroclinicity of the polar front intensified.

TEMPERATURE, WIND, POTENTIAL TEMPERATURE AND WATER VAPOR ANALYSES

The 0000Z cross-sectional analyses of the temperature and wind field for 7 and 9 January, are presented in Figures 4 and 6 while the corresponding analyses of potential temperature and water vapor are presented in Figures 5 and 7. The 0000Z surface observation and station locator numbers are shown at the base of Figures 4 and 6. The station names, locator numbers, latitude, and scale are shown on all other cross-sections as well as the maximum wind regions to be able to locate pertinent features with respect to the jet's position.

The leading and rear boundaries of the frontal zones are indicated by the heavy solid lines while the heavy dashed lines indicate tentative boundaries of frontal zones with weaker thermal support. The heavy dashed line on the cross-sections for the 7th indicates the upper boundary of a bubble of a very shallow modified cA air associated with a previous arctic outbreak. The polar frontal zone over Green Bay separates the extremely cold shallow cA and deep tropospheric cP air to the north from the modified mP air over the central U. S. As noted before, the temperature contrast between mP air over the U. S. and the mT air over

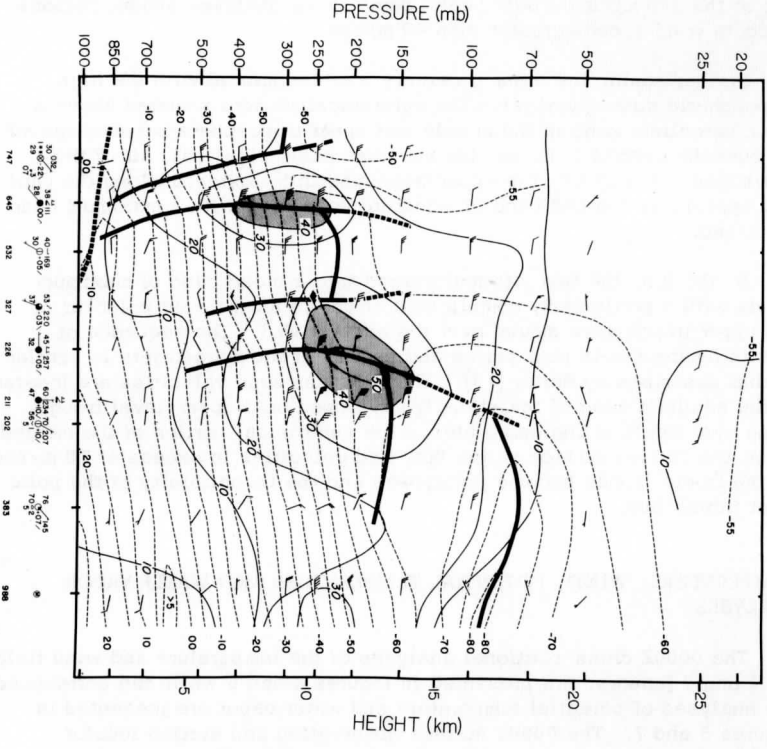

Figure 4. Temperature (°C) and wind (m/sec) analysis, 0000Z, 7 January 1961. For the plotted winds whole barbs indicate 10 m/sec., half barbs indicate 5 m/sec. Shaded regions delineate region of wind speeds greater than 40 m/sec. Heavy solid vertical lines indicate leading and rear boundaries of frontal zones with strong thermal support, dashed lines indicate frontal zones with weak thermal support. Heavy solid horizontal lines indicate tropopause.

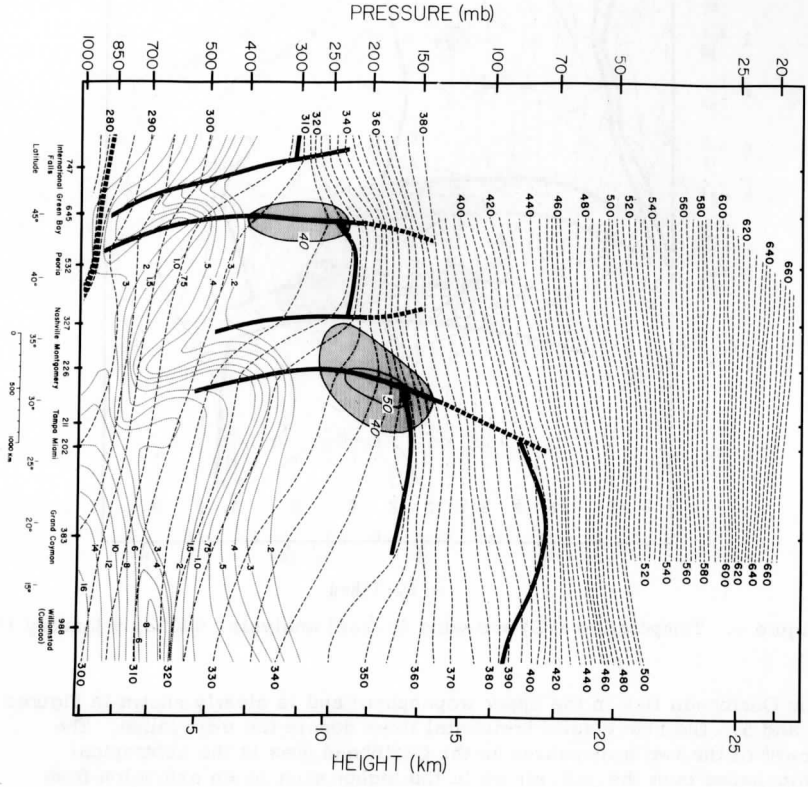

Figure 5. Potential temperature (°K) and water vapor (gm/kg) analysis, 7 January 1961.

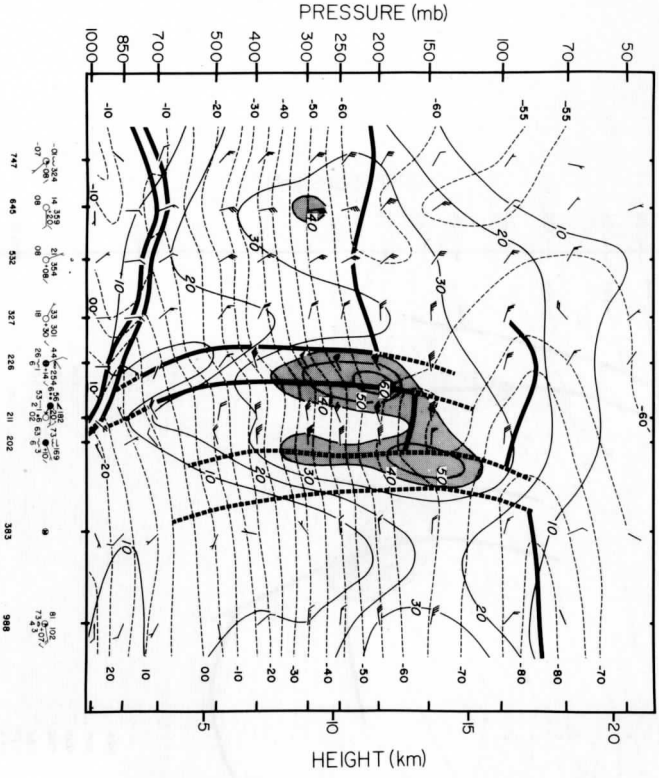

Figure 6. Temperature (°C) and wind (m/sec) analysis, 0000Z, 9 January 1961.

the Caribbean lies in the upper troposphere and is clearly shown in Figures 4 and 5. The heavy solid horizontal lines denote the tropopause. The lower of the two tropopauses in the Caribbean area is the subtropical tropopause over the mT air while the higher must be an extension from the low latitudes of the very high tropical tropopause.

The rising warmer moist air south of the two frontal zones on the 7th and of the polar front on the 9th is clearly delineated from the subsiding dryer air to the north by the water vapor analysis. The observations for Green Bay and Montgomery on the 7th and Montgomery on the 9th indicated increasing moisture with height as the radiosonde ascended through the frontal zones. Thus, the maximum horizontal gradient of the moisture field was positioned in the frontal zones. The water vapor contrast across the front indicating the opposing vertical motions, is likely evidence of a

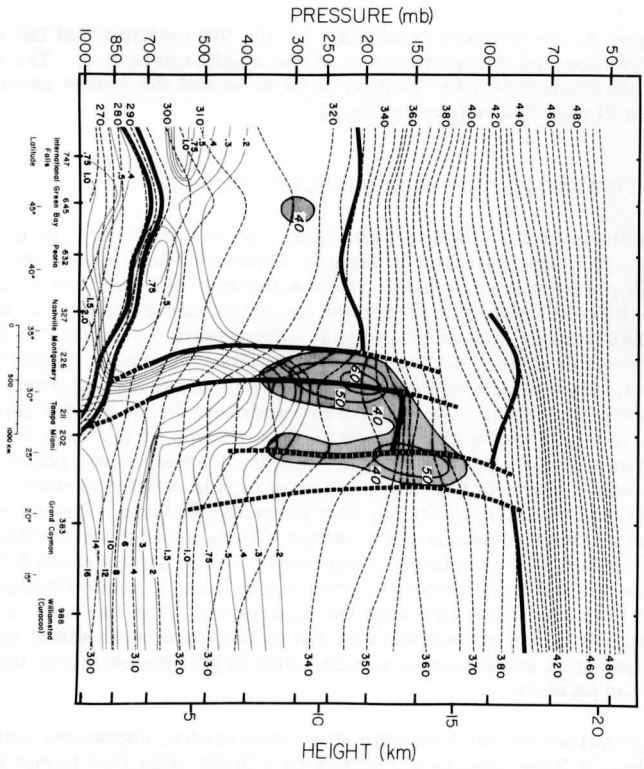

Figure 7. Potential temperature (°K) and water vapor (gm/kg) analysis, 0000Z, 9 January 1961.

thermally direct vertical circulation of the type proposed by Eliassen [5]. From quasi-geostrophic theory Eliassen notes that a transverse circulation of the direct type should exist for tropospheric cold fronts.

At the base of Figure 4, the surface weather conditions on the 7th indicate a region of extensive cloudiness north of Green Bay associated with the developing unstable wave. The other area of extensive cloudiness from Nashville to Tampa was associated with the subtropical jet. Generally fair weather conditions existed from just south of Green Bay to Nashville and to the south of Tampa. The cloudy and precipitating regions are emphasized since these conditions greatly attenuate the components of infrared irradiance.

In Figure 6, the weather conditions for the 9th indicate that the region of extensive cloudiness was confined to the southeastern U. S. The cloudiness was associated with the trailing polar front and the stable wave off the western Florida coast (see Figure 2).

UPWARD, DOWNWARD AND NET IRRADIANCE PROFILES

The profiles of the upward, downward, and net irradiance (ly/min) for 7 January, 1961, are portrayed in Figures 8 through 10. Profiles for the 8th and 9th were prepared to study the continuity of the irradiance fields. However, the results are not presented since the time continuity is excellent and they display similar processes. The principle variation in the cross-sections of upward and downward irradiance occurs in the vertical with the magnitude of the components of irradiance decreasing from the earth's surface upwards. The well known decrease in the upward directed irradiance is explained by the absorption of a portion of the earth's black body radiation by the intervening constituents of water vapor, carbon dioxide, ozone, particulates and sometimes clouds and the re-emission of a portion of the absorbed energy at a lower temperature. Exceptions to the general decrease upwards occur within clouds and the stratosphere where the upward flux is relatively constant. In the stratosphere the upward flux occasionally increases after the balloon ascends through an upper cloud boundary that lies near the tropopause. The increase of upward irradiance in the stratosphere is due to the increased radiant energy being emitted from stratospheric regions with higher temperatures than the cloud top temperature.

The magnitude of the downward irradiance always decreases with height unless a layer effectively acting as a black body lies higher in the atmosphere. Such conditions are associated with cloud layers embedded within inversions or an isothermal layer within which the density of absorbing constituents increases with height. The latter condition is indicated for the tropical stratosphere in Figure 9. The magnitude of the change is so small that the event can be explained as a presence of random instrumental errors. However, in this example and other data, there were changes in both the upward and downward irradiance which indicates significant and unexplained variations of stratospheric dust, water vapor or possibly tenuous cirrus clouds.

In contrast to the decrease of upward and downward irradiance with height, the net irradiance usually increases with height (see Figure 10). This is because the rate of decrease with height of downward irradiance is greater than that for the upward component. Exceptions to this condition occur in the vicinity of clouds.

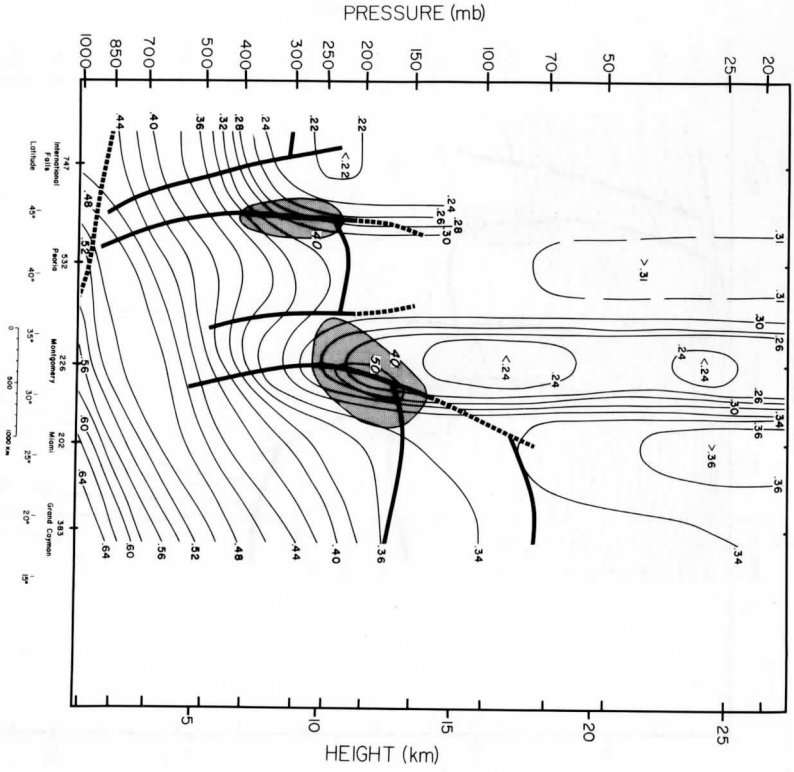

Figure 8. Upward irradiance (ly/min) analysis, 0000Z, 7 January 1961.

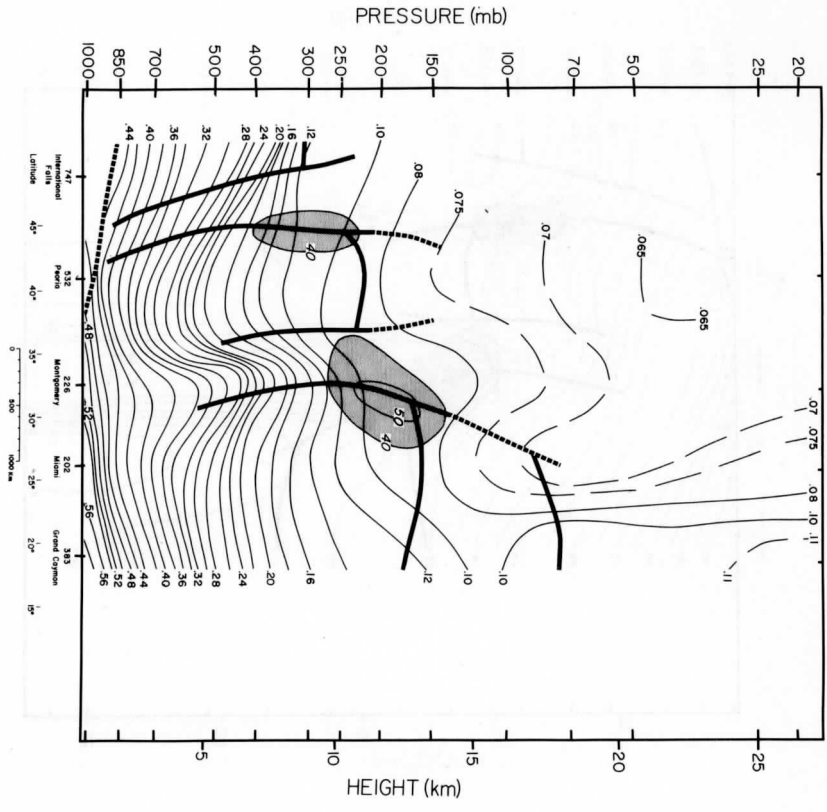

Figure 9. Downward irradiance (ly/min) analysis, 0000Z, 7 January 1961.

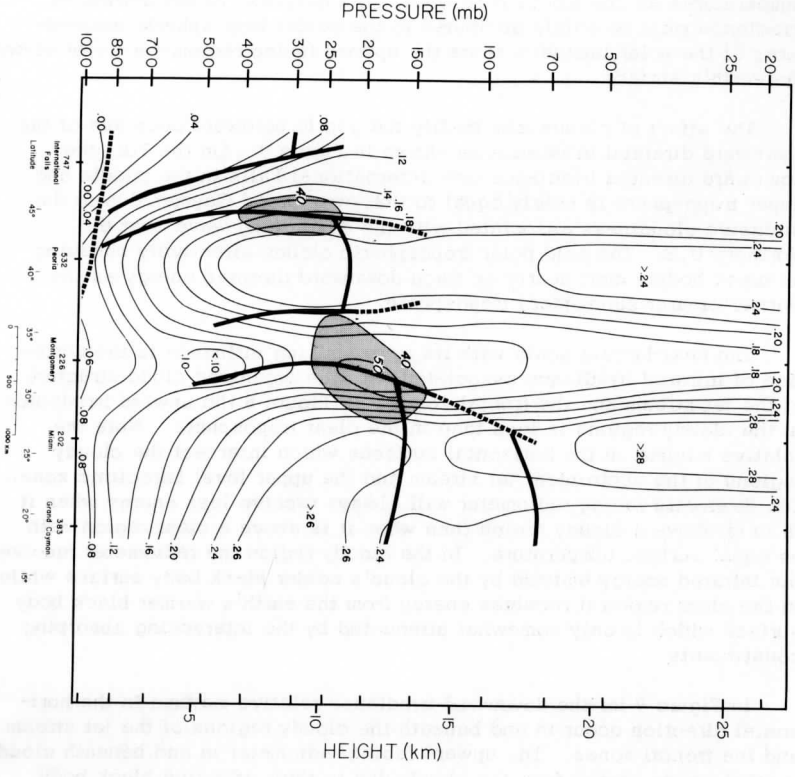

Figure 10. Net irradiance (ly/min) analysis, 0000Z, 7 January 1961.

The variation in the irradiance components associated with the largest scale, the hemispheric scale, is usually a poleward decrease at all elevations of the upward, downward, and net irradiance. The variation of the upward directed irradiance is due to the decreasing infrared emission associated with the colder surface and tropospheric temperatures as one moves northward. The decrease of the downward irradiance must be solely attributed to the colder tropospheric temperatures of the polar latitudes since the upward facing radiometer never views the earth's surface.

The effect of clouds may modify the gentle poleward decrease of the downward directed irradiance as shown in Figure 9. On the 7th, the downward directed irradiance over International Falls in the middle and upper troposphere is nearly equal to that over Grand Cayman due to the intensive cloudiness associated with the developing wave over the Northern U. S. The cold polar tropospheric clouds effectively behaving as black bodies emit nearly as much downward directed energy as the warmer clearer subtropical troposphere.

The next largest scale with its more striking influence is the variation of infrared irradiance associated with the organized cloud structure of the jet stream and the frontal zones. In Figure 8 the upward irradiance in the cloudy regions is less than in the clear troposphere. Note the relative minima on the horizontal surfaces which intersect the cloudy regions of the subtropical jet stream and the upper level baroclinic zone. The downward facing radiometer will always receive less energy when it is in or above a cloudy region than when it is above a clear region with an equal surface temperature. In the cloudy region the radiometer receives the infrared energy emitted by the cloud's colder black body surface while in the clear region it receives energy from the earth's warmer black body surface which is only somewhat attenuated by the intervening absorping constituents.

In Figure 9 for the downward irradiance relative maxima in the horizontal direction occur in and beneath the cloudy regions of the jet stream and the frontal zones. The upward facing radiometer in and beneath clouds receives more energy from the clouds due to their effective black body behavior than if it were at an equivalent pressure surface with a clear overlying atmosphere. The greatest contrasts for the horizontal variation of downward irradiance occur in the high troposphere and are depicted in the irradiance cross sections above Montgomery on the 7th.

The effects of high and middle clouds are even more striking in the profiles of net irradiance in Figure 10. On the 7th in the free atmosphere the minimum values of net irradiance on a horizontal surface occur within

the multi-layer cloud structure over Montgomery and International Falls. Note that snow is falling at International Falls. The effect of organized middle and high level clouds on the upward irradiance near the top of the atmosphere for this scale of motion is clearly portrayed by the magnitude of the upward irradiance at the top of Figure 8. At the 150 mb level a minimum value of approximately .24 ly/min of upward irradiance is indicated over the subtropical jet while a maximum value of .35 ly/min is indicated for the subtropical Caribbean, these are representative values that are observed by the satellite infrared sensors.

INFRARED COMPONENT OF ATMOSPHERIC HEATING

As noted in the introduction, the sole component of diabatic heating that serves to discharge thermal energy from the earth-atmosphere system is that due to infrared emission. Lorenz [9] and others have considered the problem of explaining why the intensity of the atmosphere's circulation is so low in comparison to the total energy received and emitted by the atmosphere. Our purpose is not to explore this question but to note that the role of infrared emission is a fundamental consideration in the answer to this problem. From classical thermodynamic considerations, the efficiency of the "thermodynamic engine" in producing mechanical energy not only depends on the temperature at which the heat is added but also on the temperature at which it is extracted. The coupling process for the thermal energy source and sink which produces the mechanical energy is the adiabatic expansion phase. These fundamental thermodynamic considerations were emphasized by Mintz [10] and the importance of these considerations in the generation of available potential energy for the atmosphere's circulation is evident in the results of Dutton and Johnson [4]. From the concept of available potential energy as a basis for their diagnostics, they obtained a generation due to the infrared component of 1.61 watts/m^2, which was 29 percent of the total generation of zonal available potential energy. The large positive value is due to the efficiency of the generation process in the cold polar troposphere coupled with the significant infrared emission from that portion of the atmosphere.

At scales of atmospheric motion intermediate to the zonal and the cloud convection scale the importance of infrared cooling is largely undetermined. However, the cross-sections of instantaneous infrared cooling due to the infrared divergence for both the 7th and 9th of January are presented to gain some insight into representative values for the large planetary, secondary and convective scales of the atmosphere.

In the cross-section of infrared cooling for the 7th and 9th (Figure 11 and 12) the dominant patterns are due to the effects of clouds. To a lesser degree there is a hemispheric scale associated with the poleward decrease of temperature for on the 9th the mean cooling of the subtropical region is approximately 1.7° C/day while it is near 1.0° C/day in the polar region.

The effects of clouds on the 9th is evidenced by the heating of 3° C/day at the base of the middle cloud and the cooling of 4 to 5° C/day at the top of the multi-layered clouds over Miami. Undoubtedly this vertical variation of the infrared component of diabatic heating is important in determining the structure and intensity of the ascending and descending motions within the cloud by which latent heat is released and both water vapor and sensible heat are redistributed through the cloud destabilization process. The rate of destabilization is greater the higher the cloud (Moller [11]) and the larger its effective emissivity. In addition, the process is enhanced when the clouds are above warm surfaces as over Florida and the tops reach the high troposphere so there is little back radiation from the overlying atmospheric mass to offset the effective black body cooling of the cloud top. The destabilization process is also portrayed to a lesser extent by the profile of infrared cooling above International Falls on the 7th. In this case, there is little heating at the cloud's base since the clouds are multilayered and over a snow covered surface. Thus the differences in the upward impinging irradiance and the downward emitted irradiance at the cloud's base over International Falls is much less than at the middle cloud base above Miami the 9th.

One interesting feature of the cooling profile on the 7th (Figure 11) is the small positive heating of 1.0°/day near 550 mb over Montgomery. The only cloud reported at 0000Z is a high overcast of cirrostratus. The first indication of lower clouds is an observation at 0340Z of 8/10 coverage of altocumulus with an estimated base of 18,000 ft. The two possibilities are that either the observer missed the lower deck of clouds under the cirrostratus overcast in his night-time observation at 0000Z or the radiometer is sensing the moisture contained in an isentropic layer that is being advected ahead of the visible cloud structure. The latter explanation seems preferable since the cirrostratus is reported to be a high overcast from before sunset to 0140Z, then broken between the 0140Z observation and the 0340Z observation. This indicates that the observer was able to estimate some characteristics of the cloud structure in his night-time observation, thus adding evidence to his observation of no reportable clouds below the high cirrostratus overcast.

In both Figures 11 and 12, a slight heating of the region near the tropopause is indicated. On the 7th the heating rate is generally positive but less than 1° /day. On the 9th higher heating rates are indicated

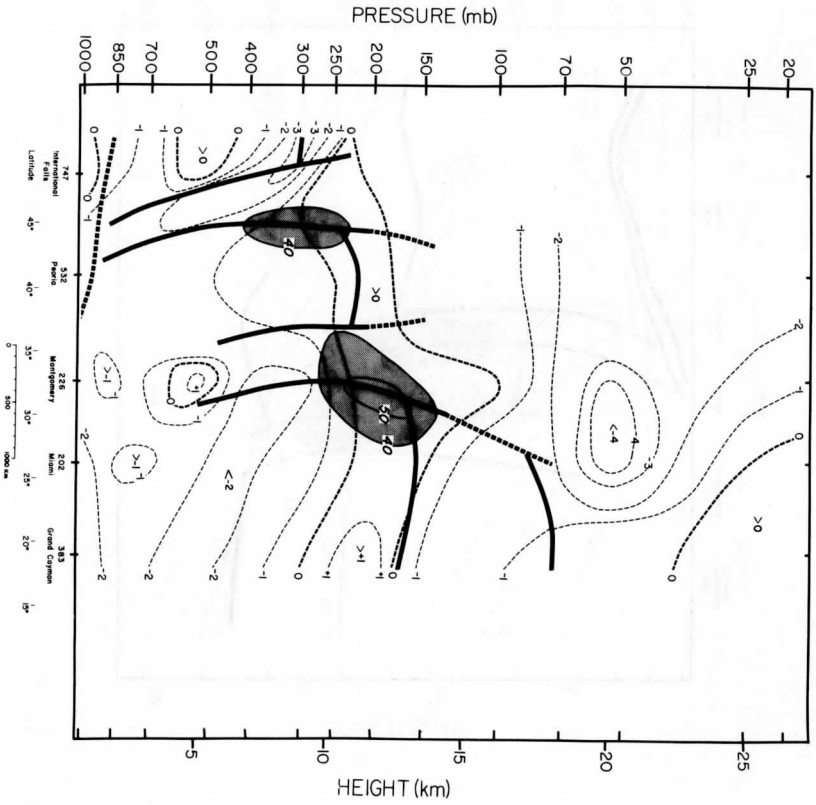

Figure 11. Analysis of instantaneous atmospheric heating (°C/day) by net irradiance divergence, 0000Z, 7 January 1961.

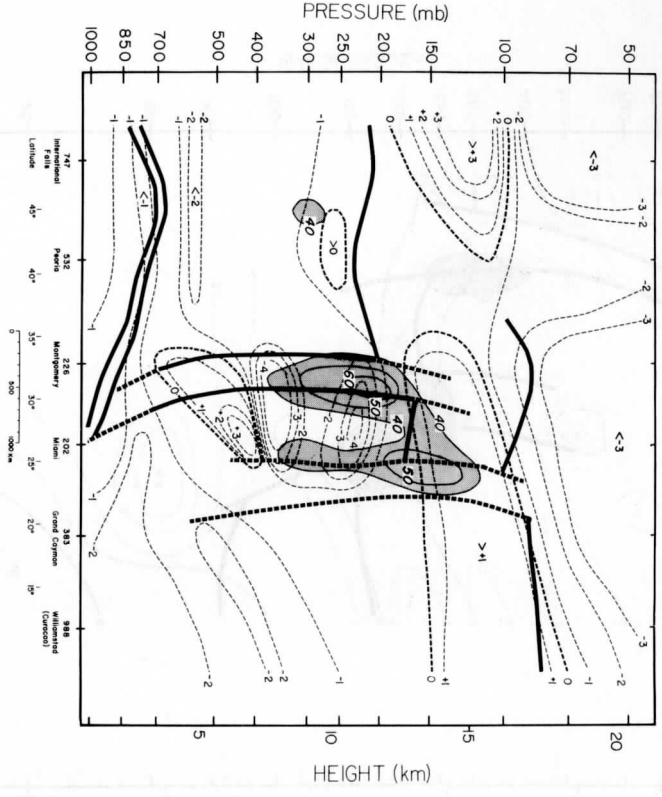

Figure 12. Analysis of instantaneous atmospheric heating (°C/day) by net irradiance divergence, 0000Z, 9 January 1961.

although less clearly organized. These results agree with Darkow's conclusion [3] that the infrared component generally serves to heat the region of the tropopause.

One of the most interesting but speculative results of this study is the stratospheric field of infrared cooling on the 9th. On both the 7th and 9th (Figures 11 and 12) relative intense cooling is indicated for the stratospheric region near 20 km above the high clouds of the subtropical jet. The actual magnitude of the cooling may be questionable since the cooling estimates for the stratospheric region are less reliable then for tropospheric regions and the sounding at Miami terminated before reaching 50 mb. However, the data indicates that the cooling rates of the stratospheric regions above high tropospheric clouds tend to exceed the cooling rates above clear areas. This difference can be partially attributed to the fact that there is 30 - 50% less upward directed irradiance to be absorbed by the stratospheric mass over the high cloudy regions than over a clear area with a high surface temperature. Quite likely there must also be a higher concentration of the variable effective emitters, either particulates, ozone, water vapor or ice crystals, to account for the increased loss of radiant energy in localized regions of the stratosphere.

Another interesting feature in Figure 12 is the region of heating and cooling in the stratospheric air above International Falls on the 9th. In the surface observation, high thin cirrus is reported one hour prior to 0000Z but at 0000Z only a layer of 2/10 altocumulus at 8000 ft. is reported. The most likely explanation for the heating and cooling in the stratospheric regions is that tenuous cirrus actually exists in the stratosphere near 100 mb. On the surface chart for the 9th, Figure 2, a weak occluded system lies over the western Dakotas. The subtropical tropopause associated with this system is near 100 mb, thus indicating that the attenuating layer over International Falls near 100 mb may be a tenuous layer of cirrus being advected isentropically ahead of the occluded system into the stratospheric regions over the cold polar air mass. This process associated with the secondary circulation scale serves to inject water vapor from the troposphere into the stratosphere and can be readily detected by radiometersonde observations.

RELATIONSHIP OF SATELLITE AND RADIOMETERSONDE IRRADIANCE OBSERVATIONS

Radiometersonde observations of upward irradiance high in the stratosphere above any organized attenuating layers are directly comparable with satellite infrared observations if certain geometrical relations are satisfied and both instruments possess similar spectral sensitivity. The horizontal variations of the absorbed and re-emitted energy of the intervening mass between a radiometer high in the stratosphere and a satellite are extremely small in comparison to the magnitude range of both observational series.

Our immediate purpose in this discussion is to illustrate how satellite irradiance data contains information for locating jet streams if associated cloud patterns are present. Previous results indicate that both cloud photographs (Oliver, Anderson and Ferguson [12]; Whitney, Timchalk and Gray [15]) and satellite radiation data (Allison, Gray and Warnecke [1]) are useful for locating the jet stream axis. Whitney, et al., present an excellent summary and discussion of the physical processes that produce characteristic cirrus shield with a sharply defined poleward edge. Although both location techniques primarily depend on the presence of a cirrus shield, the two techniques used jointly will provide greater reliability than each used separately. Our upward irradiance cross-section, Figure 8, illustrates the effects of organized clouds in creating variations in the upward irradiance field of the stratosphere. Since the same cloud features will produce similar variations in the satellite observational series, the radiometersonde values at the top of the cross section can be considered representative of satellite data. Spectrally, such a given hypothetical satellite series is comparable to TIROS II channel 4 observations of the 7-32 micron region of the terrestrial infrared spectrum (TIROS II Radiation Data User's Manual [14]).

Returning to Figure 8 for the upward irradiance, and assuming that the values of the upward irradiance at the top of the cross-section are representative of the satellite observations, it is apparent that the effect of clouds associated with the jet stream produce significant variations in the hypothetical satellite irradiance. In Figure 8 the upward irradiance between the cloudy and clear regions of the subtropical Caribbean ranges from approximately .24 to .34 ly/min. These are representative values observed by the satellite experiments. Note that the maximum gradient is located at the equatorward edge of the jet stream which agrees with Winston's [17] result that the magnitudes of the westerlies and the gradient of upward irradiance observed by satellites are positively correlated. The effects of high clouds in producing variations in satellite observations will be the greatest when the

contrast between the background upward irradiance of the earth surface and the cloud top irradiance is greatest. Thus, the larger the difference in the equivalent black body temperatures of the two radiating surfaces, the better is the detection capability. Subtropical jets should be easier to detect than polar jets since the contrast in the upward irradiance emitted by the jet stream cirrus shield and the earth's tropical surface is greater than the corresponding contrast at higher latitudes. Furthermore the usually more dense subtropical cirrus shield lying higher in the troposphere will probably possess the coldest equivalent black body temperatures. The latter condition partially depends on the effective emissivity of the cloud layer (Kuhn and Suomi [7]). For a jet stream over a very cold surface, a cyclonic upper level cold core vortex with extensive clouds or any similar low valued irradiance background region, the satellite irradiance location technique may fail to discriminate the jet stream location. Satellite data may also fail over jet cores that do not have high level clouds to produce attenuation of the irradiance field. The satellite irradiance data would be particularly valuable when photographic techniques fail because the shadow cast on lower cloud surfaces or on the earth (Whitney et al., [15]) cannot be detected due to an unfavorable geometric arrangement of the sun, earth and satellite. Furthermore, at night, the irradiance data is the only satellite observation that can provide information on the detection of this important feature.

CONCLUDING REMARKS

While not emphasized, the fields of the irradiance components and infrared cooling were all determined from filtered radiometersonde data. From the detailed structure shown in the cross sections, it is clear that the use of filtering polynomials does not obscure the basic structure of the fields even in the vicinity of the cloud boundaries. Without filtering, it is not possible to determine the detailed structure of the infrared cooling profiles due to the dominating effects of the random error component.

In conclusion, we simply note that our threefold purpose presented in the introduction was fulfilled. The results presented are tentative due to the sparsity of data in time and space, but they portray a new dimension of information for the zonal, secondary and convective scales that would be extremely valuable for both research and operational purposes in meteorology.

ACKNOWLEDGMENTS

We wish to express our appreciation to Professors V. E. Suomi and L. H. Horn of the University of Wisconsin for their encouragement in the preparation of this paper. We gratefully acknowledge the assistance of Messrs. Charles Hutchins, David Barber, Mark Lipschutz and Miss Susan Koebel in the preparation of the data and drafting, and of Dr. Peter M. Kuhn in making available the radiometersonde data.

This work was supported by the Environmental Sciences Services Administration through WBG's 25 and 52.

BIBLIOGRAPHY

1. Allison, L. J., T. I. Gray, Jr. and G. Warnecke, 1964: "A quasi-global presentation of TIROS III radiation data," NASA SP-53, Goddard Space Flight Center, NASA, Greenbelt, Maryland.

2. Astling, E. G. and L. H. Horn, 1964: Some geographical variations of terrestrial radiation measured by TIROS II, Journal of Atmospheric Sciences, Vol. 21, No. 1, pp. 30-34.

3. Darkow, G. L., 1963: A study of infrared measurements in the vicinity of the subtropical tropopause. Ph.D. thesis, Department of Meteorology, University of Wisconsin.

4. Dutton, J. A. and D. R. Johnson, 1967: The theory of available potential energy and a variational approach to atmospheric energetics, Advances in Geophysics, Vol. 12, pp. 333-436.

5. Eliassen, A., 1962: On the vertical circulation in frontal zones, V. Bjerknes Cent. Vol., Geofys. Publikasjones, Norske Videnskaps Akad. Oslo, Vol. 24, pp. 148-160.

6. Kuhn, P. M. and Suomi, V. E., 1960: Infrared radiometer soundings on a synoptic scale, Journal of Geophysical Research, Vol. 65, No. 11, pp. 3669-3677.

7. Kuhn, P. M. and V. E. Suomi, 1965: Airborne radiometer measurements of effects of particulates on terrestrial flux, Journal of Applied Meteorology, Vol. 4, No. 2, pp. 246-252.

8. Kuhn, P. M. and D. R. Johnson, 1966: Improved radiometersonde observations of atmospheric infrared irradiance, Journal of Geophysical Research, Vol. 71, No. 2, pp. 367-373.

9. Lorenz, E. N., 1960: Generation of available potential energy and the intensity of the general circulation. In Dynamics of Climate (R. L. Pfeffer, ed.), Pergamon Press, Oxford, pp. 86-92.

10. Mintz, Y., 1947: On the kinematics and thermodynamics of the general circulation of the atmosphere in the higher latitudes, Transactions, American Geophysical Union, Vol. 28, No. 4, pp. 539-544.

11. Moller, F., 1951: Long wave radiation, Compendium of Meteorology, American Meteorological Society, Boston, Massachusetts, pp. 34-39.

12. Oliver, V. J., R. K. Anderson and E. W. Ferguson, 1964: Some examples of the detection of jet streams from TIROS photographs, Monthly Weather Review, Vol. 92, No. 10, October 1964, pp. 441-448.

13. Reiter, Elmar R., 1963: Jet Stream Meteorology, University of Chicago Press, Chicago.

14. Staff Members, 1961: TIROS II radiation data user's manual, Goddard Space Flight Center, Greenbelt, Maryland, p. 57.

15. Whitney, L. T. Jr., A. Timchalk and T. I. Gray Jr.: On locating jet streams from TIROS photographs, Monthly Weather Review, Vol. 94, No. 3, pp. 127-138.

16. Winston, J. S. and K. Rao, 1962: Preliminary study of planetary-scale outgoing longwave radiation as derived from TIROS II measurements, Monthly Weather Review, Vol. 90, No. 9, pp. 307-310.

17. Winston, J. S., 1967: Zonal and meridonal analysis of 5-day averaged outgoing longwave radiation data from TIROS IV over the Pacific sector in relation to the northern hemisphere circulation. Journal of Applied Meteorology, Vol. 6, No. 3, pp. 453-563.

Scanner's note:

This page is blank.

JOURNAL OF GEOPHYSICAL RESEARCH VOL. 71, NO. 24 DECEMBER 15, 1966

The Effect of Bias and Random Radiometersonde Temperature Errors in the Estimation of Atmospheric Downward, Upward, Net, and Equivalent Infrared Irradiance

DONALD R. JOHNSON

Department of Meteorology, University of Wisconsin, Madison

The effects of instrumental errors of the radiometersonde on the downward, upward, net, and equivalent irradiance estimates of the true atmospheric infrared radiative functions are presented. The first and second moments of the irradiance error distributions are related to the moments of the radiometersonde temperature error distributions. Bias irradiance estimates are equated to bias temperature errors. The random error variance of the downward, upward, net, and equivalent irradiance is firmly established for the first time and presented in graphical form. A significant reduction in the irradiance variance is achieved by using a 'least-squares' approximating polynomial to evaluate the temperature lag term of the irradiance equations. The normal distribution of irradiance errors is heuristically justified. From these results firm confidence intervals may be presented for individual irradiance estimates, given the error variance of the three radiometersonde temperature observations.

INTRODUCTION

As a result of instrumental developments during the last decade, measurements of the vertical distribution of the atmospheric infrared irradiance have become feasible. Concurrently with the radiation measurements by *Brewer and Houghton* [1956] and *Gergen* [1956], the *Suomi and Kuhn* [1958] balloon-borne radiometersonde was developed at the University of Wisconsin to provide measurements of the components of infrared flux, i.e., the upward, downward, net, and equivalent infrared irradiance. Since 1958, several thousand radiometersonde flights have been made to observe vertical radiative profiles of the atmosphere. During this period the accuracy of the instrument has been increased by minor instrumental modifications and improved data reduction techniques whereby the magnitude of bias and random error components has been reduced.

My main purpose in this investigation is to determine the effect of instrumental errors on the infrared irradiance estimates. Because infrared atmospheric cooling [*Suomi et al.*, 1958; *Staley*, 1965], effective long-wave flux emissivity [*Kuhn*, 1963], infrared diabatic vertical velocities [*Bullock*, 1965], etc., are derived from the flux density estimates, it is extremely important to establish the statistical moments and an error probability density function for the irradiance estimation errors so that the effects of both bias and random instrumental errors on the derived quantities can be determined. The bias and random error components of the derived radiative quantities are related to the bias and random error components of the three temperature observations made by the radiometersonde. The relationship is established by individually equating the bias error component of the infrared irradiance to both bias and random temperature errors and the random error component of the irradiance to the random temperature error. Thus, as the accuracy of the temperature observations is increased, the improved accuracy of the upward, downward, net, and equivalence irradiance is easily determined. Only minor emphasis is given to the possible physical causes of the instrumental error. The physical sources of error have been discussed by *Kuhn* [1961], *Bushnell and Suomi* [1961], *Bushnell* [1962], *Darkow* [1963], and *Staley* [1965].

RADIOMETERSONDE EQUATIONS AND INSTRUMENTAL ERROR

The equations for the downward, upward, net, and equivalent irradiance [*Suomi et al.*, 1958; *Businger and Kuhn*, 1960] are

$$R_d = f_1(T_t \mid 3) - f_2(T_b) - 2f_2(T_a) + \delta_d \quad (1)$$

$$R_u = f_1(T_b \mid 3) - f_2(T_t) - 2f_2(T_a) + \delta_u \quad (2)$$

$$R_n = (R_u - R_d)$$
$$= f_1(T_b \mid 4) - f_1(T_t \mid 4) + \delta_n \quad (3)$$

$$R_E = \tfrac{1}{2}(R_u + R_d) = \tfrac{1}{2}[f_1(T_b \mid 2)$$
$$+ f_1(T_t \mid 2) - 4f_2(T_a)] + \delta_E \quad (4)$$

where R_d, R_u, R_n, and R_E are the downward, upward, net, and equivalent irradiance of the earth-atmosphere system and T_t, T_b, and T_a are the top, bottom, and air radiometersonde temperatures, respectively. δ_d, δ_u, δ_n, and δ_E are errors in the calculation of radiation 'due to the neglect of absorption and emission of the polyethylene films, adiabatic air temperature changes inside the radiometer, and other small effects' [*Suomi et al.*, 1958]. The functions f_1 and f_2 are

$$f_1(T_l \mid K_m) = C_1 T_l^4 + K_m C_2 T_l^2$$
$$+ K_m C_3 T_l + C_4 \, dT_l/dt \quad (5)$$

$$f_2(T_l) = C_2 T_l^2 + C_3 T_l \quad (6)$$

where the subscript l denotes either the top, t, bottom, b, or air, a, temperature sensors and K_m is the fixed constant equal to 3, 3, 4, or 2 for the upward, downward, net, and equivalent irradiance, respectively.

The vertical bar in the argument of the function $f(T \mid K_m)$ means 'given the parameter' and is a conditional statement indicating that the quantity following the bar is a parameter upon which the function or its independent variables depend. The time operator, d/dt, in the last term of (5), the temperature lag term, should not be confused with the top temperature subscript, t. The constants are

$$C_1 = 8.17 \times 10^{-11} \text{ cal cm}^{-2} \text{ min}^{-1} \text{ deg } (A)^{-4}$$

$$C_2 = 2.750 \times 10^{-6} \text{ cal cm}^{-2} \text{ min}^{-1} \text{ deg } (A)^{-2}$$

$$C_3 = 3.065 \times 10^{-4} \text{ cal cm}^{-2} \text{ min}^{-1} \text{ deg } (A)^{-1}$$

$$C_4 = 1.015 \times 10^{-2} \text{ cal cm}^{-2} \text{ deg } (A)^{-1}$$

These equations imply that the true continuous functions of height exactly satisfy (1), (2), (3), and (4). The equation relating the true downward-directed irradiance to the true continuous temperature functions is

$$\gamma_d = (C_1 \eta_t^4 + 3C_2 \eta_t^2 + 3C_3 \eta_t + C_4 \, d\eta_t/dt)$$
$$- (C_2 \eta_b^2 + C_3 \eta_b) - 2(C_2 \eta_a^2 + C_3 \eta_a) + \delta_d$$
$$= f_1(\eta_t \mid 3) - f_2(\eta_b) - 2f_2(\eta_a) + \delta_d \quad (7)$$

where γ_d and η_l are the true functions relating the true flux of radiation in the atmosphere to the three observed temperatures. It should be noted that the functions η_t and η_b are not the actual radiation temperatures of the downward and upward streams in the atmosphere but are first-order estimates of these temperatures which are adjusted for the conduction and lag of the radiometer. In illustrating the effects of the random and bias temperature errors, I shall present only the complete set of equations for the downward irradiance. The development of the equations for the other three components is analogous, and only a few of the derived equations are presented.

The equation relating the three observed temperatures to the true but unknown temperature functions is

$$T_l = \eta_l + \epsilon_l \quad (8)$$

where $\epsilon_l = \epsilon_t, \epsilon_b$, and ϵ_a represent the three instrumental errors composed of a nonrandom bias component and a random stochastic component. For this development, the instrumental error component is the combination of all errors that are primarily due to the sensors, telemetry system, data reduction, etc. These errors should not be confused with true continuous error functions δ_d, δ_u, δ_n, and δ_E, which are present because of the neglect of higher-order terms and effects in the derivation of (1), (2), (3), and (4). The complete set of equations relating the estimates of R_d, R_u, R_n, and R_E to the true continuous functions and the errors are given by substitution of (8) into the temperature functions of (1), (2), (3), and (4). The expansion of the binomial term $\eta_l + \epsilon_l$ in the temperature functions of f_1 and f_2 for the downward irradiance yields

$$R_d = \Big\{ C_1 \sum_{i=0}^{4} \binom{4}{i} \eta_t^{4-i} \epsilon_t^{\,i}$$
$$+ 3C_2 \sum_{i=0}^{2} \binom{2}{i} \eta_t^{2-i} \epsilon_t^{\,i}$$
$$+ 3C_3(\eta_t + \epsilon_t) + C_4 \frac{d}{dt}(\eta_t + \epsilon_t) \Big\}$$

$$- \left\{ C_2 \sum_{i=0}^{2} \binom{2}{i} \eta_b^{2-i} \epsilon_b^{\,i} + C_3(\eta_b + \epsilon_b) \right\}$$

$$- \left\{ 2C_2 \sum_{i=0}^{2} \binom{2}{i} \eta_a^{2-i} \epsilon_a^{\,i} + 2C_3(\eta_a + \epsilon_a) \right\} + \delta_d \tag{9}$$

where $\binom{4}{i}$ and $\binom{2}{i}$ are the binomial coefficients. The time derivative in the lag term of (9) is the derivative of a stochastic process and is to be defined in the sense of convergence in mean square [*Parzen*, 1962].

Equation 9 is the basic equation for the subsequent development and discussion. Although instrumental error is implicit in (1) through (4), equation 9 allows an orderly development that clearly demonstrates the effect of instrument error on the derived irradiance estimates. The main emphasis is given to the effect of the errors, both bias and random, on the estimates R_i of the true irradiance functions γ_i.

Expected Value, Bias and Random Error of Irradiance Estimates

The separate effects of the random and the bias error components of the temperature observations in the irradiance estimates of the radiative flux can be determined by defining a cumulative probability density function of error, P, such that

$$P(\mathbf{T} \mid \mathbf{n}\lambda p) = \int_{\alpha}^{\beta} p(\boldsymbol{\epsilon} \mid \mathbf{n}\lambda p)\, d\boldsymbol{\epsilon} \tag{10}$$

where $\mathbf{T}$ is the vector of the three temperature observations T_t, T_b, and T_a; $\mathbf{n}$ is the vector of the true functions η_t, η_b, and η_a; $\boldsymbol{\lambda}$ is the vector of the bias functions; p is pressure; $\boldsymbol{\epsilon}$ is the vector of errors ϵ_t, ϵ_b, and ϵ_a; and $d\boldsymbol{\epsilon}$ is the vector of differential elements $d\epsilon_t$, $d\epsilon_b$, and $d\epsilon_a$. The event $\mathbf{T}$ corresponds to a value of $\boldsymbol{\epsilon}$ between α and β, where again the vertical bar means given the values of $\mathbf{n}$, $\boldsymbol{\lambda}$, and p.

The mean or the expected value of any of the three observed temperatures is

$$E(T_t \mid \mathbf{n}\lambda p) = \int T_t p(\boldsymbol{\epsilon} \mid \mathbf{n}\lambda p)\, d\boldsymbol{\epsilon} \tag{11}$$

$$E(T_t \mid \mathbf{n}\lambda p) = \eta_t + E(\epsilon_t) \tag{12}$$

For biased measurements the expected error is

$$E(\epsilon_t) = \lambda_t \neq 0 \tag{13}$$

where $\lambda = 0$ for unbiased observations. According to the law of large numbers, if simultaneous temperature observations could be made at any instant by one instrument during the flight, the mean of the observed quantities would approach $\eta_t + \lambda_t$ as the number of observations increased. In this formulation, the probability of observing a temperature T_t is determined by the joint probability density, which is a function of $\mathbf{n}$, $\boldsymbol{\lambda}$, and p. In general, the form of the probability distribution is not specified and may be different for each sensor, each instrument, each operator, etc. However, because these errors are minimized by careful calibration and operation, we shall consider that the probability density function is a function of the pressure and the three temperature functions.

From (8) and (12) the three temperature observations T_t are related to the true functions η_t by the sum of the bias nonrandom components λ_t and the random stochastic components ϵ_{Rt}, where

$$T_t = \eta_t + \lambda_t + \epsilon_{Rt} \tag{14}$$

Hereafter, ϵ_{Rt} without the subscript R is the random error component. In a similar manner, the irradiance estimates defined to be composed of three components, a measurement of the true function, a bias component, and a random error component, are

$$R_i = \gamma_i + \lambda_i + \epsilon_i \tag{15}$$

The expected value of the irradiance estimate in suppressed notation is, by definition,

$$\begin{aligned} E(R_i) &= E(R_i \mid \mathbf{n}\lambda p) \\ E(R_i) &= \int R_i p(\boldsymbol{\epsilon} \mid \mathbf{n}\lambda p)\, d\boldsymbol{\epsilon} \end{aligned} \tag{16}$$

The expected value of the downward irradiance is

$$E(R_d) = \gamma_d + \lambda_d = E\{f_1(T_b \mid 3) - f_2(T_t) - 2f_2(T_a)\} + \delta_d \tag{17}$$

$$E(R_d) = \left\{ C_1 \sum_{i=0}^{4} \binom{4}{i} (\eta_t + \lambda_t)^{4-i} E(\epsilon_t^{\,i}) + 3C_2[(\eta_t + \lambda_t)^2 + \sigma_t^{\,2}] + 3C_3(\eta_t + \lambda_t) + C_4\left[\frac{d(\eta_t + \lambda_t)}{dt} + E\left(\frac{d\epsilon_t}{dt}\right) \right] \right\}$$

$$- \{C_2[(\eta_b + \lambda_b)^2 + \sigma_b^2] + C_3(\eta_b + \lambda_b)\}$$
$$- 2\{C_2[(\eta_a + \lambda_a)^2 + \sigma_a^2]$$
$$+ C_3(\eta_a + \lambda_a)\} + \delta_d \qquad (18)$$

where the variance, σ_i^2, is the expected value of the squared random error, given $\mathbf{n}$, $\boldsymbol{\lambda}$, and p. Equations 15 and 16 require that the irradiance random error component be defined by

$$\epsilon_i = R_i - E(R_i) \qquad (19)$$

This step is necessary to separate arbitrarily the effects of the bias and random components of the temperature observations of (14). The irradiance random error component is most easily obtained from (9) by substituting $\eta_i + \lambda_i$ for each η_i and by considering ϵ_t, ϵ_b, and ϵ_a of this equation to be merely the random error component. Thus (19) defines the random error of the upward, downward, net, and equivalent irradiance, which for the downward component is

$$\epsilon_d = \left\{C_1 \sum_{i=1}^{4} \binom{4}{i}(\eta_t + \lambda_t)^{4-i}[\epsilon_t{}^i - E(\epsilon_t{}^i)]\right.$$
$$+ 3C_2[2(\eta_t + \lambda_t)\epsilon_t + (\epsilon_t{}^2 - \sigma_t{}^2)]$$
$$\left. + 3C_3\epsilon_t + C_4\left[\frac{d\epsilon_t}{dt} - E\left(\frac{d\epsilon_t}{dt}\right)\right]\right\}$$
$$- \{C_2[2(\eta_b + \lambda_b)\epsilon_b + (\epsilon_b{}^2 - \sigma_b{}^2)] + C_3\epsilon_b\}$$
$$- 2\{C_2[2(\eta_a + \lambda_a)\epsilon_a + (\epsilon_a{}^2 - \sigma_a{}^2)] + C_3\epsilon_a\} \qquad (20)$$

The expected value of (20) is zero, thus satisfying the definition of a random error component. The complete linear function which determines the bias errors λ_d of the downward irradiance is easily obtained by the subtraction of (7) from (18). The last equations clearly show that the definition of both a random and a bias error in the irradiance estimates is satisfied. One notes, however, the complexity of the mixed products of the errors in (18). Because the even moments of the random error component produce a small bias error, the downward, upward, and equivalent irradiance estimates will invariably contain a bias error unless both error components are zero. The bias error of the net irradiance estimates is negligible when the bias and random error components of the top and bottom sensors are equal. To simplify (18) and (20), two assumptions are necessary.

Assumption I. The probability density function of the random temperature error is symmetric.

Assumption II. The probability density function for an individual component is independent of the true function, the bias error, the pressure, and the probability density functions of the other two random components.

Therefore

$$p(\boldsymbol{\epsilon} \mid \mathbf{n}\boldsymbol{\lambda}p) = p(\epsilon_t)p(\epsilon_b)p(\epsilon_a) \qquad (21)$$

and

$$d(p(\boldsymbol{\epsilon}))/d\eta = 0 \qquad (22)$$

On the basis of previous studies [*AWSTR 105-133*, 1955; *Kuhn*, 1961] both assumptions appear to be satisfied. As a result of assumption I, all odd moments of the random error component vanish. However, since the sources of bias error from the second, third, and fourth moments of the random error component are negligible quantities, this is a minor assumption.

The necessary and sufficient condition for the time derivative dT_i/dt to exist in the sense of convergence in mean square is that $\eta_i + \lambda_i$ be differentiable and that the mixed second derivative of the time covariance of $\eta_i(s) + \lambda_i(s)$ and $\eta_i(t) + \lambda_i(t)$ with respect to any time, s and t, exist and be continuous [*Parzen*, 1962]. I shall assume that these conditions are satisfied. $\eta_i + \lambda_i$ is a continuous and differentiable function of height; thus the expected value of the observations from an ascending balloon having a continuous and differentiable vertical velocity becomes the differentiable function of time $\eta_i(t) + \lambda_i(t)$. Observations also indicate that the covariance function is differentiable. Satisfaction of the sufficient conditions allows the interchange of the operations of expectation and differentiation [*Parzen*, 1962], and the expected value of the lag term is given by

$$E\left(\frac{d}{dt}[\eta_i + \lambda_i + \epsilon_i]\right)$$
$$= \int \frac{d}{dt}(\eta_i + \lambda_i + \epsilon_i)p(\boldsymbol{\epsilon})\, d\boldsymbol{\epsilon} \qquad (23)$$

$$E\left(\frac{d}{dt}\left[\eta_i + \lambda_i + \epsilon_i\right]\right) = \frac{d}{dt}\int (\eta_i + \lambda_i + \epsilon_i)p(\epsilon)\,d\epsilon \quad (24)$$

$$E\left(\frac{d}{dt}\left[\eta_i + \lambda_i + \epsilon_i\right]\right) = \frac{d}{dt}(\eta_i + \lambda_i) \quad (25)$$

Until recently, the lag term was evaluated by a noncentered finite difference of the jth minus the $(j-1)$th observation. Such an evaluation is easily biased in regions of curvature of the top or bottom temperature function. By Rolle's theorem [*Stiefel*, 1963], if the data were exact the finite estimate would be unbiased for at least one point on the temperature function between the observations. However, for data with a random error component, there is no assurance that the finite estimate is equal to the true derivative of the temperature function for any point between two observations.

The main disadvantage of the finite difference was that the linear contribution of $(\eta_j - \eta_{j-1})/\Delta t$ to the irradiance estimates was less than the random linear effect of $(\epsilon_j - \epsilon_{j-1})/\Delta t$. Thus excessive random error variance was introduced, causing the oscillations of the irradiance estimates due to the random temperature component to be amplified. The lag term has recently been evaluated by differentiating a 'least-squares' second-degree approximating polynomial centered with respect to two adjacent temperature observations on either side of the midpoint observation. The estimate of the derivative is applied only to the midpoint observation, i.e., the observation for which an individual irradiance estimate is determined. The advantage of the polynomial evaluation is a significant reduction in the random error variance of the irradiance estimates. This reduction of variance is presented later in the determination of the irradiance random error variance.

The differentiated polynomial provides unbiased estimates of the derivative of $\eta_i + \lambda_i$ if the estimated polynomial is unbiased [*Johnson*, 1965]. From the continuous nature of radiation profiles and the analysis of more than 100 flights, it is evident that the second-degree polynomial determination of the derivative of $\eta_i + \lambda_i$ provides an unbiased estimate for the entire profile except possibly at the lower and upper boundaries of clouds. The possible bias error does not appear to be the result of oversmoothing, but is due to the lack of sufficient data points at the cloud's boundary to determine an unbiased estimate by any technique. It is evident, however, that the basic structure of the irradiance profiles is clearly delineated in the vicinity of clouds, and an increased sampling rate will be required for small-scale studies of the radiative field at the boundaries of clouds.

The most important assumption to be satisfied in determining valid irradiance estimates is that the instrumental errors are unbiased, but it is difficult to determine when a bias error ceases to be a problem. If the bias error is known as a function of η_i, the equations may be modified to provide unbiased estimates of the irradiance γ_i by subtracting the bias terms. Furthermore, in many studies bias estimates are entirely satisfactory, particularly if the bias term is constant or its variation is small in relation to the variation of the measured function. To study the possible influence of a bias error, I simplified a set of equations by deleting from (20) and the corresponding equations for the other three components all terms that are two orders of magnitude less than the leading error term for each sensor. In the atmosphere, the function η varies between 200 and 300°K; the bias error component, if it exists, is probably less than 1°C, and the rms of the random temperature error variance is approximately 0.2°C. For order of magnitude considerations, 3° will be used as the maximum for the bias error while 1° is used for the random error component. Using these values, we obtain the expected value of the downward, upward, net, and equivalent irradiance:

$$\begin{aligned} E(R_d) \approx \gamma_d &+ \{4C_1\eta_t{}^3\lambda_t + 6C_2\eta_t\lambda_t \\ &+ 3C_2\lambda_t{}^2 + 3C_3\lambda_t + C_4\, d\lambda_t/dt\} \\ &- \{2C_2\eta_b\lambda_b + C_3\lambda_b\} \\ &- \{4C_2\eta_a\lambda_a + 2C_3\lambda_a\} + \delta_d \end{aligned} \quad (26)$$

$$\begin{aligned} E(R_u) \approx \gamma_u &+ \{4C_1\eta_b{}^3\lambda_b + 6C_2\eta_b\lambda_b \\ &+ 3C_2\lambda_b{}^2 + 3C_3\lambda_b + C_4\, d\lambda_b/dt\} \\ &- \{2C_2\eta_t\lambda_t + C_3\lambda_t\} \\ &- \{4C_2\eta_a\lambda_a + 2C_3\lambda_a\} + \delta_u \end{aligned} \quad (27)$$

$$E(R_n) \approx \gamma_n + \{4C_1\eta_b{}^3\lambda_b + 8C_2\eta_b\lambda_b + 4C_2\lambda_b{}^2 + 4C_3\lambda_b + C_4\, d\lambda_b/dt\} - \{4C_1\eta_t{}^3\lambda_t + 8C_2\eta_t\lambda_t + 4C_2\lambda_t{}^2 + 4C_3\lambda_t + C_4\, d\lambda_t/dt\} + \delta_n \quad (28)$$

$$E(R_E) \approx \gamma_E + \tfrac{1}{2}\{4C_1\eta_b{}^3\lambda_b + 4C_2\eta_b\lambda_b + 2C_2\lambda_b{}^2 + 2C_3\lambda_b + C_4\, d\lambda_b/dt\} + \tfrac{1}{2}\{4C_1\eta_t{}^3\lambda_t + 4C_2\eta_t\lambda_t + 2C_2\lambda_t{}^2 + 2C_3\lambda_t + C_4\, d\lambda_t/dt\} - \{4C_2\eta_a\lambda_a + 2C_3\lambda_a\} + \delta_E \quad (29)$$

From these equations, it can be shown that a bias error of +1°C in the top sensor causes an error of approximately 0.007 ly/min. In (28) we note that any bias error in the telemetry system of the radiometersonde has a negligible influence on the estimates of net irradiance estimates, for the bias errors in the top and bottom temperature measurements cancel. The region of the atmosphere where a systematic bias error in the temperature observation might be most serious is the stratosphere, particularly when one is studying the infrared cooling from the divergence of long-wave radiation. This is a problem if the true error function or bias error is a function of height. If the bias error for the net irradiance estimates is constant with height, any bias error in the estimates of cooling will be eliminated by cancellation in the determination of the net radiative divergence. For the troposphere and the lower stratosphere the experimental work of *Bushnell* [1962] indicates that bias errors are negligible at pressures greater than 30 mb. Thus, in this region, they are not a serious problem in the estimation of the downward, upward, net, or equivalent irradiance. At pressures less than 30 mb, when the magnitude of the downward radiation stream is small, bias errors are possibly present. Additional research is necessary to determine whether they are present and significant.

Variance of the Irradiance Estimates

In the determination of the variance of the irradiance estimates, one should note that the equation for temperature measurements (14) contains two variance components; the first is due to the systematic bias error and the second to the random component. Likewise, since the expected value of the irradiance is a function of a true and a bias temperature function, the variance of the irradiance estimate is composed of a bias and a random component. By definition, the variance of the irradiance estimate about the true function is

$$V(R_i) = \sigma_i{}^2 + \lambda_i{}^2 \quad (30)$$

where the variance of the random component is

$$\sigma_i{}^2 = E([R_i - E(R_i)]^2) \quad (31)$$

and the systematic variance is

$$\lambda_i{}^2 = [E(R_i) - \gamma_i]^2 \quad (32)$$

This component of variance is the squared distance between the true function and the expected value function.

In the irradiance calculation, any bias error is an unknown factor whose variation as a function of height is probably negligible. Thus, in the following, the variance will be simply defined as the variance about the expected value of irradiance which is given by (31). By this definition the variance of the random error component becomes

$$V(R_i) = E\{R_i - (\gamma_i + \lambda_i)\}^2 \quad (33)$$

In general, since the irradiance estimates are obtained from a linear combination of three temperatures, the variance of the downward irradiance expressed as the variance of a linear function is

$$V(R_d) = V(f(T_t)) + V(f(T_b)) + V(f(T_a)) + 2C\,V(f(T_t), f(T_b)) + 2C\,V(f(T_t), f(T_a)) + 2C\,V(f(T_b), f(T_a)) \quad (34)$$

where $CV(\ )$ is the covariance of two terms.

Similar expressions exist for the upward, net, and equivalent irradiance. Although (34) can be completely determined by binomial expansions, a third assumption is made which eliminates the covariant terms involving the three temperature observations.

Assumption III. The random observational error component of each temperature series l is independent of the error probability density function for each of the two remaining temperature series m; thus for all i, j

$$E(\epsilon_{li}\epsilon_{mj}) = E(\epsilon_{li})E(\epsilon_{mj}) \quad (35)$$

From this assumption all the covariant terms of the functions of temperature are identically zero. Thus the equations for the variance of the downward, upward, net, and equivalent irradiance are

$$V(R_d) = V(f_1(T_t \mid 3)) + V(f_2(T_b)) + 4V(f_2(T_a)) \quad (36)$$

$$V(R_u) = V(f_1(T_b \mid 3)) + V(f_2(T_t)) + 4V(f_2(T_a)) \quad (37)$$

$$V(R_n) = V(f_1(T_t \mid 4)) + V(f_1(T_b \mid 4)) \quad (38)$$

$$V(R_E) = \tfrac{1}{4}\{V(f_1(T_b \mid 2)) + V(f_1(T_t \mid 2)) + 16V(f(T_a))\} \quad (39)$$

The variance of $f_1(T_l|K_m)$ is

$$\begin{aligned} V(f_1(T_l \mid K_m)) &= C_1^2 V(T_l^4) + K_m^2 C_2^2 V(T_l^2) \\ &+ K_m^2 C_3^2 V(T_l) + C_4^2 V(dT_l/dt) \\ &+ 2K_m C_1 C_2 C V(T_l^4, T_l^2) \\ &+ 2K_m C_1 C_3 C V(T_l^4, T_l) \\ &+ 2C_1 C_4 C V(T_l^4, dT_l/dt) \\ &+ 2K_m^2 C_2 C_3 C V(T_l^2, T_l) \\ &+ 2K_m C_2 C_4 C V(T_l^2, dT_l/dt) \\ &+ 2K_m C_3 C_4 C V(T_l, dT_l/dt) \end{aligned} \quad (40)$$

and the variance of $f_2(T_l)$ is

$$V(f_2(T_l)) = C_2^2 V(T_l^2) + C_3^2 V(T_l) + 2C_2 C_3 C V(T_l^2, T_l) \quad (41)$$

To solve these two equations and the remaining expressions of (37), (38), and (39), the variance and covariance are determined from general binomial expansions. However, before expressing the general binomial expansions, we make a fourth assumption.

Assumption IV. The random observational errors of each temperature series l are independent of each other for all $i \neq j$; thus

$$E(\epsilon_{li}{}^c \epsilon_{lj}{}^d) = E(\epsilon_{li}{}^c)E(\epsilon_{lj}{}^d) \quad (42)$$

From assumptions I and IV, let

$$E(\epsilon^i) = \begin{cases} \kappa_0\sigma^0 = 1 & \text{for } i = 0 \\ \kappa_i\sigma^i & \text{for } i = 4, 6, 8 \\ 0 & \text{for } i = 1, 3, 5, 7 \end{cases} \quad (43)$$

where the κ_i are positive numbers relating the higher moments to the variance of the temperature observations. If the probability density function for the temperature errors is assumed to be a spherical normal distribution, κ equals 3, 15, and 105 for i equal to 4, 6, and 8.

The variance of an arbitrary power of temperature is

$$V(T_l^c) = E(T_l^c - E(T_l^c))^2 \quad (44)$$

$$V(T_l^c) = E(T_l^{2c}) - [E(T_l^c)]^2 \quad (45)$$

Substitution of (14) and a binomial expansion yields

$$V(T_l^c) = \sum_{i=0}^{2c} \binom{2c}{i} (\eta_l + \lambda_l)^{2c-i} \kappa_i \sigma_l{}^i - \sum_{i=0}^{c}\sum_{j=0}^{c} \binom{c}{i}\binom{c}{j} (\eta_l + \lambda_l)^{2c-(i+j)} \kappa_i \kappa_j \sigma_l{}^{i+j} \quad (46)$$

where, for c equal to 4, the variance of the fourth power of temperature is

$$\begin{aligned} V(T_l^4) &= 16(\eta_l + \lambda_l)^6 \sigma_l{}^2 + (68\kappa_4 - 36) \\ &\cdot (\eta_l + \lambda_l)^4 \sigma_l{}^4 + (28\kappa_6 - 12\kappa_4) \\ &\cdot (\eta_l + \lambda_l)^2 \sigma_l{}^6 + (\kappa_8 - \kappa_4{}^2)\sigma_l{}^8 \end{aligned} \quad (47)$$

For c equal to 2, the variance of temperature is

$$V(T_l^2) = 4(\eta_l + \lambda_l)^2 \sigma^2 + (\kappa_4 - 1)\sigma^4 \quad (48)$$

The covariance between the two arbitrary powers of temperature is, by definition,

$$CV(T_l^c, T_l^d) = E(T_l^{c+d}) - E(T_l^c)E(T_l^d) \quad (49)$$

which yields

$$CV(T_l^c, T_l^d) = \sum_{i=0}^{c+d} \binom{c+d}{i} (\eta_l + \lambda_l)^{c+d-i} \kappa_i \sigma_l{}^i - \sum_{i=0}^{c}\sum_{j=0}^{d} \binom{c}{i}\binom{d}{j} (\eta_l + \lambda_l)^{(c+d)-(i+j)} \kappa_i \kappa_j \sigma_l{}^{i+j} \quad (50)$$

For c equal to 4 and d equal to 2, the covariance is

$$\begin{aligned} CV(T_l^4, T_l^2) &= 8(\eta_l + \lambda_l)^4 \sigma_l{}^2 + (14\kappa_4 - 6) \\ &\cdot (\eta_l + \lambda_l)^2 \sigma_l{}^4 + (\kappa_6 - \kappa_4)\sigma_l{}^6 \end{aligned} \quad (51)$$

For c equal to 4 and d equal to 1, the covariance is

$$C\,V(T_l^4, T_l) = 4(\eta_l + \lambda_l)^3\sigma_l^2 + 4\kappa_4(\eta_l + \lambda_l)\sigma_l^4 \quad (52)$$

and for c equal to 2 and d equal to 1, it is

$$C\,V(T_l^2, T_l) = 2(\eta_l + \lambda_l)\sigma_l^2 \quad (53)$$

The variance of the differentiated polynomial estimate of the lag term for the midpoint for evenly time spaced observations is [*Johnson*, 1965]

$$V(dT/dt_i) = V(B_{1i}/2\,\Delta t) \quad (54)$$

where Δt is the time interval between adjacent observations and B_{1i} is the estimated regression coefficient of the linear term of the second-degree polynomial. The linear relation of the estimated regression coefficient B_{1i} to the five temperature observations, $j = (i-2), \ldots, (i+2)$, is given by

$$B_{1i} = \left(\sum_{j=i-2}^{i+2} w_j T_j\right)_i \quad (55)$$

where the five values of w_j are $(-2/5, -1/5, 0, 1/5, 2/5)$ for $j - 2$ to $j + 2$, respectively. The variance of the lag term is, by definition,

$$V\left(\frac{dT}{dt_i}\right) = \frac{1}{(2\Delta t)^2}\{E(B_i^2) - [E(B_i)]^2\} \quad (56)$$

$$V\left(\frac{dT}{dt_i}\right) = \frac{1}{(2\Delta t)^2}\left\{E\left(\sum_{j=i-2}^{i+2} w_j T_j\right)_i^2 - \left[E\left(\sum_{j=i-2}^{i+2} w_j T_j\right)_i\right]^2\right\} \quad (57)$$

$$V\left(\frac{dT}{dt_i}\right) = \frac{1}{(2\Delta t)^2} \cdot\left\{\sum_{r=0}^{2}\binom{2}{r}\left[\sum_{j=i-2}^{i+2} w_j(\eta_j + \lambda_j)\right]^{2-r} \cdot E\left[\sum_{j=i-2}^{i+2} w_j\epsilon_j\right]^r - \left[\sum_{j=i-2}^{i+2} w_j(\eta_j + \lambda_j)\right]^2\right\} \quad (58)$$

For $r = 0$, the first and second right-hand terms are identical; for $r = 1$, the first right-hand term is zero. Thus, by assumption IV, the variance of the lag term is

$$V\left(\frac{dT}{dt_i}\right) = \frac{\sigma^2}{4(\Delta t)^2}\sum_{j=i-2}^{i+2} w_j^2 \quad (59)$$

$$V(dT/dt_i) = \sigma^2/10(\Delta t)^2 \quad (60)$$

The covariance of a power of the temperature and the lag term is

$$C\,V\left(T_{1i}^c, \frac{dT}{dt_{1i}}\right) = C\,V\left[T_{1i}^c, \left(\sum_{j=i-2}^{i+2} w_j T_j\right)_{1i}/2\Delta t\right] \quad (61)$$

By assumption IV, the covariance becomes

$$C\,V\left(T_{1i}^c, \frac{dT}{dt_{1i}}\right) = C\,V[T_{1i}^c, (w_i T_{1i}/2\Delta t)] \quad (62)$$

Since w_i for the midpoint observation i in the estimate of B_{1i} is always zero, the covariance of the power of temperature and the lag term is identically zero.

The linear contribution, LC (poly), of the variance of the lag term from an approximating polynomial estimate to the variance of the flux estimates is

$$LC(\text{poly}) = C_4^2(\sigma/\Delta t)^2/10 \quad (63)$$

This contribution may be compared with that by the finite estimation, LC (finite), from *Johnson* [1965].

$$LC(\text{finite}) = 2C_4^2(\sigma/\Delta t)^2 + 2C_1C_4 \cdot\{4(n + \lambda)^3\sigma^2/\Delta t + 4\kappa_4(n + \lambda)\sigma^4/\Delta t\} + 6C_2C_4\{2(n + \lambda)\sigma^2/\Delta t\} + 6C_3C_4\sigma^2/\Delta t \quad (64)$$

The first right-hand term of (64) is 20 times greater than the single term of (63), and the second term for normal atmospheric values of η is approximately 10 times greater. Clearly,

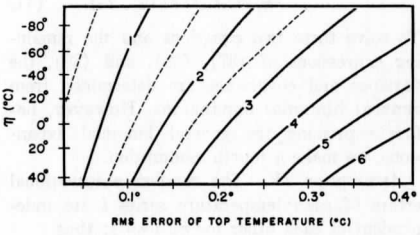

Fig. 1. Isopleths of standard deviation of downward or upward irradiance (units, 10^{-3} ly/min). The ordinate is the true temperature.

the polynomial evaluation of the lag term significantly reduces the propagation of the random temperature errors on the irradiance errors and demonstrates the power of a thorough statistical analysis. This reduction of random error variance is very important in the net and equilibrium irradiance estimates because their equations contain two lag terms. Comparative estimates will be presented later.

The complete expressions for the variance of the downward, upward, net, and equivalent irradiance are given by substitution of these general expansions into (36) through (39). However, because of their length, only the expression for the downward irradiance is presented, which is (see note, p. 5825)

$$
\begin{aligned}
V(R_d) = {} & C_1^2\{16(\eta_t + \lambda_t)^6\sigma_t^2 \\
& + (68\kappa_4 - 36)(\eta_t + \lambda_t)^4\sigma_t^4 \\
& + (28\kappa_6 - 12\kappa_4)(\eta_t + \lambda_t)^2\sigma_t^6 + (\kappa_8 - \kappa_4^2)\sigma_t^8\} \\
& + 9C_2^2\{4(\eta_t + \lambda_t)^2\sigma_t^2 + (\kappa_4 - 1)\sigma_t^4\} \\
& + 9C_3^2\sigma_t^2 + 6C_1C_2\{8(\eta_t + \lambda_t)^4\sigma_t^2 \\
& + (14\kappa_4 - 6)(\eta_t + \lambda_t)^2\sigma_t^4 + (\kappa_6 - \kappa_4)\sigma_t^6\} \\
& + 6C_1C_3\{4(\eta_t + \lambda_t)^3\sigma_t^2 + 4\kappa_4(\eta_t + \lambda_t)\sigma_t^4\} \\
& + 18C_2C_4\{2(\eta_t + \lambda_t)\sigma_t^2\} + C_4^2(\sigma_t/\Delta t)^2/10 \\
& + C_2^2\{4(\eta_b + \lambda_b)^2\sigma_b^2 + (\kappa_4 - 1)\sigma_b^4\} \\
& + C_3^2\sigma_b^2 + 2C_2C_3\{2(\eta_b + \lambda_b)\sigma_b^2\} \qquad (65) \\
& + 4C_2^2\{4(\eta_a + \lambda_a)^2\sigma_a^2 + (\kappa_4 - 1)\sigma_a^4\} \\
& + 4C_3^2\sigma_a^2 + 8C_2C_3\{2(\eta_a + \lambda_a)\sigma_a^2\}
\end{aligned}
$$

Discussion

Equation 65 specifies the variance of the downward irradiance from the true temperature functions and the error moments of any symmetric error distribution of the temperature observations. There is no contribution from the odd temperature moments because they are assumed to be zero. This assumption is consistent with the error analysis of *Kuhn* [1961]. Also, Kuhn's experimental data indicate that the normal distribution of errors is applicable. Thus, in the computation of the variance of the irradiance estimates, the κ's are those determined from a spherical normal distribution of temperature errors. The standard deviation of the top and bottom sensors was assumed equal because of the symmetric design of the radiometer [*Kuhn and Johnson*, 1966]. The standard deviation of the air temperature sensor was assumed to be equal to twice the value for the top and bottom sensors because it is exposed to the free air and the raw air temperature data display larger fluctuations. From considering the magnitude of the terms from each of the three sensors in the irradiance equations, it must be noted that the downward, upward, and equivalent irradiance variance is primarily determined from the contributions of the variance from the top and bottom sensors and is less sensitive to the random variance of the air temperature. The net irradiance is independent of the variance of the air temperature.

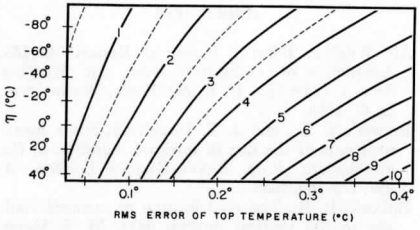

Fig. 2. Isopleths of standard deviation of net irradiance (units, 10^{-3} ly/min). The ordinate is the true temperature.

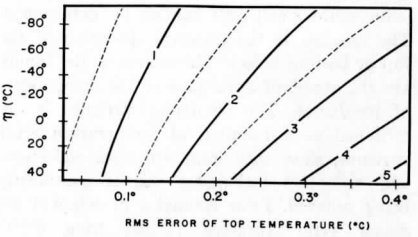

Fig. 3. Isopleths of standard deviation of equivalent irradiance (units, 10^{-3} ly/min). The ordinate is the true temperature.

The computational results of the standard deviation of the downward, upward, net, and equivalent irradiance are presented in Figures 1, 2, and 3. Figure 1 presents both the upward and downward irradiance, since, by assuming that the variance of the top and bottom sensors is equal, the variances of both components are equal. The bias temperature errors

are assumed to be zero because they are usually quite small and cannot be determined. The abscissa is the standard deviation of the top or bottom sensor. The curves of the family are the standard deviations of the components of irradiance. The irradiance variance is determined as a function of temperature error variance, since with improved data collections and reduction techniques this is continually being reduced. Prior estimates of temperature sensor error variance ranged from 0.3°C [*Johnson,* 1965] to 0.2°C in carefully edited data [*Kuhn,* 1961]. With the improved data reduction methods, the standard deviation is nearing 0.15°C. To gain the maximum utility of these figures, we need an estimate of the random temperature error variance for each radiometersonde flight. Such estimates will be available for each routine radiometersonde flight as a by-product of a 'least-squares' polynomial filtering method to reduce the effect of the random temperature errors and will be presented in a forthcoming paper on the statistical properties of filtered irradiance estimates.

The functional dependence of the irradiance variance on the true temperature functions is clearly displayed in the figures. For a fixed random temperature variance the standard deviation of the irradiance decreases with decreasing temperature. In Figure 2 for a temperature standard deviation of 0.2°C, the net irradiance standard deviation decreases from 0.0049 ly/min at 30°C to 0.0026 ly/min at −70°C. These are representative standard deviations of net irradiance for temperature observations taken in a subtropical or tropical atmosphere. It is interesting to compare these two standard deviations of net irradiance determined from a polynomial evaluation of the temperature lag term with those determined by a finite estimate of the lag term. From *Johnson* [1965], for identical conditions, the net irradiance standard deviation decreases from 0.0075 ly/min at 30°C to 0.0054 ly/min at −70°C. This is a variance reduction of 58 and 67%, respectively, and it clearly shows the power of the improved data reduction technique.

The distribution of the random error estimates of the components of irradiance is indicated by the central limit theorem [*Cramer,* 1946]. In the equation for the downward irradiance (20) and in the corresponding equations for the upward, net, and equivalence irradiance, the random irradiance error components are a linear combination of several independent terms. Furthermore, the terms with the higher-order moments, fourth and above, are small in comparison with the second-order temperature moments. Because the temperature errors tend to be normally distributed, the random irradiance errors must also tend to be nearly normally distributed. From individual temperature error variance estimates for each flight, from Figures 1, 2, and 3, and from a probability density function for the irradiance errors, firm confidence intervals can be presented for each irradiance estimate. Such confidence intervals should aid in delineating infrared radiative processes from the random effects of the inherent errors in all observations. Thus, as the accuracy of the radiometersonde temperature observations increases, smaller scales of the atmospheric structure of infrared irradiance can be investigated. To further increase the accuracy of the irradiance estimates requires temperature observations with reduced random error components or improved analysis techniques such as filtered irradiance estimates [*Johnson,* 1965; *Kuhn and Johnson,* 1966]. A detailed discussion of the over-all improvement for irradiance estimates gained by the use of approximating polynomials will be presented in a forthcoming paper.

Acknowledgments. I wish to thank Professor Lyle H. Horn for his assistance in the preparation of this paper.

This research was supported by the United States Weather Bureau through grant 25 and the National Center for Atmospheric Research through their visiting scientist program.

References

Air Weather Service Technical Report 105-133, Accuracies of radiosonde data, Air Weather Service (MATS), U. S. Air Force, Washington, D. C., 1955.

Brewer, A. W., and J. T. Houghton, Some measurements of the flux of infrared radiation in the atmosphere, *Proc. Royal Society London, A, 236,* 175–186, 1956.

Bullock, B. R., The contribution of infrared cooling to the vertical motion field, M. S. thesis, Department of Meteorology, University of Wisconsin, 1965.

Bushnell, R. H., Air investigation of the problem of the measurement of infrared radiation in the lower stratosphere, Ph.D. thesis, Department of Meteorology, University of Wisconsin, 1962.

Bushnell, R. H., and V. E. Suomi, Experimental flight verification of the economical net radiometer, *J. Geophys. Res.*, *66*(9), 2843–2848, 1961.

Businger, J. A., and P. M. Kuhn, On the observation of total and net atmospheric radiation, *J. Meteorol.*, *17*(4), 400–405, 1960.

Cramer, H., *Mathematical Methods of Statistics*, Princeton University Press, Princeton, N. J., 1946.

Darkow, G. L., A study of infrared measurements in the vicinity of the subtropical tropopause, Ph.D. thesis, Department of Meteorology, University of Wisconsin, 1963.

Gergen, J. L., Black ball: A device for measuring atmospheric infrared radiation, *Rev. Sci. Instr.*, *27*(7), 453–460, 1956.

Johnson, D. R., The role of terrestrial radiation in the generation of available potential energy, Ph.D. thesis, Department of Meteorology, University of Wisconsin, 1965.

Kuhn, P. M., Accuracy of the airborne economical radiometer, *Monthly Weather Rev.*, *89*(8), 285–287, 1961.

Kuhn, P. M., Measured effective long-wave emissivity of clouds, *Monthly Weather Rev.*, *91*(10–12), 635–640, 1963.

Kuhn, P. M., and D. R. Johnson, Improved radiometersonde observations of atmospheric infrared irradiance, *J. Geophys. Res.*, *71*(2), 367–373, 1966.

Parzen, E., *Stochastic Processes*, Holden-Clay, Inc., San Francisco, 1962.

Staley, D. O., Radiative cooling in the vicinity of inversions and the tropopause, *Quart. J. Roy. Meteorol. Soc.*, *91*(389), 282–301, 1965.

Stiefel, E. L., *An Introduction to Numerical Mathematics*, Academic Press, New York, 1963.

Suomi, V. E., and P. M. Kuhn, An economical net radiometer, *Tellus*, *10*(1), 160–163, 1958.

Suomi, V. E., D. O. Staley, and P. M. Kuhn, A direct measurement of infrared-radiation divergence to 160 mb, *Quart. J. Roy. Meteorol. Soc.*, *84*(360), 134–141, 1958.

(Received March 7, 1966.)

Note: (from page 105)

See addendum (p. 108 of this report) for the variance equations of the upward, net and equivalent infrared irradiance.

ADDENDUM

"The Variance Equations for Upward, Net and Equivalent Infrared Irradiance"

by Donald R. Johnson

In this addendum, the equations for the variance of upward, net and equivalent infrared irradiance, which were not included in the basic paper because of their length, are now added for documentation. They may be used in a computerized statistical analysis of individual radiometersonde flights. The variance equations of the upward, net and equivalent infrared irradiance are as follows:

$$V(R_u) = C_1^2\{16(\eta_b+\lambda_b)^6\sigma_b^2 + (68K_4 - 36)(\eta_b+\lambda_b)^4\sigma_b^4 +$$
$$(28K_6 - 12K_4)(\eta_b+\lambda_b)^2\sigma_b^6 + (K_8 - K_4^2)\sigma_b^8\} +$$
$$9C_2^2\{4(\eta_b+\lambda_b)^2\sigma_b^2 + (K_4 - 1)\sigma_b^4\} + 9C_3^2\sigma_b^2 +$$
$$6C_1C_2\{8(\eta_b+\lambda_b)^4\sigma_b^2 + (14K_4 - 6)(\eta_b+\lambda_b)^2\sigma_b^4 +$$
$$(K_6 - K_4)\sigma_b^6\} + 6C_1C_3\{4(\eta_b+\lambda_b)^3\sigma_b^2 + \qquad (66)$$
$$4K_4(\eta_b+\lambda_b)\sigma_b^4\} + 18C_2C_3\{2(\eta_b+\lambda_b)\sigma_b^2\} +$$
$$C_4^2/10(\sigma_b/\Delta t)^2 + C_2^2\{4(\eta_t+\lambda_t)^2\sigma_t^2 + (K_4 - 1)\sigma_t^4\} +$$
$$C_3^2\sigma_t^2 + 2C_2C_3\{2(\eta_t+\lambda_t)\sigma_t^2\} + 4C_2^2\{4(\eta_a+\lambda_a)^2\sigma_a^2 +$$
$$(K_4 - 1)\sigma_a^4\} + 4C_3^2\sigma_a^2 + 8C_2C_3\{2(\eta_a+\lambda_a)\sigma_a^2\}$$

$$V(R_n) = C_1^2\{16(\eta_b+\lambda_b)^6\sigma_b^2 + (68K_4-36)(\eta_b+\lambda_b)^4\sigma_b^4 + (28K_6 - 12K_4)\cdot$$
$$(\eta_b+\lambda_b)^2\sigma_b^6 + (K_8 - K_4)\sigma_t^8\} + 16C_2^2\{4(\eta_b+\lambda_b)^2\sigma_b^2 + (K_4 - 1)\sigma_b^4\} +$$
$$16C_3^2\sigma_b^2 + 8C_1C_2\{8(\eta_b+\lambda_b)^4\sigma_b^2 + (14K_4 - 6)(\eta_b+\lambda_b)^2\sigma_b^4 +$$
$$(K_6 - K_4)\sigma_b^6\} + 8C_1C_3\{4(\eta_b+\lambda_b)^3\sigma_b^2 + 4K_4(\eta_b+\lambda_b)\sigma_b^4\} +$$
$$32C_2C_3\{2(\eta_b+\lambda_b)\sigma_b^2\} + C_4^2/10(\sigma_b/\Delta t)^2 +$$
$$C_1^2\{16(\eta_t+\lambda_t)^6\sigma_t^2 + (68K_4 - 36)(\eta_t+\lambda_t)^4\sigma_t^4 + (28K_6 - 12K_4)\cdot$$
$$(\eta_t+\lambda_t)^2\sigma_t^6 + (K_8 - K_4)\sigma_t^8\} + 16C_2^2\{4(\eta_t+\lambda_t)^2\sigma_t^2 + (K_4 - 1)\sigma_t^4\} +$$
$$16C_3^2\sigma_t^2 + 8C_1C_2\{8(\eta_t+\lambda_t)^4\sigma_t^2 + (14K_4 - 6)(\eta_t+\lambda_t)^2\sigma_t^2 +$$

$$(K_6 - K_4)\sigma_t^6\} + 8C_1C_3\{4(\eta_t + \lambda_t)^3\sigma_t^2 + 4K_4(\eta_t + \lambda_t)\sigma_t^4\} +$$

$$32C_2C_3\{2(\eta_t + \lambda_t)\sigma_t^2\} + C_4^2/10(\sigma_t/\Delta t)^2 \tag{67}$$

$$V(R_E) = \frac{1}{4}[C_1^2\{16(\eta_b + \lambda_b)^6\sigma_b^2 + (68K_4 - 36)(\eta_b + \lambda_b)^4\sigma_b^4 +$$

$$(28K_6 - 12K_4)(\eta_b + \lambda_b)^2\sigma_b^6 + (K_8 - K_4^2)\sigma_b^8\} +$$

$$4C_2^2\{4(\eta_b + \lambda_b)^2\sigma_b^2 + (K_4 - 1)\sigma_b^4\} + 4C_3^2\sigma_b^2 +$$

$$4C_1C_2\{8(\eta_b + \lambda_b)^4\sigma_b^2 + (14K_4 - 6)(\eta_b + \lambda_b)^2\sigma_b^4 +$$

$$(K_6 - K_4)\sigma_b^6\} + 4C_1C_3\{4(\eta_b + \lambda_b)^3\sigma_b^2 + 4K_4(\eta_b + \lambda_b)\sigma_b^4\} +$$

$$8C_2C_3\{2(\eta_b + \lambda_b)\sigma_b^2\} + C_4^2/10(\sigma_b/\Delta t)^2] +$$

$$\frac{1}{4}[C_1^2\{16(\eta_t + \lambda_t)^6\sigma_t^2 + (68K_4 - 36)(\eta_t + \lambda_t)^4\sigma_t^4 + \tag{68}$$

$$(28K_6 - 12K_4)(\eta_t + \lambda_t)^2\sigma_t^6 + (K_8 - K_4^2)\sigma_t^8\} +$$

$$4C_2^2\{4(\eta_t + \lambda_t)^2\sigma_t^2 + (K_4 - 1)\sigma_t^4\} + 4C_3^2\sigma_b^2 +$$

$$4C_1C_2\{8(\eta_t + \lambda_t)^4\sigma_t^2 + (14K_4 - 6)(\eta_t + \lambda_t)^2\sigma_t^4 +$$

$$(K_6 - K_4)\sigma_t^6 + 4C_1C_3\{4(\eta_t + \lambda_t)^3\sigma_t^2 + 4K_4(\eta_t + \lambda_t)\sigma_t^4\} +$$

$$8C_2C_3\{2(\eta_t + \lambda_t)\sigma_t^2\} + C_4^2/10(\sigma_t/\Delta t)^2] +$$

$$4C_2^2\{4(\eta_a + \lambda_a)^2\sigma_a^2 + (K_4 - 1)\sigma_a^4\} + 4C_3\sigma_a^2 +$$

$$8C_2C_3\{2(\eta_t + \lambda_t)\sigma_t^2\}$$